MULTICONSTITUENT NONLINEAR VISCOELASTIC FRAMEWORK FOR MODELING ASPHALT BINDERS AND MIXTURES

A Dissertation

by

BHASKAR VAJIPEYAJULA

Submitted to the Graduate and Professional School of
Texas A&M University
in partial fulfillment of the requirements for the degree of

DOCTOR OF PHILOSOPHY

Chair of Committee,	K.R. Rajagopal
Co-Chair of Committee,	Eyad Masad
Committee Members,	Alan D Freed
	Zachary Grasley
Head of Department,	Andreas A Polycarpou

August 2021

Major Subject: Mechanical Engineering

ABSTRACT

The mechanical response of asphaltic material is complex and usually nonlinear depending on the applied stresses and strains. The material exhibits nonlinearity in several ways, such as non-proportional responses to external loading, shear-thinning/thickening, and generation of normal force when sheared. Moreover, asphalt mixtures have several constituents and are sensitive to factors like time, temperature, and confinement pressure, among others. The importance of accounting for nonlinearity in the response of asphaltic materials has been well documented in the literature. However, most available models only account for specific nonlinear aspects of materials (usually the non-proportional response to external loading) and have several inherent shortcomings. For example, the model proposed by Schapery [1] was to violate conservation of angular momentum for large deformation [2] and the integral models developed by Cheung and Cebon [3] cannot account for the normal force generated when the material is sheared [4].

This research aims to develop a framework to account for the nonlinear behavior of asphalt binders and mixtures. For this reason, thermodynamics-based constitutive models were developed. First, this framework is used to understand and account for the contribution of the individual constituents of asphalt mixtures to overall nonlinear behavior. This allows one to understand and better design the material constituents so mixtures can last longer in the field. The model is corroborated with experimental data obtained from subjecting asphalt mixtures to various experimental protocols. Second, the model is further developed to represent the behavior of blended asphalt mixtures containing reclaimed (recycled) asphalt and virgin binder. Lastly, the model is modified to account for confinement and temperature effects on asphalt mixture behavior. The outcome of this research is the development of a comprehensive nonlinear viscoelastic framework that analyzes asphaltic materials and accounts for the effects of their constituents.

The findings of this research highlight the importance of using appropriate testing protocols and choosing the correct model to analyze asphaltic material response. This research will pave the way for developing a fundamental understanding of the responses of asphalt mixtures subjected to

different confinement conditions, while accounting for the densification and implicit response of the material. Consequently, the outcome of this study can be used to predict material responses in the field with greater accuracy.

DEDICATION

To my parents.

ACKNOWLEDGEMENTS

I would like to thank my committee chair, Prof. K. R. Rajagopal, and Prof. Eyad Masad for their guidance over the years. I wish to express the deepest gratitude to my research guide, Prof. K. R. Rajagopal for his belief in me and for the opportunity to pursue this research. Today I see his advice to select this topic as the most appropriate one, as I enjoyed every day of my Ph.D. work. It was a great privilege to have a man with his depth and breadth of knowledge as my advisor. His classes on mechanics were inspiring and exhilarating. I thank him for his guidance, support, and inspiration during the course of my education at this institution.

I also thank Professor Masad. I appreciate the time and support he has given me all these years and am I am deeply thankful for the amount of time he spent in thought-provoking discussions, painstakingly correcting write-ups, and above all, getting things going even in the not-so-good situations in research. His guidance was highly valuable in enhancing my knowledge in the subject and in providing a proper shape and direction to this research. Also, I am grateful to Prof. Alan Freed and Prof. Zachary Grasley for serving on my committee.

I would like to express my sincere gratitude to Prof. Atul Narayan for his time and valuable inputs in the theoretical and computational part presented in this thesis. I appreciate the time he has spent explaining the various hurdles involved in developing a new model.

I very much appreciate the efforts of Dr. K. Lakshmi Roja in collecting data for the various experiments presented in this thesis.

Special thanks to Prof. Michael Golla of the Department of Engineering Technology and Industrial Distribution for entrusting me with a recurring teaching assistant position and providing me with much-needed financial stability.

I especially need to thank all of my lab mates, Manoj, Tejasvi Krishna, Pavitra, Alagappan, and Juan, for making the workplace a lot of fun. I also recognize the special role played by several brainstorm sessions with Manoj in forwarding my research and my understanding of various concepts in continuum mechanics. I acknowledge my mentors Abhijth, Tejasvi, Alagappan, Aditya,

and Vivek who have always guided me during tough times.

Lastly, I would like to thank my parents for being a positive influence and supporting me through this journey during the many trying times.

CONTRIBUTORS AND FUNDING SOURCES

Contributors

This work was supported by a dissertation committee consisting Prof. Kumbakonam Rajagopal, Prof. Eyad Masad, Prof. Alan Freed of the Department of Mechanical Engineering and Prof. Zachary Grasley of the Department of Civil Engineering. The data used for the analysis in chapter is Contributed by Prof. Eyad Masad and Dr. Mohammed Sadeq and is published in Vajipeyajula et al. [5]. The data used in Chapter 4 was contributed by Prof. Eyad Masad and Prof. Emad Kassem as a part of the Asphalt Research Consortium at Texas A&M University and is published in Rahmani et al. [6], Bazzaz et al. [7], Rahmani et al. [8], and Rushing et al. [9].

Funding sources

Part of the Graduate study was funded by Prof. Kumbakonam Rajagopal, Prof. Eyad Masad.

Part of the Graduate study was funded through Teaching Assistanship provided by Professor Michael Golla of the Department of Engineering Technology and Industrial Distribution.

TABLE OF CONTENTS

Page

LIST OF FIGURES

FIGURE Page

LIST OF TABLES

TABLE Page

1. INTRODUCTION

Asphalt binders, whether natural or processed from petroleum, are all mixtures of hydrocarbons. Recently, interest in adding various polymers to increase the life of the asphalt pavements has spiked. Polymer additives, along with the long-chain hydrocarbons in asphalt binders are a mixture of reacting and diffusing constituents [10]–[12]. Thus, asphalt binders are made of constituents with different chemical compositions that exhibit a wide range of responses to external stimuli.

Traditionally, the linearized viscoelastic constitutive relation has been used to model asphalt binder and mixture behaviors. Studies relying on this approach use a spring-dashpot analogy[13]–[15]. However, it has been shown that asphalt binders in the mix are subjected to high strains due to large differences in stiffnesses between aggregate and asphalt binder constituents [12]. The response of asphalt binders and mixtures was found to be nonlinear even when subjected to relatively low strains [16]. In a creep and recovery test, a material's response changes after each loading cycle, which renders linearized viscoelastic model not suitable for explaining the material's actual behavior. The response of asphaltic material in the field also changes with time due to microstructure changes due to either mechanical changes such as a reduction in air voids or chemical changes such as aging of the asphalt. Such microstructure changes and the various loading conditions experienced by asphalt pavements are the primary cause of distress phenomena such as rutting and fatigue cracking. There is a need for the development of a comprehensive nonlinear viscoelastic model that can account for asphalt binder and mixture behaviors at different stress levels, temperatures, and confinement pressures. The model should also be able to account for the effects of material constituents on the behavior and the various nonlinearities exhibited by asphaltic material. This feature will give the capability to select and design materials to optimize performance.

1.1 Problem Statement

In viewing the complex nature of asphaltic material and their diverse responses to external stimuli, developing an appropriate model that can account for all factors affecting their response is a complex task. However, it might be possible to develop a mechanical model for isothermal processes that neglects chemical effects, and pays attention to important factors. This study targets the development of a theoretical platform that can be adapted to simulate the mechanical response of asphaltic materials subjected to various loading conditions: stress relaxation, repeated creep and recovery, and random creep and recovery, repeated creep and recovery at different confinement pressures. The model developed and employed is an isothermal model capable of exhibiting compressible viscoelastic fluid-like response that can be modified in the future to account for non-isothermal phenomena. This study aims at providing a better understanding of the modeling aspects of asphaltic material that account for its nonlinearity and multi-constituent nature. Using the frameworks established in this thesis, one can optimize the design of blended binder and asphalt to attain the desired qualities and use it as feedback to understand pavement response to various loading conditions.

1.2 Objectives

The primary objectives of this study are to

- Adopt a constitutive model within the continuum mechanics that can examine the complex nonlinear behavior of asphaltic materials. The model is based on the framework presented by Rajagopal and Srinivasa [17]. This framework can describe the behavior of a material while accounting for microstructure changes as it deforms.

- Use the model to account for the nonlinear model of asphalt mixtures and constituent contributions to the overall mixture response. The framework along with the theories established in mixture theory can be used to determine individual constituents' contributions to the overall material response. The application of the model is for the analysis of warm fine aggregate mixtures (WFAM).

- Implement the model to analyze the response of blended asphalt binders consisting of reclaimed/recycled asphalt binder and virgin asphalt binder. The focus is on accounting for the effects of the constituents (i.e., reclaimed asphalt and virgin binder) on the response of the reclaimed asphalt. The model is used to develop a parameter that can describe the rutting resistance of blended binders to rutting.

- Develop a nonlinear viscoelastic constitutive model capable of accounting for confinement pressure's effects on asphalt mixture responses at various temperatures. This model can account for changes in density (compressibility of asphalt mixtures) and microstructure changes in asphalt mixtures as it deforms.

1.3 Literature Review

Having an understanding of the mechanical and thermodynamics behavior of asphaltic material is desirable because of its wide range of applications (Shell Bitumen [18] lists more than 250 known current uses for asphalt in modern times in various industries such as construction, agriculture, and the electrical industry). Before deciding on a model to capture asphaltic material response, one must understand the various complexities related to the study of constitutive behaviors of asphaltic material. The complexity of modeling the response of asphalt mixtures has been detailed in a comprehensive paper by Krishnan and Rajagopal [19]. Hence this section is divided into three sub-sections. The first section discusses the various nonlinearities exhibited by asphaltic materials. The second subsection reviews various experimental protocols used to characterize material response. The third subsection discusses the various approaches currently being used to understand the effects of confinement pressure on asphalt mixtures.

1.3.1 Nonlinearity in the Mechanical Response of Asphaltic Material

The motivation for most studies on asphaltic material has been to develop constitutive relations to understand the response of distress to which pavements in the field are subjected and to determine an experimental protocol that, along with the model, can be used to characterize the material. The rheological properties of asphalt are governed by its chemical constituents and its microstruc-

ture [11], [20], [21]. Lesueur [22] and Krishnan and Rajagopal [11] summarized developments related to asphalt microstructure. Asphaltic materials undergo reversible changes to their internal structure over time, which causes changes in density and material stiffness over time. Nonlinearity can be found in several different aspects of the mechanical response of asphaltic material. The following subsections present a review of the various nonlinearities accounted for in this thesis.

1.3.1.1 Nonproportional Viscoelastic Response

One of the first reports of nonlinearity in the response of asphaltic material was by Lethersich [23], who observed nonproportional strain responses to applied stress while conducting creep experiments. Similar trends were observed in the time domain when Cheung and Cebon [3] subjected asphalt mixtures to tensile loading and when Narayan et al. [24] subjected asphalt binders to stress relaxation, and in the frequency domain Masad et al. [25] when observed nonproportional variation of the amplitude of stress to the strain applied. In recent years, repeated creep and recovery tests at high stress levels are being employed to study rutting resistance and nonlinearity in asphalt binders [26].

1.3.1.2 Normal Force Under Shear Loading

When sheared, asphaltic material tends to expand in a direction normal to the shearing plane. Restraining this motion causes normal stress in the material. This phenomenon was first observed in asphaltic material by Dealy [27], but very few researchers have analyzed it in detail until recently. Narayan et al. [24] analyzed this phenomenon in detail in a torsional stress relaxation experiment on asphalt binders, and found that the relaxation time for normal force and stress are different. They also found that the magnitude of normal force decreases with temperature up to a threshold temperature, after which it becomes negligible.

1.3.2 Permanent Deformation in Asphalt Pavements

Permanent deformation is one of the most common forms of distress found in asphalt pavements and is one of the primary modes of failure. Thus, it is important to ensure that the pavement does not fail due to rutting during its design life. Having a well-established procedure that can rank

the rutting resistance of various binders and mixtures is crucial. Various researchers have quantified the rutting performance of asphalt binders using experimental methods that utilize aspects of linear viscoelasticity (LVE) theory [28]–[31].

The current specification of binders includes a parameter to evaluate it's rutting resistance at high temperatures. The high temperature grading is the temperature (°C) above which the parameter $\frac{G^*}{(sin\delta)}$ is less than a critical value at 10 Hz. In this parameter, G^* is the dynamic modulus and δ is the phase angle measured on the binder in a torsional strain-controlled oscillatory test. However, several researchers have found that a binder's Superpave grading correlates poorly with field observations and other simulated rutting tests [26], [32], [33]. This can be attributed to two primary reasons. The first of these is an inherent assumption of linearity for all binders at a frequency of 10 Hz at all temperatures [32]. The second is that the rutting resistance is measured at only one frequency, whereas binder response on the frequency in the strain-controlled oscillatory test.

Several researchers addressing the inherent shortcomings of Superpave specifications, have suggested using repeated creep and recovery to measure the parameters associated with the accumulation of permanent deformation. Parameters such as zero shear viscosity (ZSV) , which has been adopted by European countries as a standard to quantify rutting, have been suggested. There are various methods by which ZSV can be determined [34]. However, recent investigations found that, like Superpave grading, ZSV does not correlate well with field observations. This was attributed to the use of single stress levels in the repeated creep and recovery protocol traditionally used to calculate ZSV.

Addressing this, D'Angelo [35] developed the multiple creep and recovery test protocol. Along with this, they proposed the use of the J_{nr}(non-recoverable creep compliance) parameter based on comparing its values with the performance of pavements incorporated with different binders. The originally proposed multiple stress and creep recovery test protocol had 11 stress levels ranging from 0.25 to 25 kPa; however, this was later reduced to two stress levels (0.1 and 3.2 kPa) [36]. Several studies indicated that the 3.2 kPa stress level used in multiple stress and creep recovery is too small to differentiate among binders, and the recovery time of 9 sec is not sufficient for binders

to exhibit complete recovery [37]–[39].

1.3.3 Effects of Confinement Pressure

When pavements are subjected to repeated traffic loading, asphalt mixtures undergo large deformations. Gibson et al. [40] showed that traffic loading conditions generally induce multiaxial stress conditions within pavements. Throughout the life of pavements in the field, asphalt undergoes densification and microstructure rearrangement.

Few models have been proposed to model the effects of confinement pressure on the response of asphalt mixtures [41]–[44]. However, these models do not consider densification, the implicit response of mixtures, and the notion that mixture response usually depends on the current microstructure. For example, the study conducted by Saadeh et al. [41] presented that the nonlinear response of the material depended on the confinement pressure; however, they not did present any correlation between the model parameters and confinement stress levels. Zhao et al. [44] analyzed the effect of confinement pressure on the linear viscoelastic parameters of mixtures. However, asphalt mixture responses in the field are usually found to be nonlinear even when undergoing small deformations.

1.4 Outline of the Dissertation

This dissertation is organized following the research paper format. Chapters 2, 3, and 4 are research papers that have been or will be submitted to several refereed journals.

Chapter 1 includes the introduction, which contains the problem statement, objectives, literature review, and outline of this dissertation.

Chapter 2 presents a detailed framework to separate the contributions of individual constituents to the overall material response using the nonlinear viscoelastic model derived by Málek et al. [45]. This model was then used to analyze the response of warm fine aggregate mixtures (WFAM) when subjected to creep and recovery loading under different stress and aging conditions. This chapter also suggests modifications addressing the drawbacks of the current protocols.

Chapter 3 describes utilizing the established framework to analyze the effects of recycled as-

phalt pavement (RAP) content in RAP-blended blended binders in both the linear and nonlinear regimes. This chapter also presents the various experimental protocols being used to quantify rutting resistance along with their drawbacks.

Chapter 4 discusses using a Gibbs potential-based thermodynamic framework, and the constitutive assumptions a new constitutive model is derived to analyze the effects of confinement pressure on asphalt mixture responses. This is done by presenting a parametric analysis to understand each material parameter's sensitivity to the model response. The model is then validated by corroborating the model to data obtained from creep and recovery experiments done on asphalt mixtures at various confinement pressures.

Chapter 5 presents the major conclusions drawn from the above studies. This chapter gives a summary of the studies, followed by key findings. Also discussed here are the major contributions of this work.

1.5 Scope and Limitation

The modeling of asphaltic materials is an extensive and complex task. Therefore, it would be too ambitious to consider and attempt to address all issues in a single study. Therefore, we have applied restrictions to limit the scope of the current research. The entire process is considered to be isothermal and we also ignored the chemical changes asphalt pavements experience in the field due to aging. Despite these limitations, the modeling and simulation framework developed here is demonstrated to work for asphaltic materials subjected to different loading conditions such as stress relaxation, repeated creep recovery, random creep and recovery at various temperatures, and confinement pressure.

2. A TWO-CONSTITUENT NONLINEAR VISCOELASTIC MODEL FOR ASPHALT MIXTURES*

2.1 Overview

The goal of this study is to model the creep and recovery response of fine asphalt mixtures using a thermodynamically consistent nonlinear viscoelastic model. The model considers asphalt mixtures to consist of two constituents: an aggregate structure incorporating the asphalt–aggregate interface and an asphalt binder. This study evaluates the model's efficacy using the response of warm fine aggregate mixtures (WFAM). These materials were produced using a polymer-modified binder of PG 76-22 and three warm mix additives (Sasobit, Advera, and Rediset). Unaged and aged samples were subjected to creep stress levels of 75 and 400 kPa, followed by rest periods. The model successfully the material behavior as a single set of parameters were derived from the prediction of shear and normal stress responses for both the 75 and 400 kPa stress levels. The presented model offers a unique feature in modeling the energy storage and dissipation properties of each constituent. As such, one can examine the effect of changes in individual material properties on the material's response and performance.

2.2 Introduction

modeling the response of asphalt binders and mixtures to external stimuli is a challenge as the material is inherently inhomogeneous. Additionally, the material presents a time-dependent response reflected by its ability to stress relax, creep in a nonlinear fashion, and age. An added complexity is that the material a mixture of reacting and diffusing constituents [10]–[12].

The linearized viscoelastic constitutive relation has traditionally been used to model the behavior of asphalt binders and mixtures. However, research has shown that asphalt binders are subjected

*This chapter is reprinted with permission from "B Vajipeyajula, E Masad, KL Roja, et al. "A two-constituent nonlinear viscoelastic modelfor asphalt mixtures". In:Road Materials and Pavement Design(2019), pp. 1–15."

to high strains due to large differences in stiffnesses between the aggregate and asphalt binder constituents (Masad et al. [12]). In addition, asphalt binders and mixtures are often subjected to much larger strains in creep and recovery tests (Bai et al. [46]; Laukkanen et al. [47]), leading to permanent deformation and cracking. In a creep and recovery test, a material's response changes after each loading cycle, rendering a linearized viscoelastic model unsuitable for explaining the material's actual behavior.

Krishnan and Rajagopal [16] developed a nonlinear thermodynamically consistent model to overcome the limitations of using the linearized viscoelastic model to predict the behavior of asphalt mixtures and binders. Darabi et al. [48] and Darabi et al. [49] proposed a thermo viscoelastic–viscoplastic model to separate the thermo-viscoelastic, thermo-viscoplastic, and damage responses of asphalt mixtures.

Recently Málek et al. [45] and Málek et al. [50] developed a model that recognizes that each asphalt mixture constituent may have its own "natural configuration" as the material deforms. Each constituent can store energy and produce entropy. The evolution of the natural configurations is determined by maximizing the rate of entropy production (Krishnan and Rajagopal [16]). Within a purely mechanical theory, dissipation is the only means for entropy production, and one can obtain different constitutive relations depending on the manner in which energy is stored and dissipated.

The "natural configuration" can be thought of as the configuration a body takes when all external stimuli are removed. An elastic body has only one natural configuration that is, it returns to the same natural state upon the removal of external loads. In contrast, a viscoelastic material may have infinite natural configurations (see Rajagopal [51] for a detailed description of natural configurations).

Málek et al. [45] assumed that each constituent of the mixture could have a different natural configuration. Thus, having two constituents immediately provides two ways in which the body can store energy and two ways in which it can dissipate energy. Each way of storing energy is like that in a neo-Hookean body which leads to two material constants associated with the energy storage mechanism. In addition to the dissipation associated with each of the constituents, there

is an additional term due to the interaction between the constituents (or the symmetric part of the mixture velocity gradient), yielding a total of five material parameters.

Málek et al. [50] corroborated their model against the experiments of Krishnan and Narayan [52] and Narayan et al. [24]. The torsional experiments indicated that the relaxation time for normal forces and torque were different. Existing viscoelastic models could not describe this difference in relaxation time. In addition, Málek et al. [50] simulated a variety of initial boundary value problems, including rutting and compaction under rolling action.

A thermodynamically consistent model is used in this study develop a practical tool to predict the response of individual materials (aggregate and binder) in the asphalt mixture. To characterize the mechanical response of WFAM samples in this chapter, we applied two different stress levels followed by rest periods. We developed an experimental program in such a way that the energy storage and dissipation properties of each material could quantify the response of creep and recovery and calculated the strain contribution of each individual material.

2.3 Materials and Testing

We prepared fine aggregate mixture (FAM) samples with a polymer modified binder of PG 76-22 grade. Then, we added three types of warm mix additives (Sasobit, Advera, and Rediset) to the binder. These additives belong to different categories: Sasobit is a wax-based additive, Advera is a synthetic zeolite used for foaming the binder, and Rediset is a chemical additive. The selected dosages for Sasobit, Advera, and Rediset were $2\%, 5\%,$ and 0.5%, respectively. The samples were tested after three aging conditions: unaged, 40- and 100-days40 days under UV light with oxygen and heat, and 100 days under UV light along with oxygen and heat. This aging process caused significant microstructure changes [53], [54].

The FAM samples were cored in a cylindrical shape with a diameter of 12.5 mm and height of 50 mm. The asphalt binder content used to prepare these samples was 7.9% by weight of the total mixture and the air voids were 3%. Detailed information related to the sample preparation is provided in Sadeq et al. [55].

We subjected the FAM samples to torsion in a mechanical testing device with a dynamic shear

rheometer (DSR). The ends of the samples were glued to the metal pieces as shown in Figure 1(a) and a special fixation accessory was used to apply the torsional force. The unaged and UV-aged samples underwent nine creep and recovery cycles at 25° C. The applied stress levels were 75 kPa and 400 kPa with loading times of 40 sec. We determined the rest period for each individual cycle beforehand to maintain consistency for all the samples.

We examined the repeatability of the creep and recovery test by performing two trials for each asphalt mixture. A new sample was used for each experiment and the absolute error percentage from the mean was calculated at the end of each experiment as shown in Equation 2.1. The error was found to be less than 15%.

$$\text{Error}(\%) = \frac{|x_1 - x_2|}{\text{Mean}} \times 100 \tag{2.1}$$

Here, Mean is the average of the two trials and x_1 and x_2 are the two experimental measurements.

2.4 Nonlinear Viscoelasitc Model for Asphalt Materials

As the material deforms, microstructure changes lead to the evolution of a natural configuration, which is associated with energy dissipation. In developing the model, the assumption is that the evolution of a natural configuration is determined by maximizing the rate of dissipation (in general the rate of entropy production) subject to other constraints that the body might have to meet, such as incompressibility. This assumption has been very fruitful in the development of models for a variety of material systems and mechanisms such as viscoelastic solids and fluids, twinning of metals, shape memory alloys and shape memory polymers, and mixtures consisting of fluids and solids [56]–[59]. Málek et al. [45] adopted such an approach to develop models for asphalt mixtures. This study adopts the model developed by Málek et al. [45] to describe the behavior of WFAM samples subjected to creep and recovery tests.

2.4.1 Kinematics

This section provides the basic kinematics required to describe the model. A detailed discussion of the kinematics of continua can be found in [60]. We assume $\kappa_R(B)$ as the reference

(a) (b)

Figure 2.1: (a) A sample of warm fine aggregate mix (WFAM). (b) Illustration of the testing setup in the dynamic mechanical analyzer

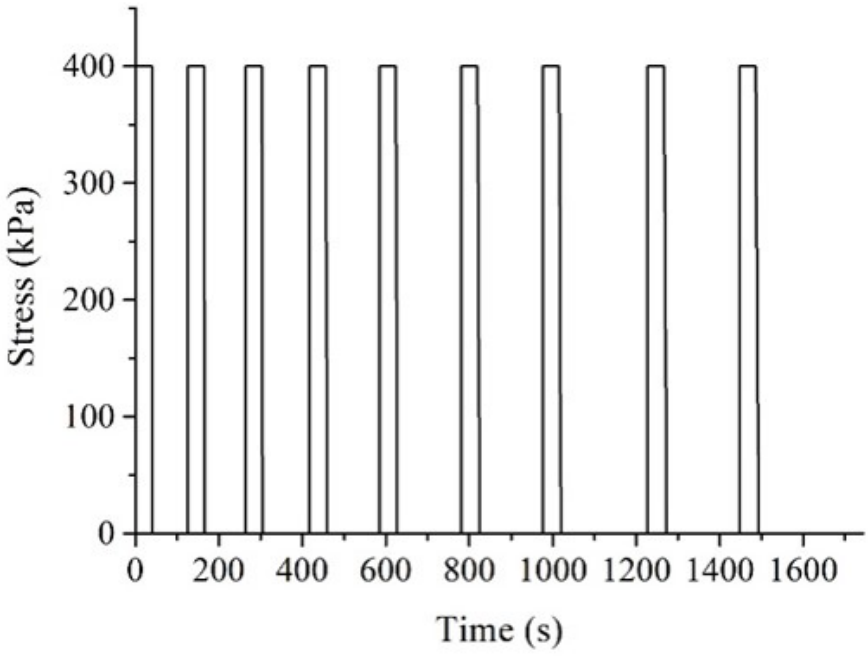

Figure 2.2: Experimental protocol

configuration of the body B and $\kappa_{c(t)}(B)$ as the current configuration of the body. If X is a point in the reference configuration and its corresponding point in the current configuration is x, then the motion of the body is given by the mapping,

$$\boldsymbol{x} = \chi_{\kappa_R}(\mathbf{X}, t). \tag{2.2}$$

The corresponding deformation gradient is defined as

$$\mathbf{F}_{\kappa_R} = \frac{\partial \chi_{\kappa_R}(\mathbf{X}, t)}{\partial \mathbf{X}}. \tag{2.3}$$

The left and right Cauchy-Green tensors associated with the above deformation gradient are

$$\mathbf{B}_{\kappa_R} = \mathbf{F}_{\kappa_R}\mathbf{F}^T_{\kappa_R}, \tag{2.4}$$

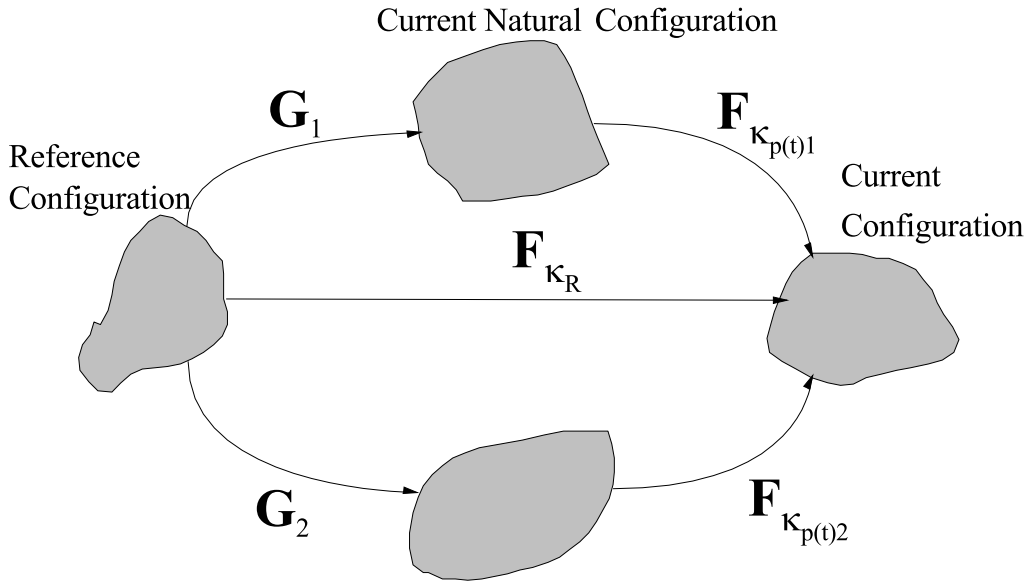

Figure 2.3: Description of motion of a body

$$\mathbf{C}_{\kappa_R} = \mathbf{F}^T_{\kappa_R}\mathbf{F}_{\kappa_R}. \tag{2.5}$$

The velocity gradient (**L**) and its symmetric part (**D**) can be expressed as,

$$\mathbf{L} = \nabla\mathbf{v} = \dot{\mathbf{F}}_{\kappa_R}\mathbf{F}^{-1}_{\kappa_R}, \tag{2.6}$$

$$\mathbf{D} = \frac{1}{2}(\mathbf{L} + \mathbf{L}^T). \tag{2.7}$$

For this model, we assume $\kappa_{p(t)_1}$ and $\kappa_{p(t)_2}$ as the two natural configurations the body can have at any given moment. The corresponding mapping between natural and current configurations are $\mathbf{F}_{\kappa_{p(t)_1}}$ and $\mathbf{F}_{\kappa_{p(t)_2}}$. $\mathbf{G}_1$ and $\mathbf{G}_2$ are the corresponding mappings between the reference configuration and the natural configuration. The relation between the mappings can be expressed as

$$\mathbf{G}_1 = \mathbf{F}^{-1}_{\kappa_{p(t)_1}}\mathbf{F}_{\kappa_R}, \tag{2.8}$$

$$\mathbf{G}_2 = \mathbf{F}^{-1}_{\kappa_{p(t)_2}} \mathbf{F}_{\kappa_R}. \tag{2.9}$$

The material is assumed to be incompressible, which is reflected by having the determinant of the deformation gradient be equal to unity.

$$det(\mathbf{F}_{\kappa_R}) = 1. \tag{2.10}$$

The response between $\kappa_{p(t)_i}$ and κ_R is to be purely elastic and incompressible, thereby

$$det(\mathbf{F}_{\kappa_{p(t)_1}}) = 1, \tag{2.11}$$

$$det(\mathbf{F}_{\kappa_{p(t)_2}}) = 1. \tag{2.12}$$

The inertial term is ignored while modeling the evolution of $\mathbf{B}_{\kappa_{p(t)}}$ as the motion is considered to be slow. As discussed earlier, the two natural configurations are associated with the bulk binder and the aggregate structure incorporating the binder interface, respectively.

2.4.2 Model Description

This section summarizes the main constitutive equations for a thermodynamically compatible model used by Málek et al. [61] to model asphalt binder behavior.

- Balance of mass

$$\dot{\rho} + \rho \,\mathrm{div}\, \mathbf{v} = 0. \tag{2.13}$$

Under the assumption that the material is incompressible, the above equation reduces to

$$\mathrm{div}\, \mathbf{v} = 0. \tag{2.14}$$

- Balance of linear momentum

$$\rho \dot{\mathbf{v}} = \rho \mathbf{b} + \mathrm{div}\, \mathbf{T}. \tag{2.15}$$

- The rate of entropy production is assumed to be

$$\xi = 2\mu_3 \mid \mathbf{D} \mid^2 + \mu_1 \mid \mathbf{D}_{\kappa_{p(t)_1}} \mid^2 + \mu_2 \mid \mathbf{D}_{\kappa_{p(t)_2}} \mid^2 . \tag{2.16}$$

- Balance of angular momentum in the absences of any internal body couples

$$\mathbf{T} = \mathbf{T}^T. \tag{2.17}$$

- Using the aforementioned balance laws and assumptions, the constitutive equation for the model can be expressed as

$$\mathbf{T} = -p\mathbf{I} + 2\mu_3\mathbf{D} + G_1\mathbf{B}^d_{\kappa_{p(t)_1}} + G_2\mathbf{B}^d_{\kappa_{p(t)_2}}, \tag{2.18}$$

$$\check{\mathbf{B}}_{\kappa_{p(t)_i}} = -2\frac{G_i}{\mu_i}\mathbf{B}_{\kappa_{p(t)_i}}\mathbf{B}^d_{\kappa_{p(t)_i}}, \tag{2.19}$$

where *i* can be 1 or 2 for 3D and $\mathbf{A}^d$ is the deviatoric part of the tensor **A**

$$\mathbf{A}^d = \mathbf{A} - \frac{1}{3}tr(\mathbf{A})\mathbf{I} \quad \text{in 3D}, \tag{2.20}$$

$$\mathbf{A}^d = \mathbf{A} - \frac{1}{2}tr(\mathbf{A})\mathbf{I} \quad \text{in 2D}. \tag{2.21}$$

We define a quantity p as

$$p = -\frac{1}{3}tr\mathbf{T}. \tag{2.22}$$

In these equations, ρ is the density, **v** is the velocity, **B** is the volume force, ξ is the rate of entropy production, **D** is the symmetric part of the velocity gradient, **T** is the Cauchy stress tensor, μ_3 is the viscosity, and G_1 and G_2 are the shear moduli, *p* is the pressure, $(G_1/\mu_1)^{-1}$ and $(G_2/\mu_2)^{-1}$are the two relaxation times. $\check{\mathbf{A}}$ is the upper convected Oldroyd derivative of the tensor. The model is derived with the intention of modeling multiple complex problems using a single set of parameters.

The shearing flow is assumed to have the form

$$\mathbf{v} = (0, \frac{\dot{\Omega} r z}{h}, 0), \tag{2.23}$$

where $\dot{\Omega}$ is the angular velocity at the top of the plates, r is the radius, z is the distance from the bottom plate, and h is the gap between the plates. The velocity gradient field for the corresponding motion will be of the form

$$\mathbf{L} = \nabla \mathbf{v} = \begin{bmatrix} 0 & -\frac{\dot{\Omega} z}{h} & 0 \\ \frac{\dot{\Omega} z}{h} & 0 & \frac{\dot{\Omega} r}{h} \\ 0 & 0 & 0 \end{bmatrix}. \tag{2.24}$$

The evolution equation will be of the form

$$\check{\mathbf{B}}_{\kappa_{p(t)_i}} = \dot{\mathbf{B}}_{\kappa_{p(t)_i}} - \mathbf{L}\mathbf{B}_{\kappa_{p(t)_i}} - \mathbf{B}_{\kappa_{p(t)_i}}\mathbf{L}^T = -2\frac{G_i}{\mu_i}\mathbf{B}_{\kappa_{p(t)_i}}\mathbf{B}^d_{\kappa_{p(t)_i}}, \tag{2.25}$$

$$\dot{\mathbf{B}}_{\kappa_{p(t)_i}} = \mathbf{L}\mathbf{B}_{\kappa_{p(t)_i}} + \mathbf{B}_{\kappa_{p(t)_i}}\mathbf{L}^T - 2\frac{G_i}{\mu_i}\mathbf{B}_{\kappa_{p(t)_i}}\mathbf{B}^d_{\kappa_{p(t)_i}}. \tag{2.26}$$

The inertial terms are couple of orders of magnitude smaller than the remaining terms in the equation. Ignoring the inertial terms and using the initial condition yields

$$\mathbf{B}_{\kappa_{p(t)}i} = \begin{bmatrix} B_{irr} & B_{ir\phi} & B_{irz} \\ B_{i\phi r} & B_{i\phi\phi} & B_{i\phi z} \\ B_{irz} & B_{iz\phi} & B_{izz} \end{bmatrix} = \mathbf{I}, \tag{2.27}$$

$$\mathbf{T} = \begin{bmatrix} T_{rr} & T_{r\phi} & T_{rz} \\ T_{\phi r} & T_{\phi\phi} & T_{\phi z} \\ T_{rz} & T_{z\phi} & T_{zz} \end{bmatrix} = \mathbf{0}. \tag{2.28}$$

One can calculate the evolution of $\mathbf{T}$ and $\mathbf{B}_{\kappa_{p(t)}i}$ to be

$$T_{rr} = -p + \frac{G_1}{3}(2B_{1rr} - B_{1\phi\phi} - B_{1zz}) + \frac{G_2}{3}(2B_{2rr} - B_{2\phi\phi} - B_{2zz}), \tag{2.29}$$

$$T_{\phi\phi} = -p + \frac{G_1}{3}(2B_{1\phi\phi} - B_{1rr} - B_{1zz}) + \frac{G_2}{3}(2B_{2\phi\phi} - B_{2rr} - B_{2zz}), \tag{2.30}$$

$$T_{zz} = -p + \frac{G_1}{3}(2B_{1zz} - B_{1rr} - B_{1\phi\phi}) + \frac{G_2}{3}(2B_{2zz} - B_{2rr} - B_{2\phi\phi}), \tag{2.31}$$

$$T_{\phi z} = G_1 B_{1\phi z} + G_2 B_{2\phi z} + \mu_3 \frac{r\dot{\Omega}}{h} \tag{2.32}$$

$$\dot{B}_{i\phi z} = \frac{r\dot{\Omega}}{h} B_{izz} + \frac{2G_i}{3\mu_i} B_{i\phi z}(B_{irr} - 2B_{i\phi\phi} - 2B_{izz}), \tag{2.33}$$

$$\dot{B}_{irr} = \frac{2G_i}{3\mu_i} B_{irr}(-2B_{irr} + B_{i\phi\phi} + B_{izz}), \tag{2.34}$$

$$\dot{B}_{i\phi\phi} = \frac{2G_i}{3\mu_i} B_{i\phi\phi}(+B_{irr} - 2B_{i\phi\phi} + B_{izz}) - \frac{2G_i}{\mu_i} B_{i\phi z}^2 + \frac{2r\dot{\Omega}}{h} B_{i\phi z}, \tag{2.35}$$

$$\dot{B}_{izz} = \frac{2G_i}{3\mu_i} B_{izz}(+B_{irr} + B_{i\phi\phi} - 2B_{izz}) - \frac{2G_i}{\mu_i} B_{i\phi z}^2. \tag{2.36}$$

Using the above equations and initial conditions, we solve the evolution of B_i as an initial boundary value problem. To solve the set of ordinary differential equations, we used the Runge-Kutta fifth-order (ODE45) in Matlab has been used.

The solution for pressure *p* should be known to calculate the normal stress or normal force. To avoid this, we eliminate the pressure term using the remaining two stress terms (T_{rr},$T_{\phi\phi}$) in the following manner.

$$0 = \frac{\partial T_{rr}}{\partial r} + \frac{T_{rr} - T_{\phi\phi}}{r}, \tag{2.37}$$

$$T_{zz}(r) = T_{rr}(r) + (T_{zz}(r) - T_{rr}(r)), \tag{2.38}$$

$$T_{zz}(r) = \int_R^r \frac{\partial T_{rr}}{\partial r} dx + (T_{zz}(r) - T_{rr}(r)), \tag{2.39}$$

$$T_{zz}(r) = \int_R^r \frac{T_{rr} - T_{\phi\phi}}{x} dx + (T_{zz}(r) - T_{rr}(r)). \tag{2.40}$$

2.5 Data Analysis and modeling

2.5.1 Nonlinearity Check

The material behavior is considered linear only if the obtained response satisfies linear scaling and superposition. This study checked for linear scaling with the data in the same way as presented in [24]. where the angle of rotation was divided by the amount of torque applied. As shown in Figure 2.6, the normalized angle of rotation is found to be independent of the torque applied, indicating that the material does not satisfy the scaling criterion, which implies that the material behavior is nonlinear when subjected to a loading of 400 kPa.

In addition to this linear scaling check, we attempted to model the behavior of the WFAM samples using the Burgers linear viscoelastic model. The Burgers model parameters were determined using data obtained from testing at 75 kPa as shown in Figure 2.4. We then used the same model parameters to predict the response at a higher stress conditions of 400 kPa as shown in Figure 2.5. The results showed that the linear model could not predict the behavior of the WFAM samples at a higher stress condition (400 kPa). Based on these results, one can clearly conclude that the behavior of the WFAM sample is nonlinear when subjected to a load of 400 kPa and is linear when subjected to a load of 75 kPa.

2.6 Nonlinear Viscoelastic Modeling

The model expresses the Cauchy stress **T** as a function of G_1, G_2, μ_1, μ_2, and μ_3. The aim of the modeling work is to find a single set of parameters capable of capturing the behavior of a WFAM sample over a range of loading conditions. This study introduced a new scalar parameter, expressed as:

$$J(G_1, G_2, \mu_1, \mu_2, \mu_3) = \int_0^T |E(t) - Omega(G_1, G_2, \mu_1, \mu_2, \mu_3)|dt, \tag{2.41}$$

where *E (t)* is the angle of twist obtained from the experimental data. The parameters are then found by minimizing the scalar function $J(G_1, G_2, \mu_1, \mu_2, \mu_3)$.

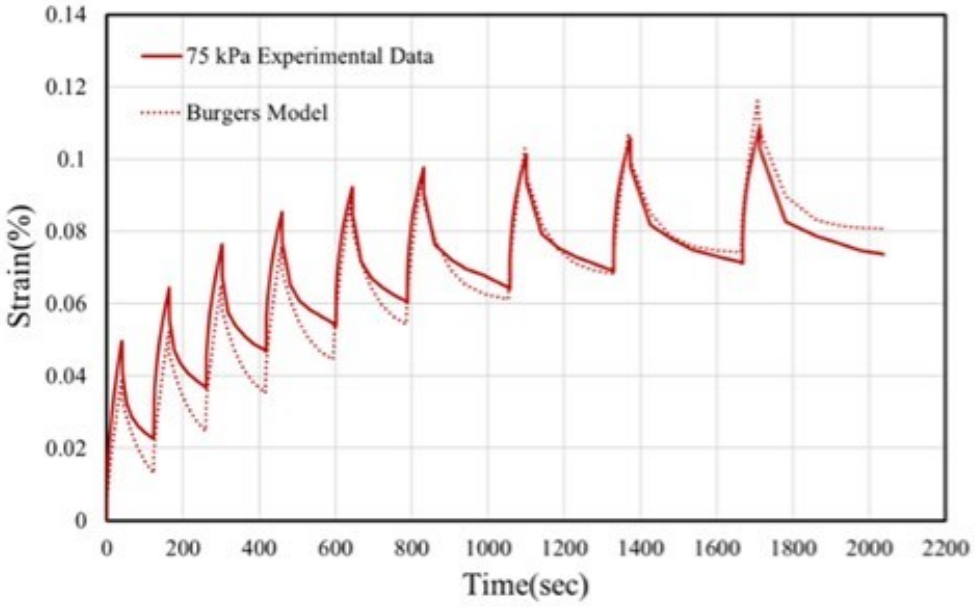

Figure 2.4: Burgers model fit at 75 kPa for the WFAM sample with Advera

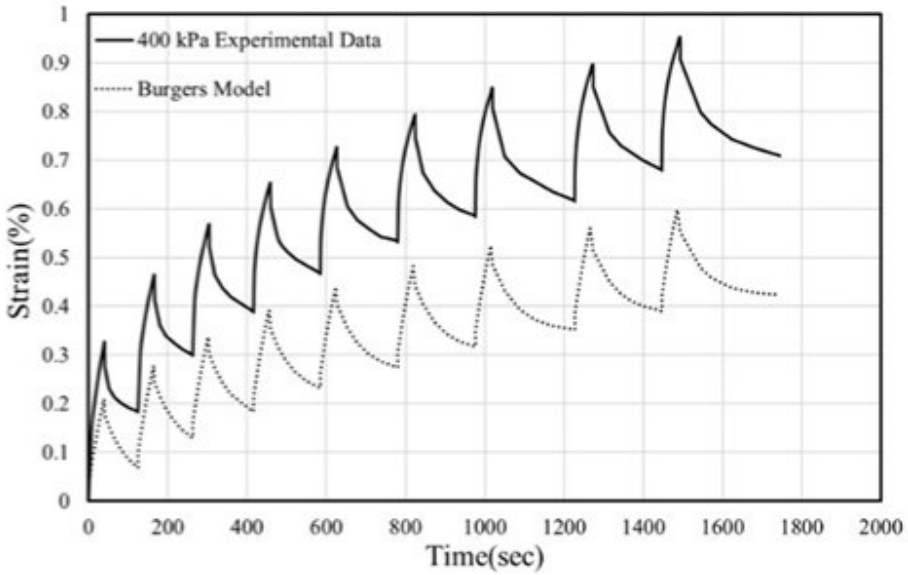

Figure 2.5: Burgers model verification of the model at 400 kPa for the WFAM sample with Advera

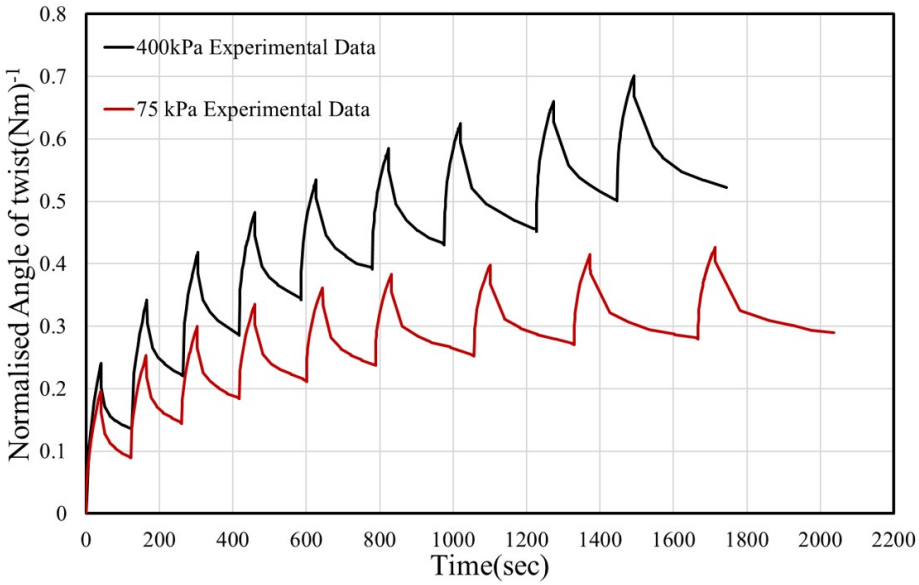

Figure 2.6: Normalized angle of rotation vs time curves at various stress levels during the first creep level for the WFAM sample with Advera

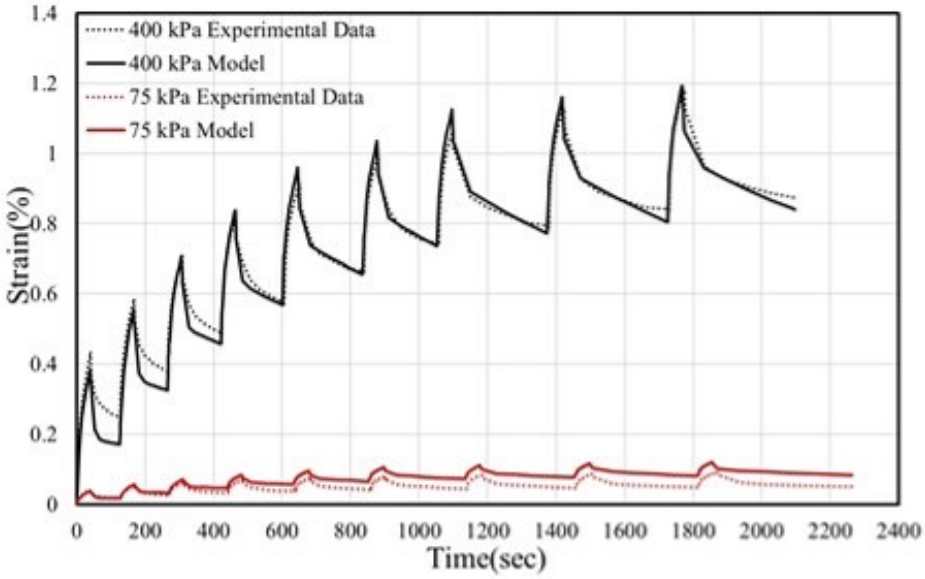

Figure 2.7: Nonlinear analysis at 400 kPa and verification of the model at 75 kPa for the Control Mixture

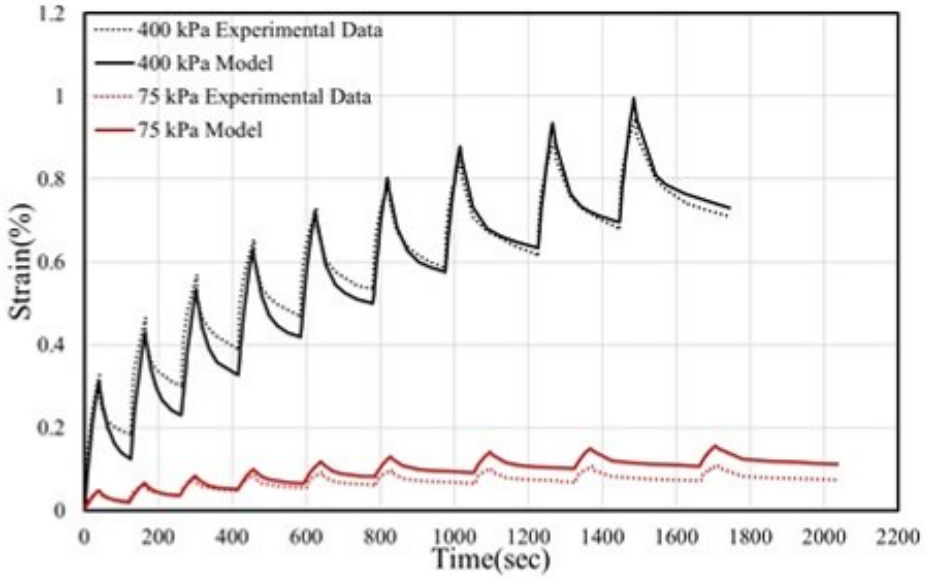

Figure 2.8: Nonlinear analysis at 400 kPa and verification of the model at 75 kPa for the WFAM sample with Advera

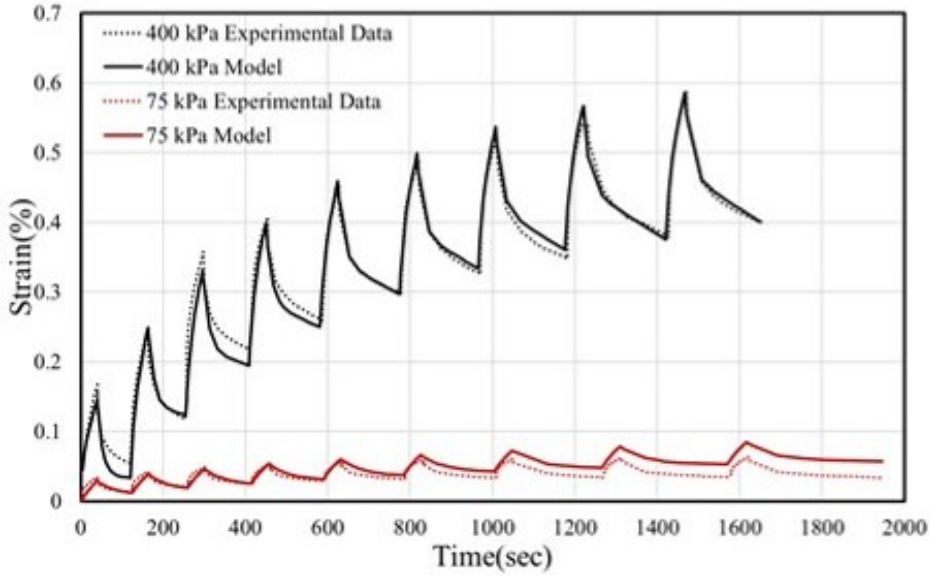

Figure 2.9: Nonlinear analysis at 400 kPa and verification of the model at 75 kPa for the WFAM sample with Sasobit

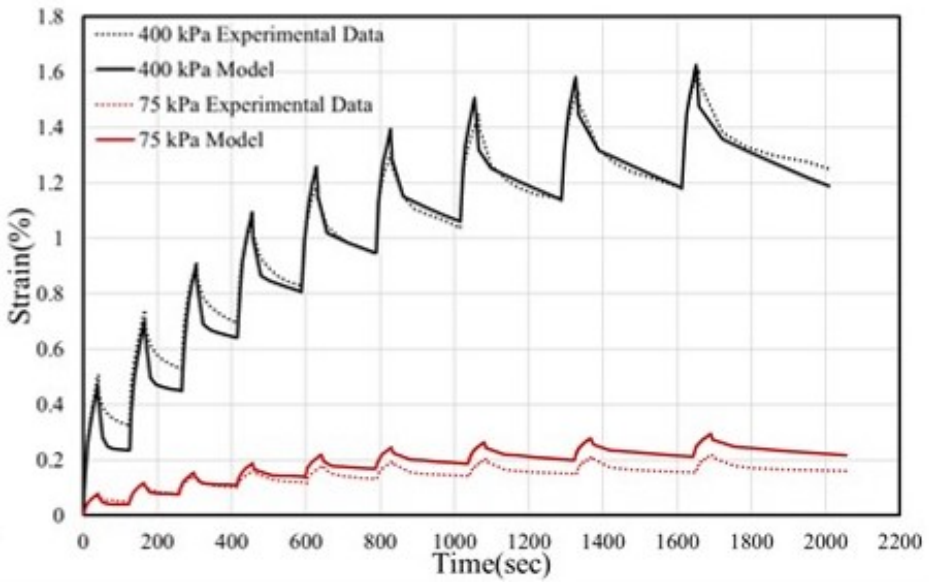

Figure 2.10: Nonlinear analysis at 400 kPa and verification of the model at 75 kPa for the WFAM sample with Rediset additives

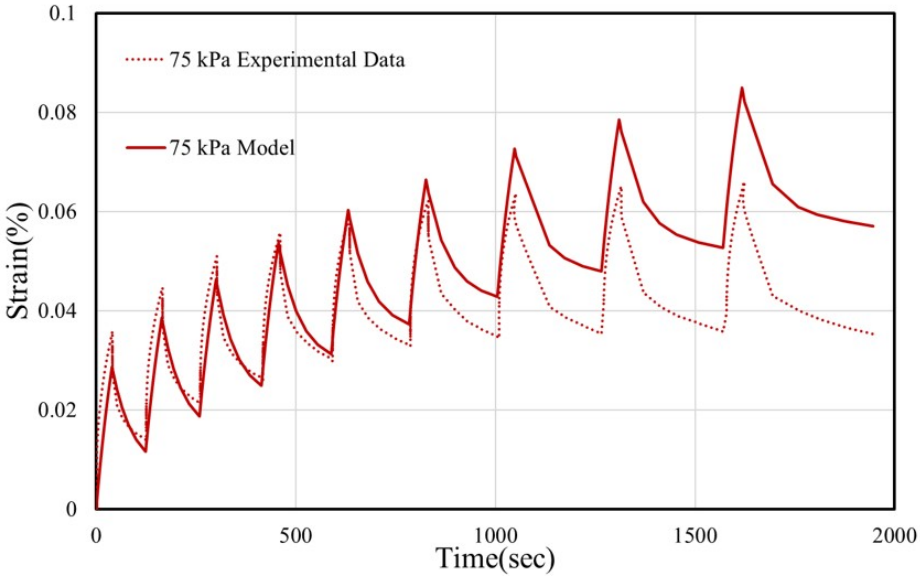

Figure 2.11: Model prediction and experimental data for WFAM sample with Sasobit

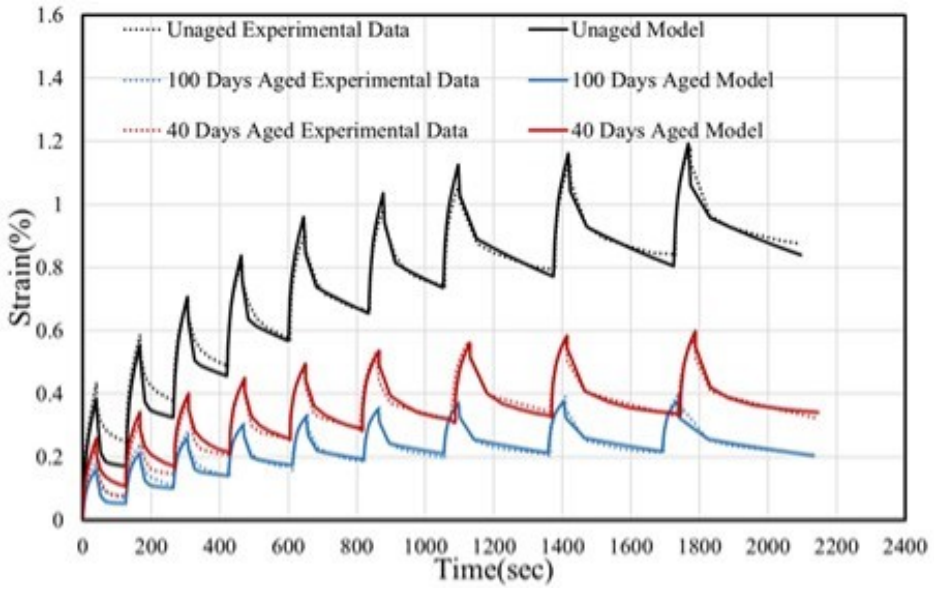

Figure 2.12: The effects of aging at 400 kPa for the control mixture

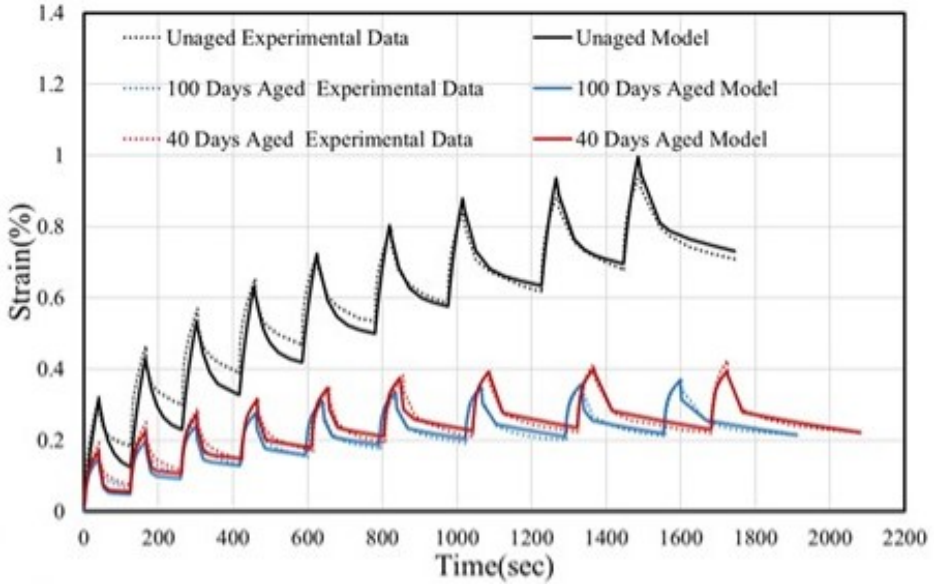

Figure 2.13: The effects of aging at 400 kPa for the WFAM sample with Advera

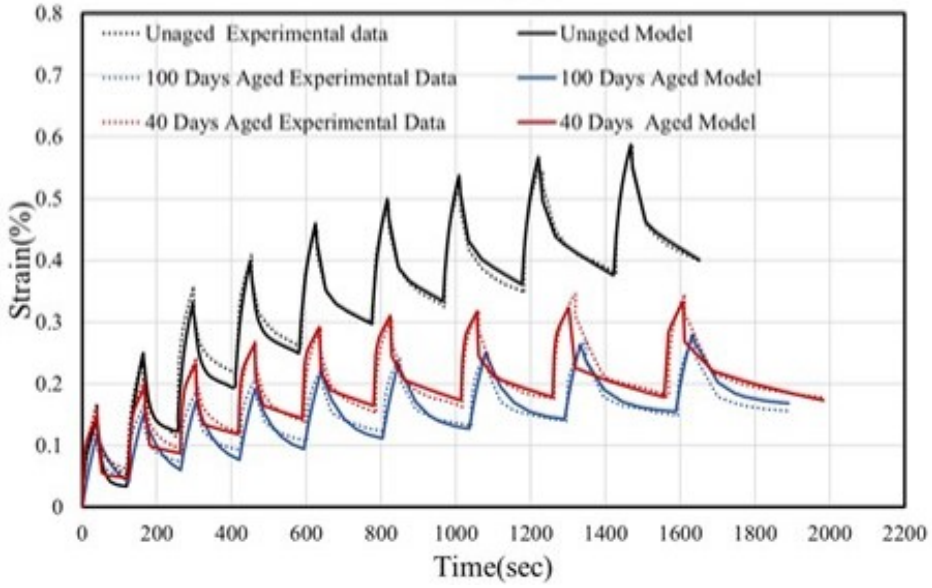

Figure 2.14: The effects of aging at 400 kPa for the WFAM sample with Sasobit

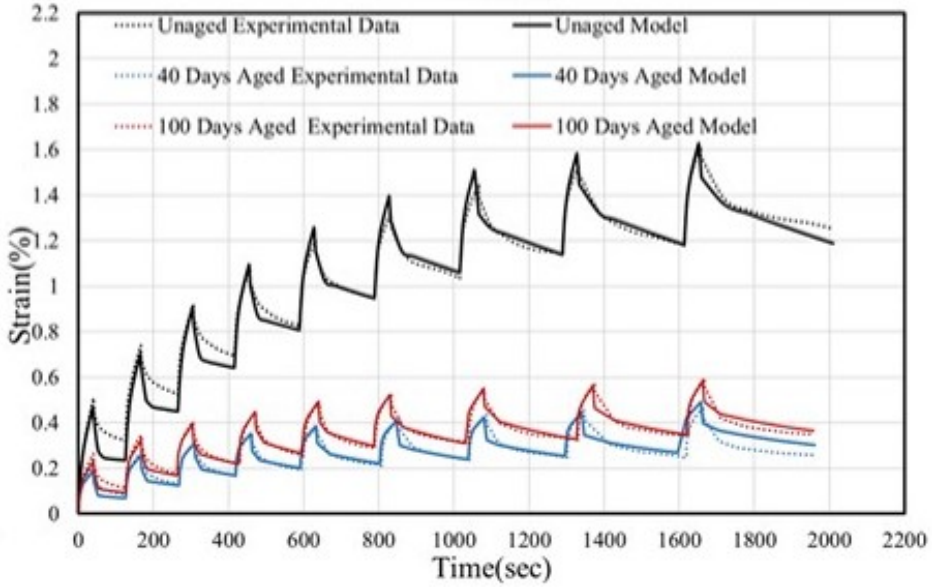

Figure 2.15: The effects of aging at 400 kPa for the WFAM sample with Rediset

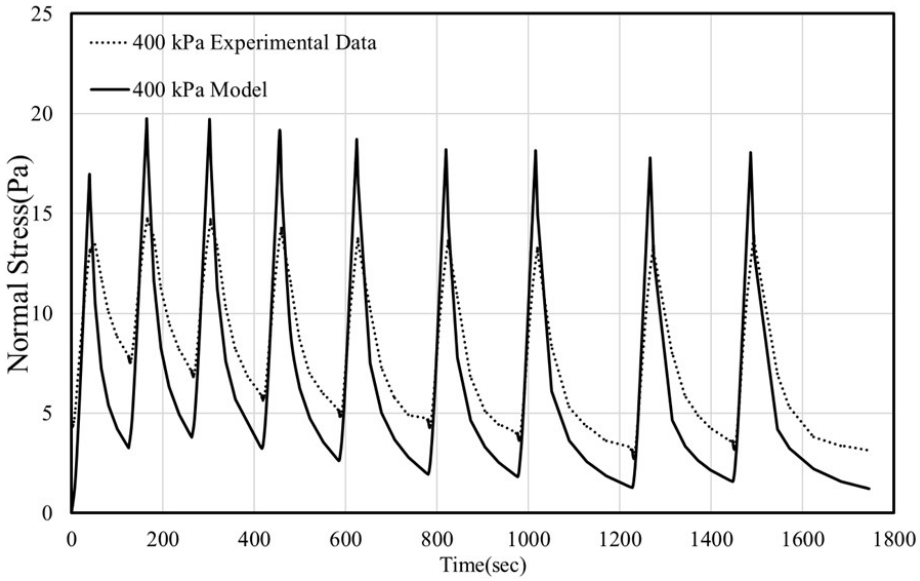

Figure 2.16: Normal stress vs time plot for WFAM sample with Advera additive at 400 kPa loading

The data obtained from repeated creep and recovery experiments were the stress (input) and the angle of rotation as function of time (output). The values of each of the parameters were restricted by an upper limit and a lower limit. The former to reduce the computational time and the latter was set to a value of zero to ensure non-negative values of the parameters. The parameters are then adjusted to minimize the scalar function $J(G_1, G_2, \mu_1, \mu_2, \mu_3)$. The obtained parameters are considered as the material parameters. If the fit is satisfactory, as shown in Table 2.1, the parameters from the higher stress condition (400 kPa) are then used to model the angle of rotation at the lower stress condition (75 kPa). The model was found to be effective for both stress levels, and the results are shown in Figures 2.7, 2.8, 2.9, and 2.10. The error percentage for the prediction of 75 kPa data by the model is calculated as

$$Error(\%) = \frac{|x_{mt} - xet|}{x_{et}} \times 100 \tag{2.42}$$

where x_{mt} and x_{et} are the modeling prediction and experimental value at time t, respectively.. The error percentages between the model prediction and experimental data at the end of the experiment for 75 kPa data are shown in Table 2.2. The error percentage values are high due to low strain values

obtained when the WFAM samples were subjected to a loading of 75 kPa and the accumulation of error with the progress of time as shown in Figure 2.11. As the model has not been formulated to consider the effect of aging, we carried out the analysis for each material subjected to different aging conditions separately as shown in Figures 2.12, 2.13, 2.15, and 2.15.

WFAM sample	R square values
Control mixture	0.93
WFAM samples with Advera	0.90
WFAM samples with Sasobit	0.92
WFAM samples with Rediset	0.91

Table 2.1: R square values of the nonlinear model at 400 kPa

WFAM sample	Error at the end of the test
Control mixture	40.01%
WFAM samples with Advera	62.5%
WFAM samples with Sasobit	61.7%
WFAM samples with Rediset	35%

Table 2.2: Error between the model and experimental data at the end of the test at 75 kPa

The data obtained from repeated creep and recovery experiments were the stress (input) and the angle of twist as function of time (output). The values of each of the parameters were restricted by an upper limit and a lower limit. The former to reduce the computational time and the latter was set to a value of zero to ensure non-negative values of the parameters. If the fit was satisfactory, the parameters from the higher stress condition (400kPa) were then used to model the angle of twist per unit length at the lower stress condition (75kPa). The model was found to be effective for both stress levels and the results are shown in Figures 2.7, 2.8, 2.9, and 2.10. As the model had not been

formulated to consider the effect of aging, we carried out the analysis for each material subjected to different aging conditions separately as shown in Figures 2.12, 2.13, 2.15, and 2.15.

We then used the obtained parameters to model the normal stress using equations 2.37-2.40. Although the model seems to under predict the normal force during loading cycles and over predict it during recovery cycles, qualitatively the normal force trend is captured quite well as shown in Figure 2.16

2.7 Identification of Responses of the Two Material Constituents

The mechanical behavior of asphalt mixtures depends on the microstructure. This material response is not only complex due to the random arrangement of aggregate and binder structures, but also due to structure changes when subjected to external stimuli. The randomness in the microstructure combined with the large difference in stiffness between asphalt binder and aggregate induce a wide range of strain distribution within the mixture [62]. Understanding the strain distribution is important as the binder response to small strain (linear regime) is very different from the binder response to large strain (nonlinear regime). Here, the assumption is that the individual material experiences stress proportional to its mass fraction. This is based on the assumption that the model considers the mixture to be single continua (i.e., both the materials are present at every single point), thus separating the material properties based on mass fraction is more sound and reliable. The nonlinear model then becomes

$$\mathbf{T} = \alpha\mathbf{T} + (1-\alpha)\mathbf{T} = -p\mathbf{I} + 2\mu_3\mathbf{D} + G_1\mathbf{B}^d_{\kappa_{p(t)_1}} + G_2\mathbf{B}^d_{\kappa_{p(t)_2}}, \tag{2.43}$$

$$\alpha\mathbf{T} = \mathbf{T}_1 = -p_1\mathbf{I} + 2\mu_3\alpha\mathbf{D} + G_1\mathbf{B}^d_{\kappa_{p(t)_1}}, \tag{2.44}$$

where

$$X^A = \alpha X \tag{2.45}$$

$$X^B = (1-\alpha)X \tag{2.46}$$

$$\check{\mathbf{B}}_{\kappa_{p(t)_i}} = \dot{\mathbf{B}}_{\kappa_{p(t)_i}} - \mathbf{L}\mathbf{B}_{\kappa_{p(t)_i}} - \mathbf{B}_{\kappa_{p(t)_i}}\mathbf{L}^T = -2\frac{G_i^j}{\mu_i}\mathbf{B}_{\kappa_{p(t)_i}}\mathbf{B}^d_{\kappa_{p(t)_1}} \tag{2.47}$$

where α is the mass fraction, j can be A or B, and i can be 1 or 2. The evolution of $\mathbf{B}_{\kappa_{p(t)_1}}$ and $\mathbf{B}_{\kappa_{p(t)_2}}$ are similar and their corresponding stress will be of the form

$$\dot{B}_{1\phi z} = \frac{r\dot{\Omega}}{h} B_{izz} + \frac{2G_1}{3\mu_1} B_{1\phi z}(B_{1rr} - 2B_{1\phi\phi} - 2B_{1zz}), \tag{2.48}$$

$$\dot{B}_{1rr} = \frac{2G_1}{3\mu_1} B_{1rr}(-2B_{1rr} + B_{1\phi\phi} + B_{1zz}), \tag{2.49}$$

$$\dot{B}_{1\phi\phi} = \frac{2G_1}{3\mu_1} B_{1\phi\phi}(+B_{1rr} - 2B_{1\phi\phi} + B_{1zz}) - \frac{2G_1}{\mu_1} B_{1\phi z}^2 + \frac{2r\dot{\Omega}}{h} B_{1\phi z}, \tag{2.50}$$

$$\dot{B}_1 zz = \frac{2G_1}{3\mu_1} B_{1zz}(+B_{1rr} + B_{1\phi\phi} - 2B_{1zz}) - \frac{2G_1}{\mu_1} B_{1\phi z}^2, \tag{2.51}$$

$$T_{1rr} = -p_1 + \frac{G_1}{3}(2B_{1rr} - B_{1\phi\phi} - B_{1zz}), \tag{2.52}$$

$$T_{1\phi\phi} = -p_1 + \frac{G_1}{3}(2B_{1\phi\phi} - B_{1rr} - B_{1zz}), \tag{2.53}$$

$$T_{1zz} = -p_1 + \frac{G_1}{3}(2B_{1zz} - B_{1rr} - B_{1\phi\phi}), \tag{2.54}$$

$$T_{1\phi z} = G_1(B_{1\phi z}) + \mu_3 \frac{r\dot{\Omega}}{h}. \tag{2.55}$$

Using the above equations, the initial value problem for the evolution of the B_1 and B_2 was solved and the obtained values were substituted to calculate the corresponding strains for each natural configuration (material). The model responses of each individual material are shown in Figure 2.17.

2.8 Summary and Conclusions

The aim of this work was to study the behavior of fine aggregate mixture samples when subjected to repeated creep and recovery loading. We used the nonlinear model proposed by Málek et al. [45] to model the shear strain and normal stress responses. This model can describe various creep and recovery conditions by considering internal structure changes that occur during loading and unloading. The unique contribution of this chapter is showing the response of individual constituents as the mixture responds to external stimuli.

The model presented can capture nonlinear behavior of materials experiencing different aging levels. Aging causes an increase in stiffness and viscosity of the material as can be seen in Figure 2.18. These materials can be differentiated based on the values and trends of the material parameters$(G_1, G_2, \mu_1, \mu_2, \mu_3)$ obtained from the curve-fitting approach. The following conclusion can be made based the obtained results:

- The dissipation parameter (μ_3) is responsible for the viscous behavior which is almost unaffected due to aging of the WFAM sample with Sasobit additive.
- Aging seems to have a greater effect on the energy storage mechanism (G_2) than the dissipation mechanism (μ_2). For instance, there seems to be a significant increase in G_1 and G_2 values between unaged samples and those aged 40 and 100 days. However, such significant increments not seen in the μ_2 value for control, Sasobit, and Avera samples from 40 to 100 days of aging.
- The strain experienced by the binder seems to be significantly higher when compared to the actual binder-aggregate interface.

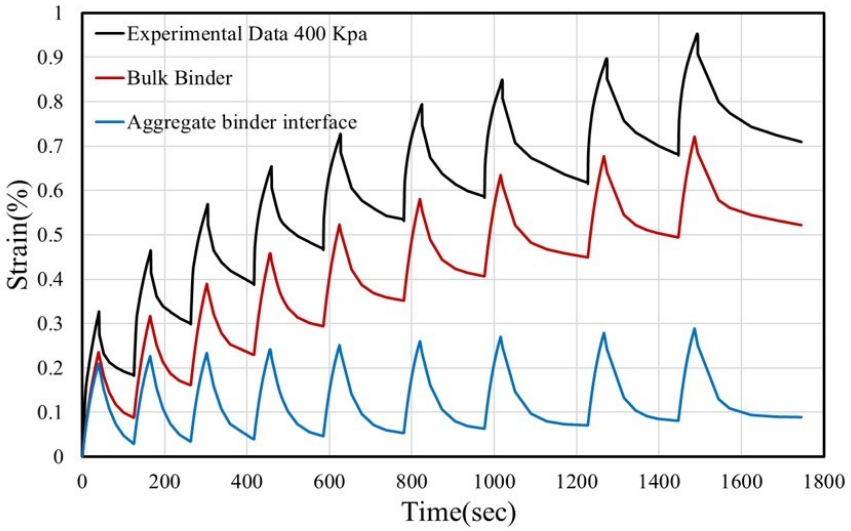

Figure 2.17: The strain response by individual constituents for the WFAM with Advera additive.

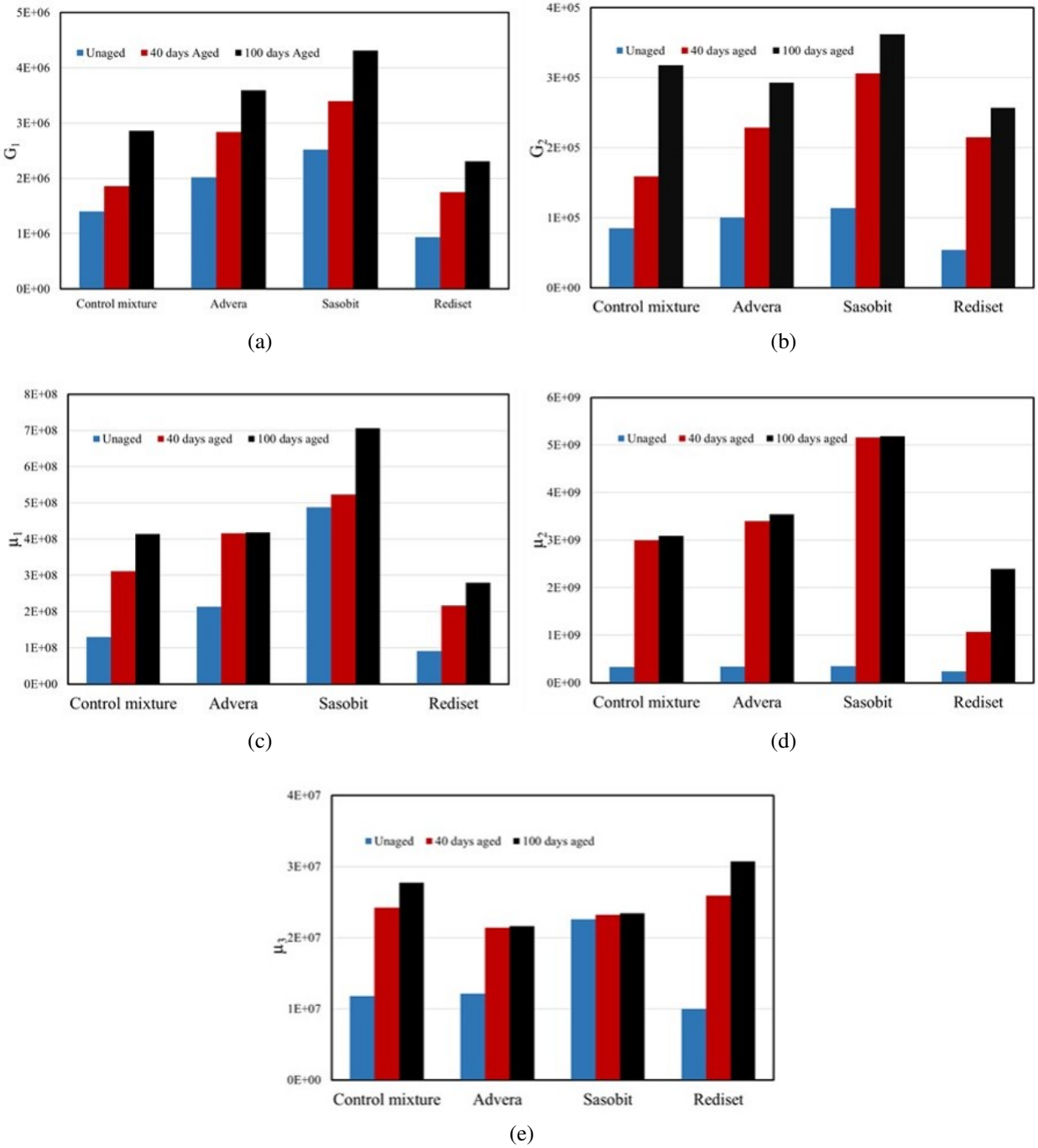

Figure 2.18: The variations of all the five parameters through the aging process.

3. ANALYSIS OF RECLAIMED ASPHALT BLENDED BINDERS USING LINEAR AND NONLINEAR VISCOELASTICITY FRAMEWORKS*

3.1 Overview

This chapter presents a comprehensive analysis of blended asphalt binders extracted from mixtures that contain various amounts of reclaimed asphalt pavements (RAP). The analysis is performed within a thermodynamically consistent nonlinear viscoelastic (NVE) modeling framework, which has the advantage of accounting for the contributions of each constituent (i.e., virgin binder and RAP binder) to the response of the blended binder.

To calibrate and validate the NVE model, we subjected RAP blended binders to different testing protocols: frequency sweep (FS), multiple stress creep and recovery (MSCR), repeated creep and recovery with multiple stress levels (RCRMS), random creep and recovery (RCR), and stress relaxation (SR). For the binders used in this study, linear viscoelasticity (LVE) was suitable to model the FS and MSCR data, but it did not capture the RCRMS results, which involved higher stress and strain levels. In contrast, the NVE model successfully described the RCRMS results. The validation was achieved by comparing the NVE model predictions with the RCR and SR test results. Lastly, this study recommends a new method based on NVE model parameters to evaluate the rutting resistance of blended asphalt binders.

3.2 Introduction

The increasing demand for asphalt materials and the depletion of natural resources (virgin aggregates and asphalt binder) have motivated the use of RAP in the construction of new pavements. Significant research has been conducted to determine RAP binder properties and their influence on the rheological properties of blended asphalt binders [63]–[66]. In recent times, rutting in the field

*This chapter is reprinted with permission from "B Vajipeyajula, KL Roja, E Masad, et al. “Analysis of reclaimed asphalt blended bindersusing linear and nonlinear viscoelasticity frameworks”. In:Materials and Structures53.5(2020), pp. 1–14."

has been quantified by analyzing the binders in the laboratory using several standard test protocols. The two test parameters typically used to quantify rutting are $G^*/sin\delta$ (G^* is the dynamic modulus and δ is the phase angle) measured using a dynamic test and J_{nr} (creep compliance) measured using the MSCR test [37], [67]–[69]. J_{nr} is the ratio of the non-recovered shear strain to the applied shear stress after applying a certain number of creep and recovery cycles. However, several studies have found several disagreements with observations made in the field and values obtained from standard experiments. For example, the studies conducted by Bahia et al. [33] and D'Angelo and Dongr [70] reported that the $G^*/sin\delta$ parameter ranked the rutting resistance of virgin binders, it did not correlate well with field observations of modified binders. For the J_{nr} value, several researchers have reported that the loading of 3.2 kPa in the MSCR test is not sufficient to capture the nonlinear behavior of asphalt binders, and the rest time of 9 seconds is also not long enough for the binder to recover completely [37]–[39], [71], [72].

Several approaches that utilize model parameters obtained from LVE analysis of RCR and SR have been proposed to rank rutting resistance of binders [73]–[75]. For example, Mangiafico et al. [76] used the normalized LVE cole-cole curves to compare the behavior of RAP blended binders with mixtures that incorporate these binders. However, LVE models are limited in considering the nonlinear responses of asphalt binders that are subjected to high strain levels in asphalt mixtures.

Recently, nonlinear approaches were used to predict the response of asphalt binders. Narayan et al. [77] and Nivitha et al. [78] proposed a rutting parameter that considers the nonlinear response of the binder. Masad et al. [25] developed an approach based on Schapery's theory [1] to capture the non-proportional response of an asphaltic material subjected to various range of creep loadings. Several other models were developed to capture the normal force generated during shearing of the asphaltic material and to better analyze transient and three-dimensional responses [16], [79]–[82]. Furthermore, Málek et al. [61] developed a thermodynamically compatible rate type fluid model to describe the behavior of asphalt binders subjected to various loading conditions. This framework can capture the nonlinear transient response and the normal force generated due to the shearing of asphalt binders. Vajipeyajula et al. [5] presented a NVE model that can be used to separate the

contributions of the constituent of a material to its overall response.

In this chapter, we evaluate rutting resistance of RAP blended binders by subjecting the blends to various standard and modified test protocols. We used LVE and NVE models to predict the response of RAP blended binders. This study mainly focused on capturing the contribution of individual constituents (virgin and RAP binder) to the overall material response using a thermodynamically developed NVE model.

3.3 Materials

This study used a base binder of Pen 60/70 (PG 64S-22) grade along with the RAP binder (PG 94E-0) extracted from roads in Qatar. Asphalt mixtures containing different proportions of RAP (0, 15, 25, 35, and 100% RAP) were then produced in the laboratory. The binders used in this study were extracted and recovered from these asphalt mixtures [83]. Because the focus of the study is on the response at high temperatures, the blended binders were subjected to short-term aging in a rolling thin film oven (ASTM: D-2872, 2004) prior to the tests discussed in the section . The properties of virgin and RAP binders are given in Table 4.3. More details about characteristics and properties of the RAP blended binders can be found in Roja et al. [20].

Table 3.1: Properties of virgin and RAP binders

Parameter	Virgin binder	RAP binder
Penetration(0.1 mm)	64	-
Specific gravity	1.032	-
Softening Point (^{o}C)	50	-
DSR G*/Sin(δ)(kPa)	1.30 at 64^oC	36.90 at 64^oC
DSR G*Sin(δ)(kPa)	4815 at 25^oC	21946 at 25^oC
BBR Stiffness(MPa)	161 at -12^oC	85 at 0^oC
BBR Slope	0.308 at -12^oC	0.300 at 0^oC

3.4 Experimental Measurements

In this study, binders were subjected to different experimental testing protocols using a dynamic shear rheometer with a 25 mm diameter parallel plate and a 1mm gap. We conducted the FS and MSCR tests were conducted to determine the suitability of the LVE and NVE models in fitting the data obtained from these standard tests. We used the RCRMS test to determine the parameters of the NVE model. We used the RCR and SR tests were used for NVE model validation. Each experiment was conducted twice to ensure repeatability. We found the error percentage to be within 6% , calculated as:

$$\text{Error}(\%) = \frac{\mid x_1 - x_2 \mid}{\text{Mean}} \times 100, \tag{3.1}$$

where x_1 and x_2 are the experimental measurements of trial 1 and 2 and Mean is the average of the two trials.

3.4.1 Frequency Sweep (FS)

We performed the FS tests using an oscillatory domain at temperatures of 45, 55, and 65^{o}C and subjected to a frequency range of 1 to 20 Hz at a rate of 1 Hz per second. At each temperature and frequency, the storage and loss moduli were recorded and presented as shown in Figure 3.1. From these values, we constructed the master curves using RHEA software [84] at a reference temperature of 64^{o}C. RHEA software follows a time-temperature superposition principle to shift the temperature isotherms and construct a master curve using the William-Landel-Ferry equation.

3.4.2 Multiple Stress Creep and Recovery (MSCR)

Each binder was tested using two different stress levels (0.1 kPa and 3.2 kPa). At each stress level, we carried out 10 loading and recovery cycles were carried out with 1 second creep loading time and 9 seconds recovery time [85].The non-recoverable creep compliance (J_{nr}) is calculated as the ratio of the average non-recoverable strain for the 10 cycles and the applied stress for those

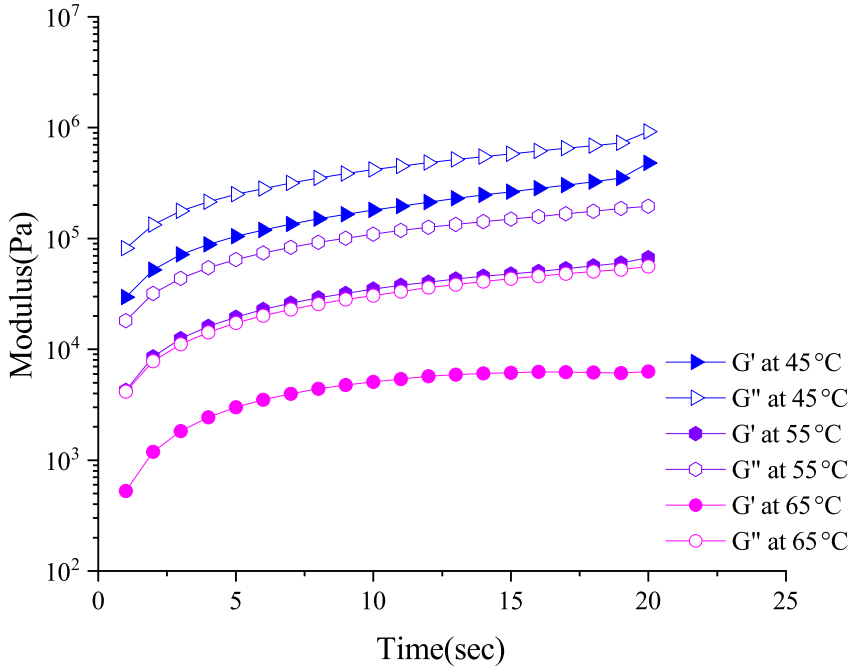

Figure 3.1: Variation of storage and loss moduli at different temperatures for a blended binder with 15% RAP

cycles, as shown in Equation 3.2:

$$J_{nr} = \frac{\sum_{i=1}^{n} \gamma_{ir} - \gamma_{io}}{\tau \times n}, \tag{3.2}$$

where γ_r and γ_o are the shear strain at the end and beginning of *i*th cycle respectively, n is the number of cycles for each stress level, and τ is the applied shear stress.

3.4.3 Repeated Creep and Recovery with Multiple Stress Levels (RCRMS)

Several researchers have reported that the loading of 3.2 kPa in the MSCR test is not sufficient to capture the nonlinear behavior of asphalt binders and the rest time of 9 seconds is also not long enough for binder to recover completely [37]–[39], [71], [72]. Therefore, several suggestions have been made to modify the MSCR protocol to include higher stress levels and varied recovery times [38], [39], [77]

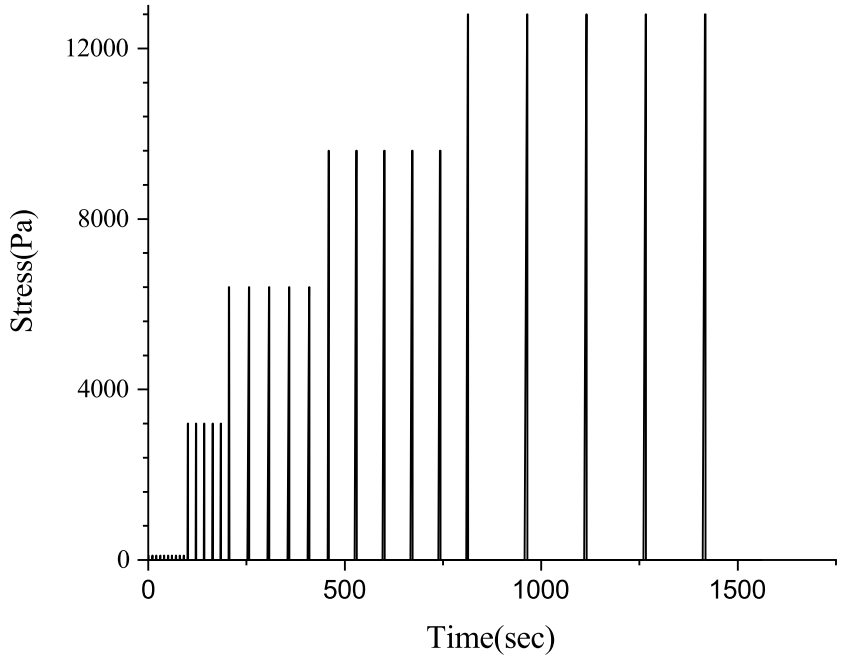

Figure 3.2: Ilustration of the loading protocol of the RCRMS loading protocol

In the RCRMS test, each binder was subjected to five different stress levels of 0.1, 3.2, 6.4, 9.6, and 12.8 kPa. At each stress level, five loading cycles were applied with a creep time of 1 second followed by varying rest periods. As shown in Figure 3.2, the selected rest periods for 0.1, 3.2, 6.4, 9.6, and 12.8 kPa were 9, 20, 50, 70, and 150 seconds, respectively. The first two stress levels were based on the standard MSCR protocol and the remaining three stress levels were selected in such a way that the linearity check (scaling and superposition) can be carried out from the obtained responses. We used the RCRMS test results to calibrate the NVE model and determine its parameters.

3.4.4 Random Creep and Recovery (RCR)

The RCR test subjected the asphalt binder to a random loading pattern in which the stress level varied within a range of 0.1 to 12.8 kPa. As shown in Figure 3.3, the creep loading time varied from 0.1 to 1 seconds and the recovery time distribution was from 1 to 10 seconds. A random

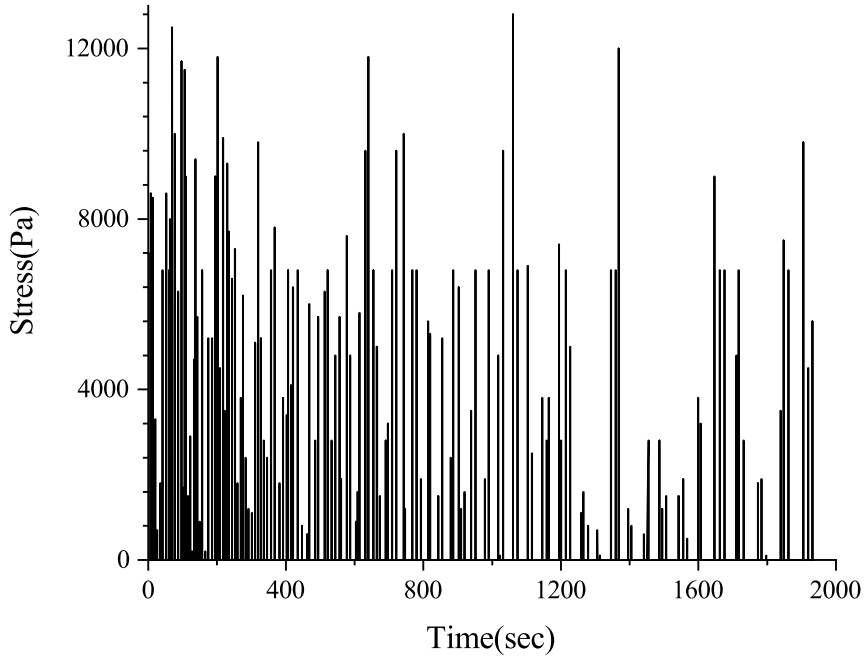

Figure 3.3: Example RCR test loading pattern

number generator function in Matlab [86] was used to generate the stress level, creep loading time, and recovery time values of each cycle. Various past researchers have used similar random loading protocols for model validation [87], [88]. In this study, the RCR data were used to validate the NVE model that was calibrated using the RCRMS test.

3.4.5 Stress Relaxation (SR)

The SR test involved applying a constant strain level while monitoring the stress needed to maintain the strain [78], [89]. This study conducted, five relaxation tests at strain levels of 30, 60, 100, 400, 600, and 800%. At each level, the ramp-up time for each strain increment was 0.1 second and each stress level was maintained constant for 600 seconds. As discussed later, this test was used for validation of the NVE model.

3.5 Linear Viscoelastic Modeling

3.5.1 LVE Modeling of FS Results

To capture the response of the binder over a wide range of frequencies, generalized LVE model was used with 9 Kelvin Voigt units and the Maxwell spring and dashpot elements connected in series. The storage (G') and loss $(G")$ moduli are related to the dynamic modulus $|G^*|$ and phase angle (δ) as shown in Equations 3.3 and 3.4,

$$G'(\omega) = |G^*(\omega)| \cos(\delta), \tag{3.3}$$

$$G"(\omega) = |G^*(\omega)| \sin(\delta). \tag{3.4}$$

The dynamic compliance (J^*) is determined as follows:

$$|J^*(\omega)| = \frac{1}{|G^*(\omega)|}. \tag{3.5}$$

Using the dynamic compliance and the corresponding phase angle at a reference temperature of 64^{o}C, one can obtain the storage compliance (J') and loss compliance (J''). The J' and J'' values can then be curve fitted using Equations 3.6 and 3.7 [90]:

$$J'(\omega) = J_M + \sum_{i=1}^{n} \frac{J_{k_i}}{(1 + \omega^2 \rho_{k_i}^2)}, \tag{3.6}$$

$$J''(\omega) = \frac{1}{\mu_M \omega} + \sum_{i=1}^{n} \frac{J_{k_i} \omega \rho_{k_i}}{(1 + \omega^2 \rho_{k_i}^2)}, \tag{3.7}$$

where ω is frequency, J_M is the instantaneous compliance, μ_M is the steady flow viscosity, ρ_{k_i} is the retardation time, and *n* is the number of the Kelvin Voigt elements. As shown in Figure 3.4, the generalized LVE model could predict the response of RAP blended binders. The model parameters obtained for 15% RAP binder are shown in Figure 3.4 .

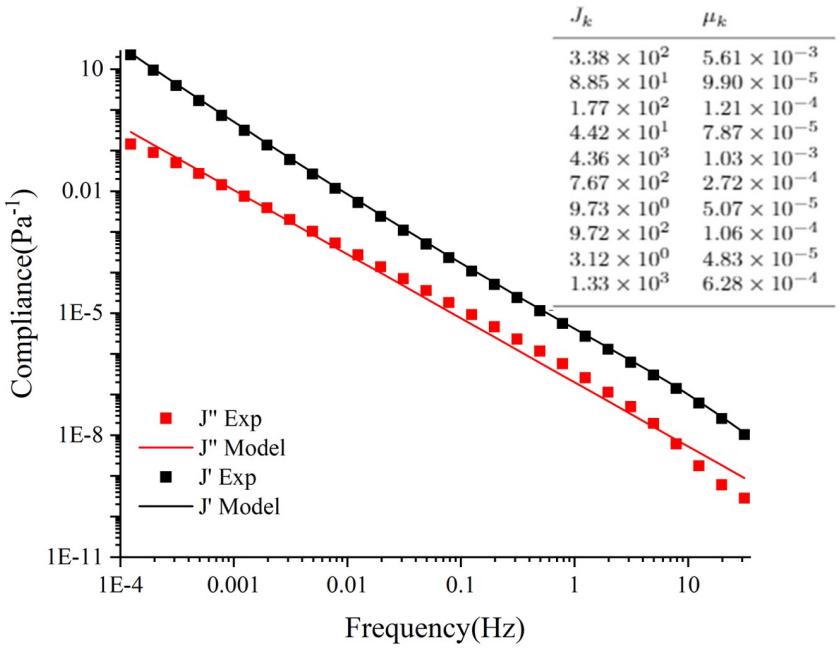

Figure 3.4: Analysis of the storage compliance and loss compliance using the generalized LVE model for 15% RAP binder at 64ºC with $J_M = 9.46 \times 10^4$ and $\mu_M = 5.68 \times 10^{-4}$.

3.5.2 LVE Modeling of MSCR Results

To evaluate the linearity of the MSCR test results, we modeled the strain response obtained from this test using the generalized model. Along with the parameters obtained from the curve fitting of the FS data, the response of the MSCR data was predicted as:

$$\epsilon_r(t) = \tau(J_M + \frac{t}{\mu_M}) + \sum_{i=1}^{n} \tau J_{k_i} \left(1 - e^{-\frac{t}{\rho_{k_i}}}\right) - \tau \left(J_M + \frac{(t - t_c)}{\mu_M}\right) - \sum_{i=1}^{n} \tau J_{k_i} \left(1 - e^{-\frac{(t-t_c)}{\rho_{k_i}}}\right), \tag{3.8}$$

where τ is the shear stress applied, ϵ is the strain, t is the time in seconds, t_c is the creep time, and $\frac{\tau}{\mu_M}$ is the instantaneous strain. The subscript c indicates creep and r indicates recovery. Figure 3.5 shows the model predictions of MSCR data.

3.5.3 LVE Modeling of RCRMS and RCR Results

We attempted to analyze the RCRMS and RCR test data with the generalized LVE model using the same set of parameters obtained from the FS and MSCR tests. As shown in Figure

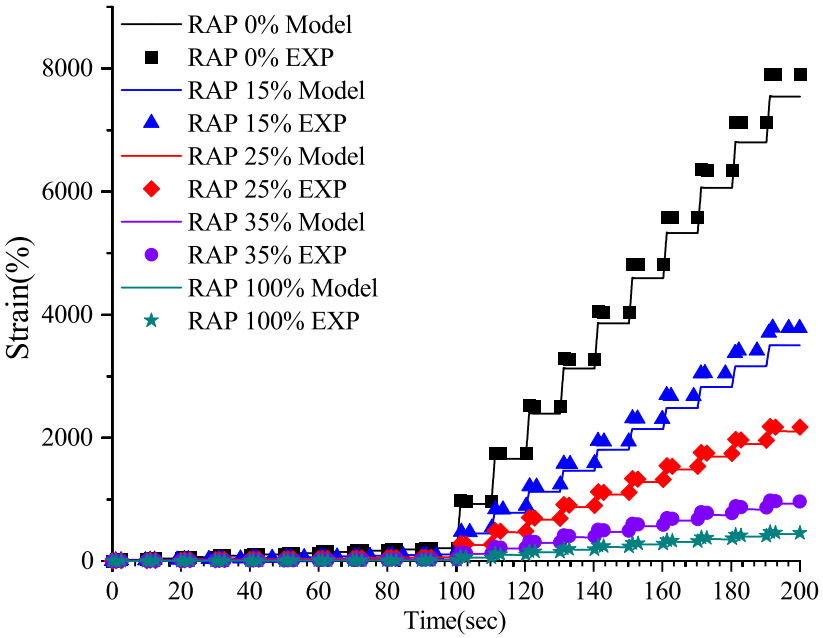

Figure 3.5: Analysis of the strain values from the MSCR test using the generalized LVE model at 64° C.

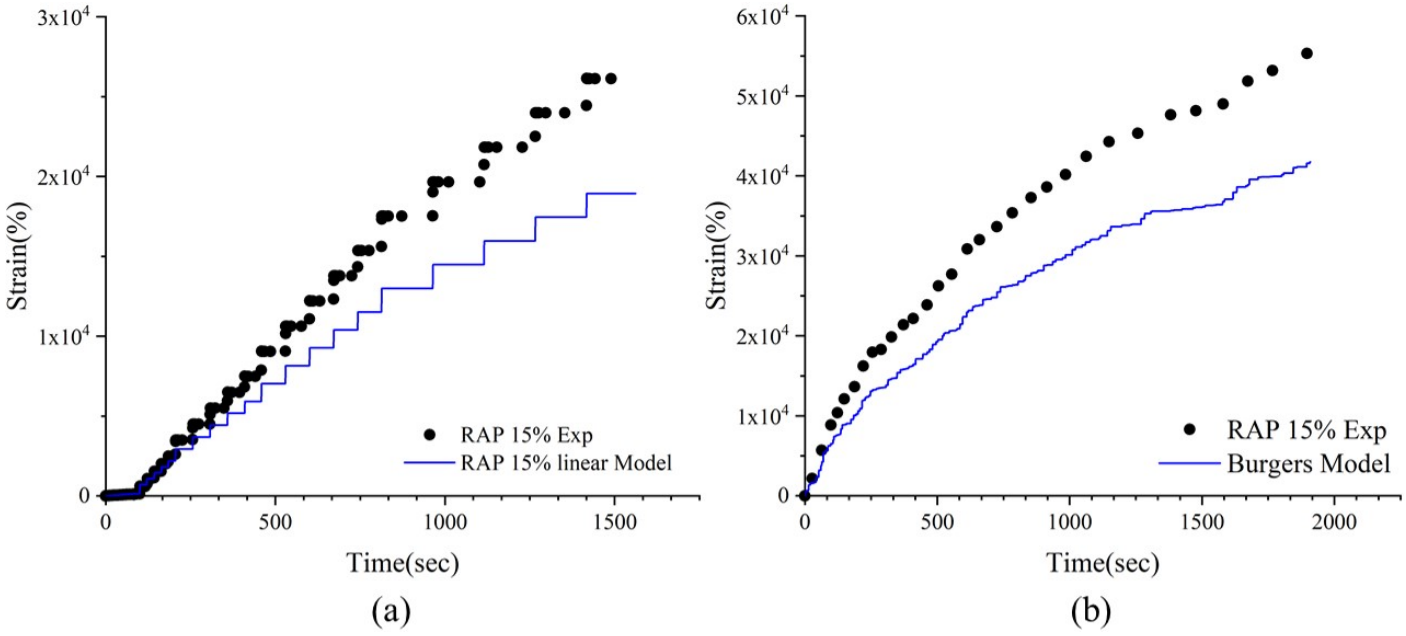

Figure 3.6: Comparison between the generalized LVE model and the RCRMS results (a); and the RCR results (b) for 15% RAP at 64^{o}C

3.6, the LVE model underpredicted the strain values obtained from the RCRMS and RCR tests. Specifically, there was a significant difference between experimental and model predicted values in the RCRMS test at higher loading conditions (greater than 3.2 kPa). Therefore, we conduct a nonlinearity check for the response of binders obtained from the RCRMS and RCR tests in section 3.6.

3.6 Nonlinearity Check of RCRMS and SR Data

Nonlinear behavior of asphalt binders when the stress or strain levels exceed certain threshold values is well documented[85]. The RCRMS tests evaluated nonlinearity by comparing the normalized strain (strain/torque) of the first cycle at different stress levels, as shown in Figure 3.7(a) for the case of 15% RAP at 64^{o}C. If the linear scaling of the normalised strain is not satisfied, the material response is considered to be nonlinear [91]. The binder response was found to be nonlinear at higher stress levels: $>$ 3.2 kPa for $0, 15, 25, and 35\%$ RAP blended binders, and $>$ 6.4 kPa for 100% RAP binder.

We evaluated the nonlinearity of the data obtained in the SR test by comparing the normalized

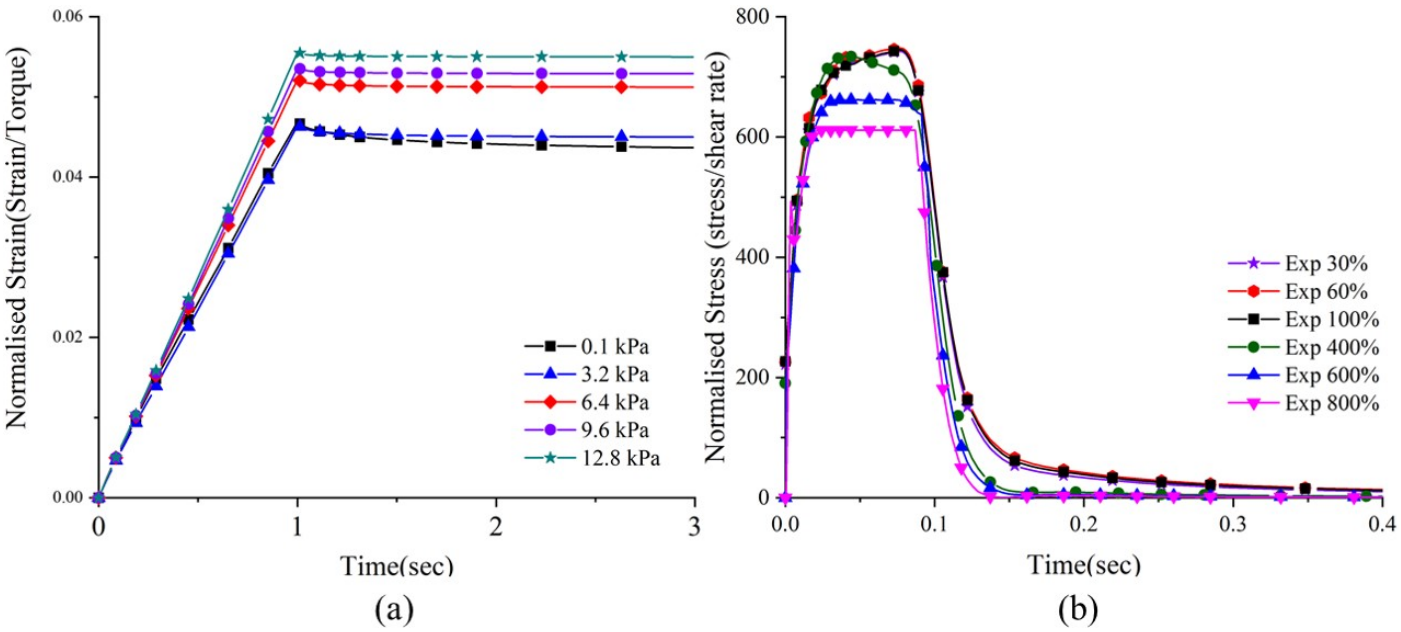

Figure 3.7: Normalized strain from RCRMS results (a) and normalized stress from SR results (b) for 15% RAP at 64^{o} C.

stress (stress/shear rate) for different strain levels as shown in Figure 3.7(b) for 15% RAP blended binder at 64^{o}C. The linear scaling was not satisfied when the binders were subjected to high strain levels of 600 and 800%. Hence, in the following sections, NVE model are determined using the RCRMS test results, and the NVE model parameters are validated using the RCR and SR data.

3.6.1 Model Calibration Using RCRMS Test Data

To simulate the binder behaviors obtained from various test protocols, this study adopted a semi-inverse method (i.e., the deformation or the velocity are assumed to be of a certain form) [5], [82]. In this case, the velocity was assumed to be

$$\mathbf{v} = (0, \frac{\dot{\Omega} r Z}{h}, 0) \tag{3.9}$$

where $\mathbf{v}$ is the velocity, $\dot{\Omega}$ is the angular velocity, Z is the vertical distance from the bottom plate, and h is the gap between two plates. Using the above velocity profile, the corresponding stress equations were derived by Málek et al. [61]. The data obtained from the RCRMS tests were curve

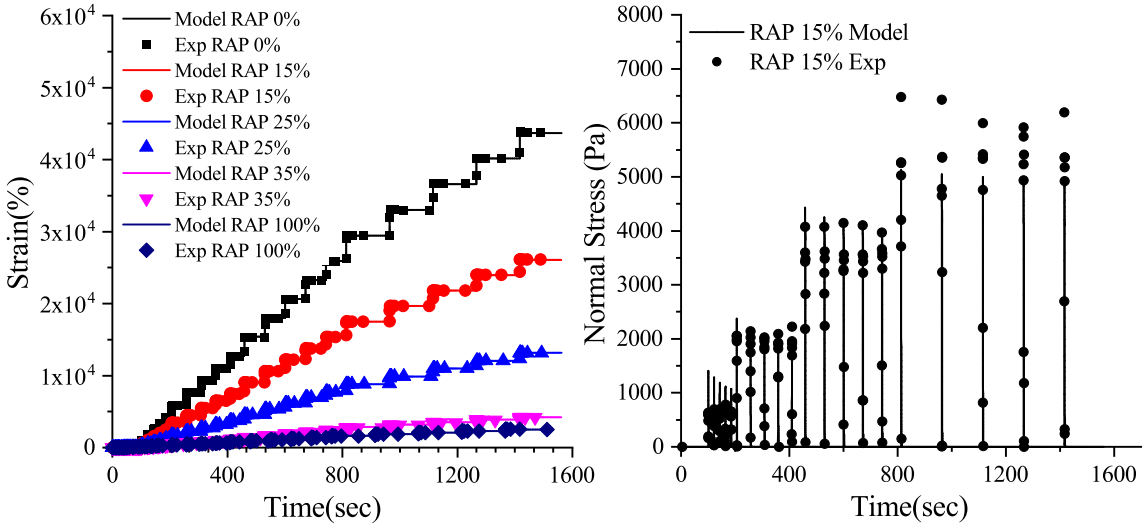

Figure 3.8: Analysis of strain and normal force values from the RCRMS experiments using non-linear modeling 64^oC

fitted with the nonlinear model using Matlab [86]. This was performed by defining a new error function:

$$\text{Er} = \sum_{i=1}^{N} \left[\frac{1}{max(S_e^i)} \left[\frac{\sum_{k=1}^{j} |S_e^i - S_m^i|^2}{j} \right] \right] + \sum_{i=1}^{N} \left[\frac{1}{max(F_e^i)} \left[\frac{\sum_{k=1}^{j} |F_e^i - F_m^i|^2}{j} \right] \right] \tag{3.10}$$

where N is the number of stress levels, S_e^i and F_e^i are the strain and normal force obtained from the experiment, respectively, S_m^i and F_m^i are the strain and the normal force obtained from the model calculations, respectively, and j is the total number of data points. This error function was then minimized to obtain the parameters. The values of each parameter were restricted by an upper limit and a lower limit. The obtained fits were able to satisfactorily capture both the shear and normal force responses for all binders, as shown in Figure 3.8.

The parameters obtained from the curve fitting of RCRMS data are shown in Figure 3.9. The shear modulus parameters (G_1, G_2) were found to increase gradually with the addition of RAP (Figure 4.9a, 4.9c), whereas the viscosity parameters (μ_1, μ_2, μ_3) gradually increased up to 25%

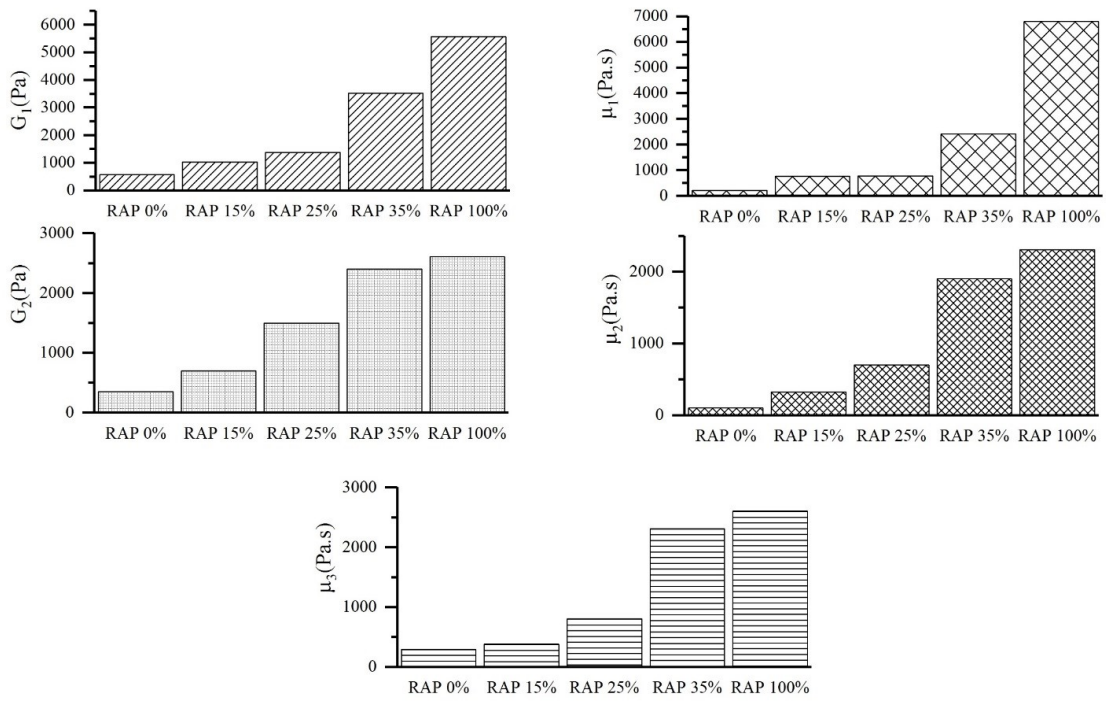

Figure 3.9: The five parameters of the nonlinear model for RAP binders

RAP, after which a rapid increment was seen. These model parameters are validated with RCRMS and SR test data in section 3.6.2.

3.6.2 Model Validation Using Random Creep and Recovery (RCR) and Stress Relaxation (SR) Test Data

The randomness in the loading history (both in the amount of load being applied and the transient condition in each cycle) makes the RCR test a good tool to validate the model's capabilities for predicting the material response. We used the NVE model described in Chapter 2 was used to predict the RCR response of binders, as shown in Figure 3.10. These results show that the model fits the RCR data quite well.

The SR experiment subjected the binders to a constant strain rate for 0.1 seconds to allow the strain to reach a predetermined value, after which the strain is kept constant, allowing the stress to

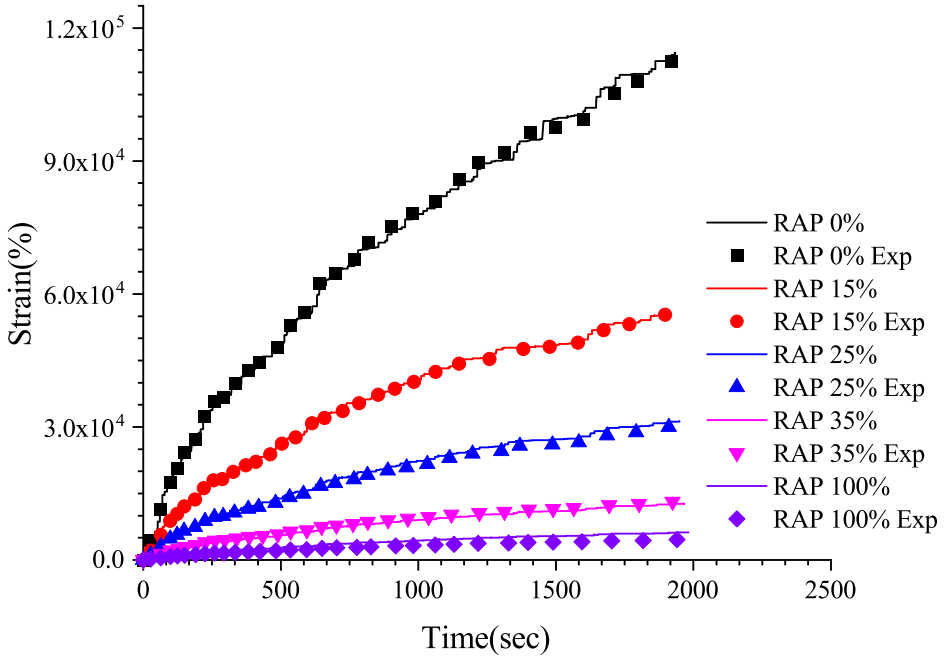

Figure 3.10: Nonlinear model validation using RCR test data.

relax. The shear rate is related to the angle of twist, expressed as: 3.11,

$$\dot{\epsilon} = \frac{r\dot{\Omega}}{h}, \tag{3.11}$$

where $\dot{\epsilon}$ is the shear rate, r is the radius, $\dot{\Omega}$ is the angular velocity, and h is the gap between two plates. The calculated angle of twist at a given time is then substituted in Equations 2.14 and 2.15 to solve for the shear stress using the ODE45' equation solver in Matlab [86]. We used the parameters obtained from the RCRMS test to model the response of stress relaxation tests, as shown in Figure 3.11. The model could predict binder response when subjected to stress relaxation to a great extent.

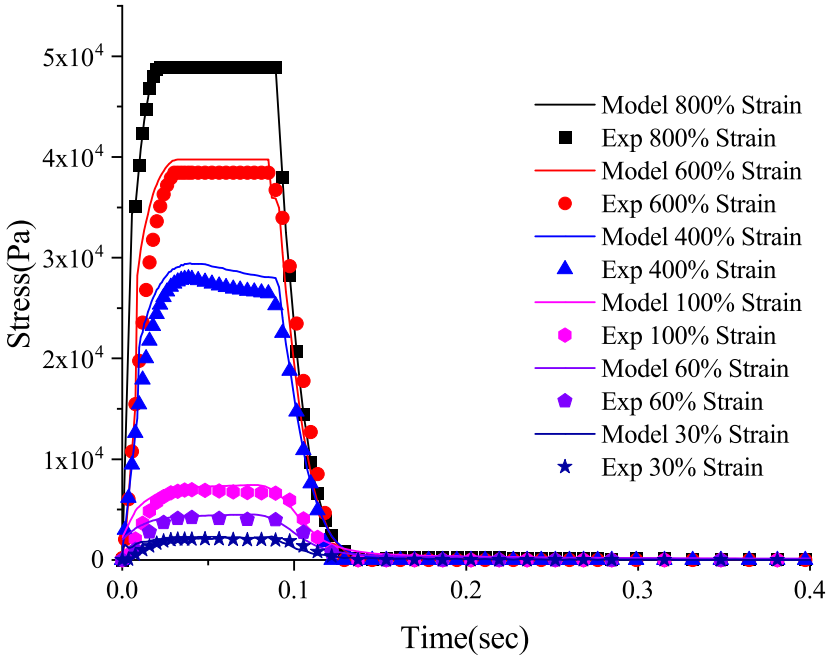

Figure 3.11: Nonlinear model validation using SR data of 15% RAP binder.

3.7 Separation of Material Response

Considering the multiconstituent nature of the RAP blended binder, it is beneficial to understand the contribution of the individual constituents (virgin binder and RAP binder) on the behavior of the blended binder. This would help to improve the design and use of high RAP mixtures. The parameters obtained from curve fitting of RCRMS data were substituted into equations 2.43-2.47, and the response of each material is shown in Figure 3.12.

From Figure 3.12, it can be inferred that the strain experienced by the virgin binder is significantly higher than the strain experienced by the RAP binder in a 15% RAP blend, which makes sense as the major component in the blend was virgin binder.

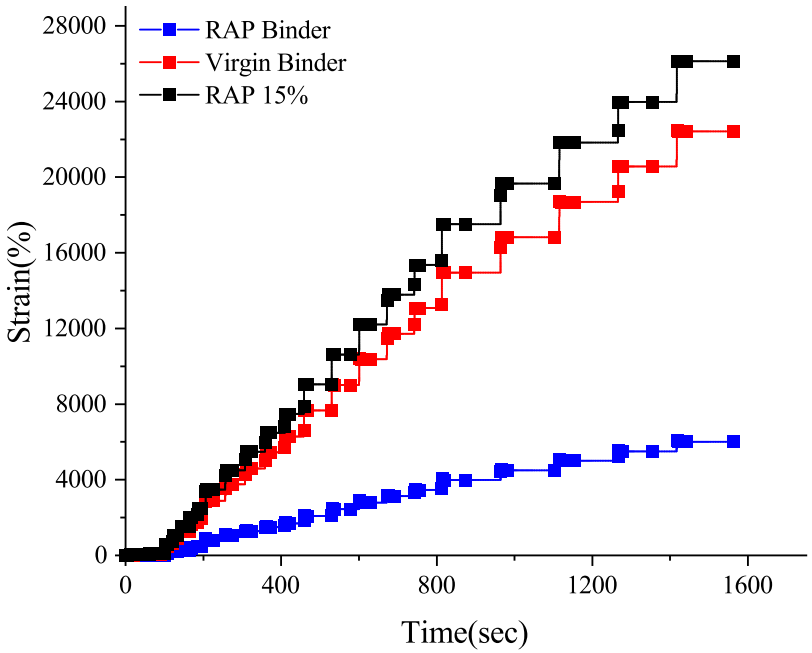

Figure 3.12: Strain response of individual constituents in 15% RAP binder.

3.8 Understanding the Effect of Adding RAP on the Permanent Deformation

We evaluated the J_{nr} value obtained from the MSCR and RCRMS tests and the viscosity parameters obtained from the nonlinear modeling of RCRMS test data for their ability to describe the resistance to permanent deformation. Figure 3.13 shows the normalized J_{nr} value obtained from the MSCR and RCRMS test data at a 3.2 kPa stress level. These values were normalized with respect to the J_{nr} of 0% RAP. For the MSCR test, the J_{nr} values were almost unchanged up to the addition of 25% RAP. However, there was a sharp drop in the J_{nr} value in the RCRMS test with the addition of RAP. The differences in the trends of J_{nr} values between these two tests are attributed to applying different stress levels (i.e., nonlinear responses of the binders), and are also due to differences in the recovery times. Because the binders were not allowed to recover completely in the MSCR test, higher J_{nr} values were obtained from the irrecoverable strain. The dependence of the J_{nr} values on the loading magnitude and recovery time is a clear indication of the nonlinear

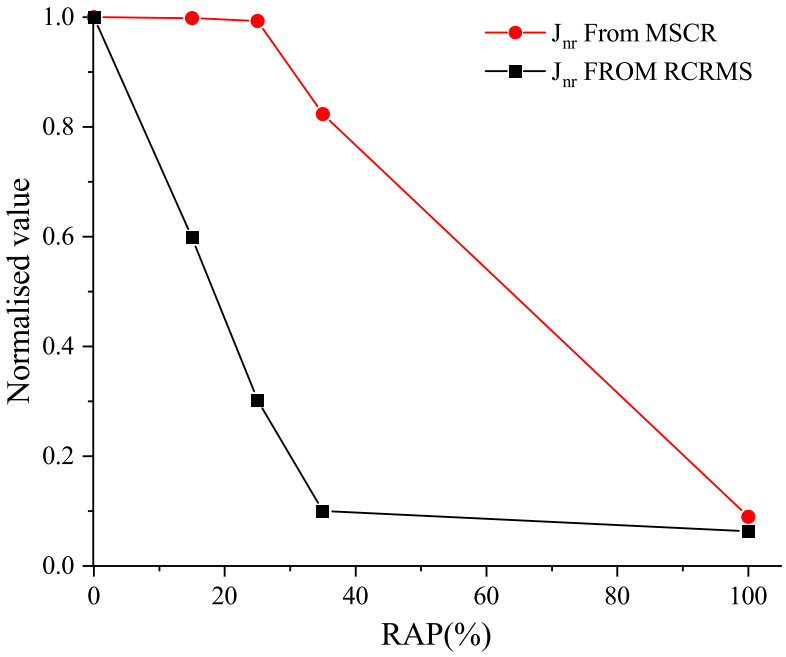

Figure 3.13: Comparison of normalized J_{nr} at 3.2kPa

behavior of binders and the need to change the MSCR test to account for this nonlinearity.

The striking dependence of J_{nr} on recovery time and creep loading demands a new parameter to quantify rutting. Narayan et al. [77] recommended using the apparent viscosity parameter derived from NVE models. Their study defined, the apparent viscosity as the ratio of the stress applied during creep to the steady state strain rate aexpressed as:

$$\eta(\tau) = \frac{\tau}{\dot{\epsilon}}, \tag{3.12}$$

where η is the apparent viscosity, τ is the shear stress, and $\dot{\epsilon}$ is the steady state strain rate. To analyze the effects of shear loading, we calculated apparent viscosity values for stress levels ranging from 1 to 10^7 Pa using the parameters obtained from the RCRMS test. Figure 3.14 shows the apparent viscosity curves of all the binders.

Unlike J_{nr}, the viscosity trends are obtained from the analysis of the complete data, and are

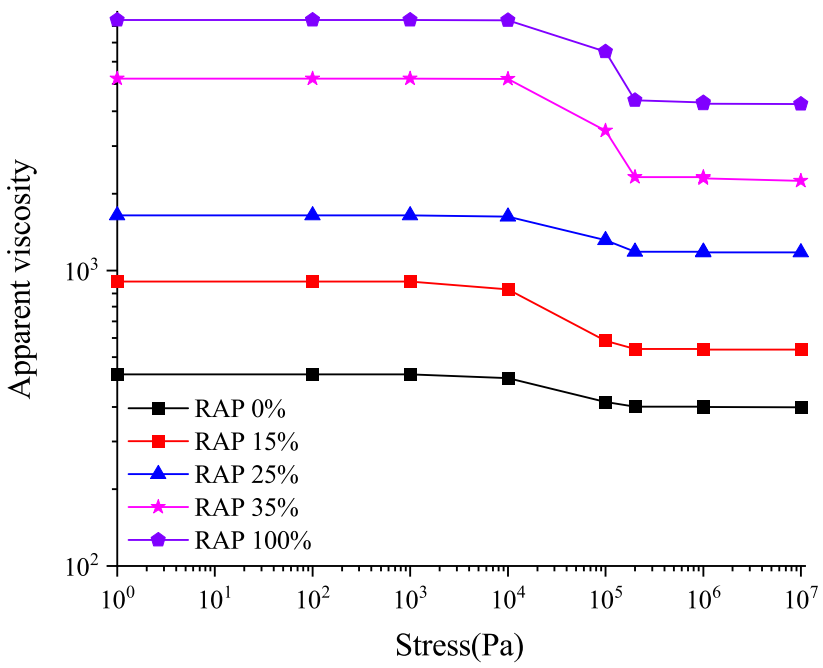

Figure 3.14: Apparent viscosity for the all the binders

found to be independent of recovery time. In addition, this apparent viscosity accounts for the non-linearity of RAP blend binder response and is the best parameter to assess permanent deformation. Therefore, in this study, we suggested using viscoelastic model parameters rather than J_{nr} values to assess permanent deformation trends.

3.9 Conclusions

This study aims to analyze the effects of adding RAP content on the rutting resistance of asphalt binders. This investigation was carried out on binders with different RAP proportions (0, 15, 25, 35, and 100%). These binders were subjected to FS, MSCR, RCRMS, RCR, and SR protocols. The FS and MSCR data were modeled successfully using a generalized LVE model for loadings of up to 3.2 kPa. The data obtained from RCRMS and SR tests were found to follow nonlinear behavior. Hence, we used a thermodynamically consistent NVE model derived by Málek et al. [61] to model the data obtained from the RCRMS test. We then validated the obtained model parameters by

capturing the response of RCR and SR protocols. The nonlinear model could predict the results of all the test protocols well.

Using the nonlinear model parameters, apparent viscosities were calculated as indicators of the rutting resistance of RAP blended binders. We also used the NVE model to predict the contribution of individual materials towards the response of RAP blended binders. The following conclusions can be drawn from the results:

- Because the binders were not allowed to recover completely in the standard MSCR test, the J_{nr} values measured from the irrecoverable strain may not represent the actual behavior of binders. The mismatch in J_{nr} values obtained from MSCR and RCRMS is a clear indication of the need to modify the standard MSCR protocol.

- The stiffness and viscosity of RAP blends increased gradually with the addition of RAP when the binder behavior is nonlinear. When the binder behavior is linear, rapid increments in stiffness and viscosity values were observed after adding 25% of RAP.

- It is recommended to use apparent viscosity rather than the J_{nr} values to assess the rutting resistance of binders. Apparent viscosity is derived from the NVE response of binders, whereas the traditional J_{nr} value is calculated assuming a LVE response in a creep and recovery cycle.

- The procedure of separating blended binder responses based on the contributions of their constituents (virgin binder and RAP) is useful to optimize the use of RAP and improve performance.

4. EFFECT OF CONFINEMENT PRESSURE ON THE NONLINEAR VISCOELASTIC RESPONSE OF ASPHALT MIXTURES

4.1 Overview

The goal of this study is to develop a constitutive model capable of accounting for the effects of confinement pressure on the response of asphalt mixtures, while also accounting for microstructure changes as the material deforms. The model used in this study considers the compressibility of the mixtures. The model is developed within a Gibbs-potential-based thermodynamic framework utilizing the notion of multiple natural configurations. Functional forms of the Gibbs potential and the dissipation rate were assumed to obtain the constitutive model. We evaluated model efficacy by corroborating with the results of experiments on asphalt mixtures at four different confinement pressures and two different temperatures. The asphalt mixture samples were subjected to cyclic creep and recovery loading at 40 and 55° C at different confinement levels [6]–[9]. It is shown that confinement pressure and the temperature significantly affect the nonlinear viscoelastic response of asphalt mixture materials. As such, one can use this model to simulate the actual loading conditions experienced by asphalt pavements in the field, as the model can simulate multi-axial loading conditions.

4.2 Introduction

Asphalt mixture is a complex material consisting of aggregates, asphalt binder, and air voids. The complex microstructure of asphalt mixtures and stiffness moduli differences between asphalt mixture consitutients induces large localized strains. These large strains contribute to the nonlinear viscoelastic response of the binder, which in turn contributes to the overall nonlinear viscoelastic response of the asphalt mixture.

When the asphalt pavement is laid down in the field it contains air voids, which causes a change in density and shearing. Mathruswamy et al. [92] reported that when subjected to constant hydrostatic pressures, asphalt mixtures exhibited densification depending on the magnitude of hy-

drostatic pressures. This in turn causes rearrangement of the microstructure. As has been noted by Krishnan and Rajagopal [11] and Masad et al. [12], the deformation resistance in asphalt mixtures is mainly derived from stiff aggregate, and viscous asphalt binders, and the way they interact with each other (i.e., microstructure). Microstructure changes due to mechanical changes such as reduction of the air voids or chemical changes such as aging of asphalt cause the material response to external stimuli to change. This also affects the mixture's ability to recover and stress relax upon load removal or keeping the strain constant, which in turn changes the material's resistance to rutting, fatigue damage, and other forms of damage.

Only a few researchers have analyzed the effects of confinement [6], [42], [43]. These studies found that the responses of asphalt mixtures varied greatly with the increase in effects of confinement pressure (e.g., material and stiffness and viscosity increased with the increase in confinement pressure). The traditional models currently being used to model the effects of confinement pressure determine a new set of parameters for each confinement pressure. This is extremely tedious, as one must determine a new set of parameters for every small change in confinement pressure. These models also do not consider the multiaxial loading conditions as they usually model the loading as uniaxial, which is far from the realistic loading conditions. The models also do not consider the evolution of microstructure as the material deforms, which is known to significantly affect material response.

Rajagopal and Srinivasa [17] developed a framework appealing to the concept of maximizing the rate of dissipation. This framework recognizes material microstructure changes through the changes in the material's natural configuration. A similar framework was later used by several studies([45], [50], [89], [93]–[95]), and has shown great promise in capturing complex asphaltic material response such as rutting, compaction under rolling action, and nonlinear shear flow.

In this chapter, a model considering confinement pressure's effects on asphalt mixtures is developed within a thermodynamic framework appealing to the notion of the body existing in multiple natural configurations and treating the material as a continuum. This model has been developed primarily to capture the non-proportional and multiaxial response of asphalt mixtures. The ma-

terial also shows a clear sensitivity to the interaction between temperature and confinement (as shown in section 4.3). In light of this, these aspects of the complex mechanical behavior of the asphalt mixtures were also considered during model development.

4.3 Experimental Data

The data presented in the chapter were collected by the Asphalt Research Consortium at Texas A&M University [6]–[9].

Cylindrical specimens were prepared in the laboratory using a Superpave Gyratory Compactor, which was used to compact 15.2 cm diameter by 17.8 cm height specimens. The prepared specimens were then cored and cut to 10 cm diameter by 15.2 cm height. The average percent air voids of the test specimens as 7.0 ± 0.5%. Limestone aggregate and binder PG 67-22 were used to prepare the test specimens.

The samples were subjected to repeated creep and recovery loading with a creep time of 0.4 seconds, with a ramp-up time of 0.05 seconds, creep loading of 0.35 seconds, and a recovery time of 30 seconds [6]. Each loading block included eight creep recovery cycles with increasing axial stresses. This test was conducted in compression at two different temperatures (i.e., 40^o C and 55^o C) and four confinement levels (i.e., $0, 70, 140, and 380$ kPa), which were kept constant during the test. The axial stresses for the first cycle was chosen to be 140 kPa and the axial stress for each subsequent cycle was ensured to be 1.2 times the axial stress of the preceding cycle. Each block contains eight creep and recovery cycles. The first axial stress level for the next block is the same as the third stress level in the previous block as shown in Figure 4.2. The specimens were attached with three axial and three radial LVDT's to measure the axial and radial strains during the test as shown in Figure 4.1. The specimens were conditioned for 2 hours at the confinement pressure before any axial loading was applied.

The analysis results of the repeated creep and recovery test at different confinement levels show that the mixture response depends on the current pressure being applied on the materials, as shown in Figure 4.3. The effect of temperature on the material's mechanical response was as expected. At higher temperatures, the accumulated strain was considerably higher than at lower temperatures, as

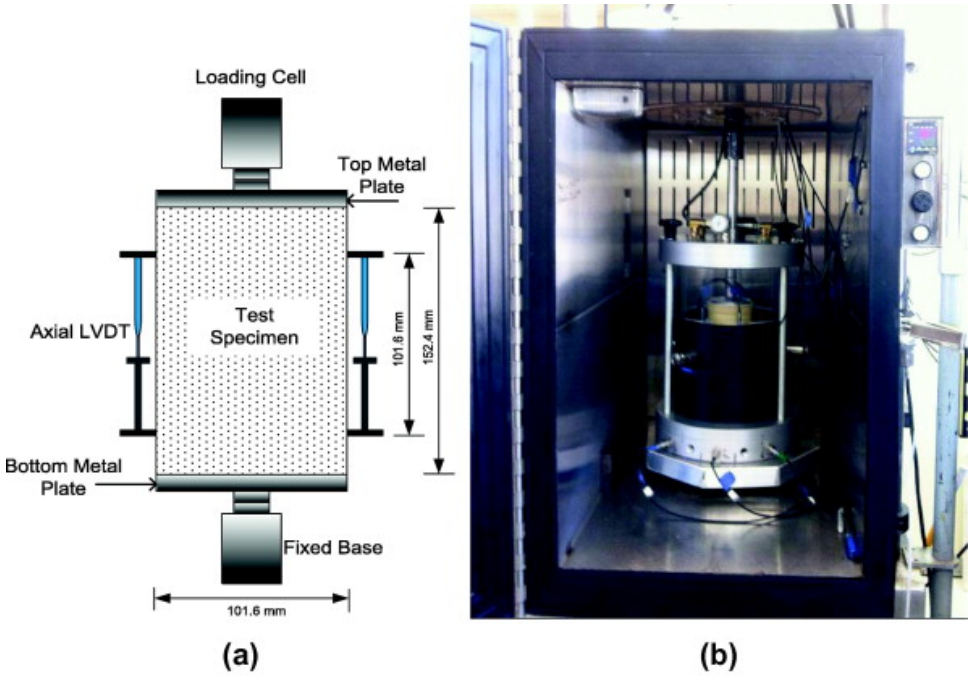

Figure 4.1: Experimental testing setup. (a) Schematic view of test specimen with mounted axial LVDTs. (b) Tri-axial cell equipped with radial LVDTs inside environmental chamber. Reprinted with permission from [6]

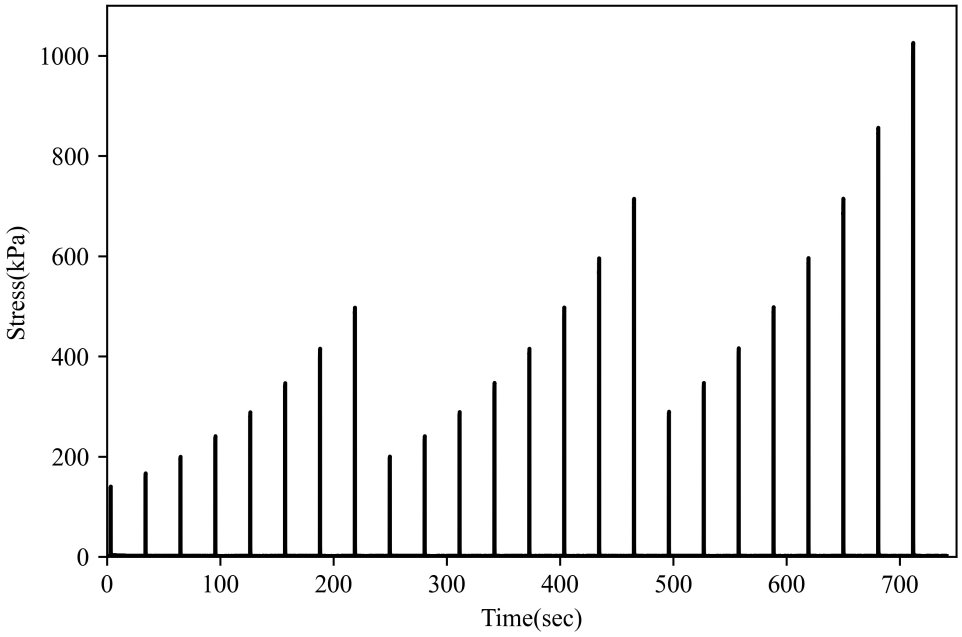

Figure 4.2: Schematic experimental test protocol. Reprinted with permission from [6]

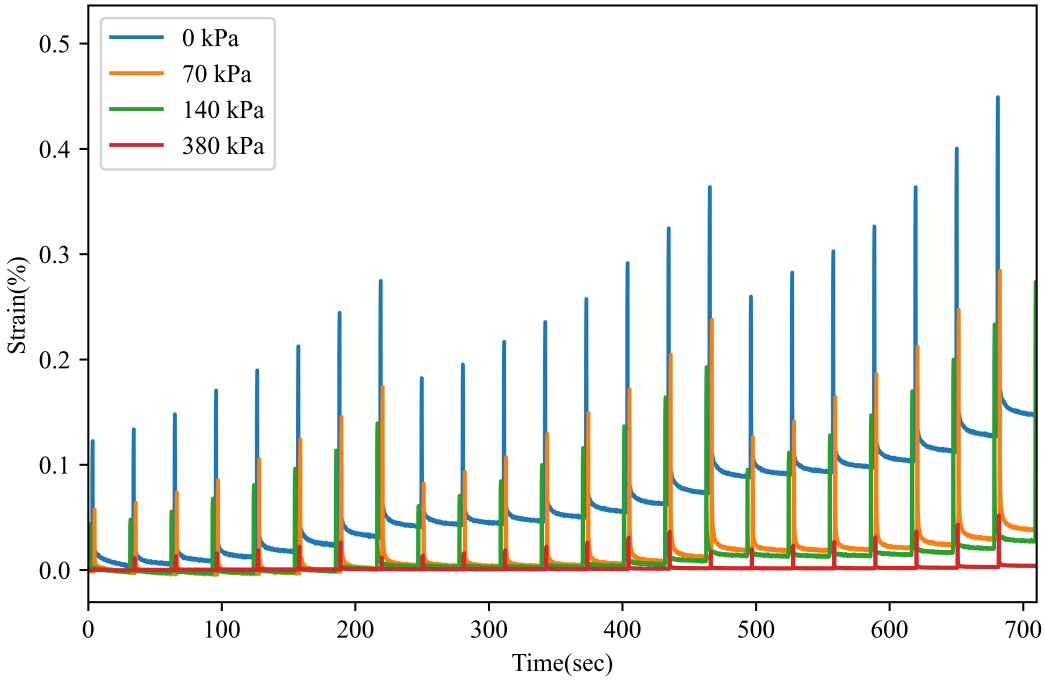

Figure 4.3: Axial strain response of asphalt mixtures when subjected to various confinement pressures

shown in Figure 4.4. This is a clear indicator that the material parameters are a function of current multi-axial stresses acting on the material. This requires an implicit compressible viscoelastic model.

4.3.1 Linearity Check

Because of its complex composition, asphalt mixtures tend to display a nonlinear response even when subjected to small strains. Hence, we performed a nonlinearity check by comparing the normalized strain (strain/applied stress) for various stress levels in the first block when the mixtures were subjected to a 0 kPa confinement pressure. If the linear scaling of the normalized strain is not satisfied, the material response is considered to be nonlinear. The mixture response was found to be nonlinear at stress levels greater than 165 kPa as shown in Figure 4.5

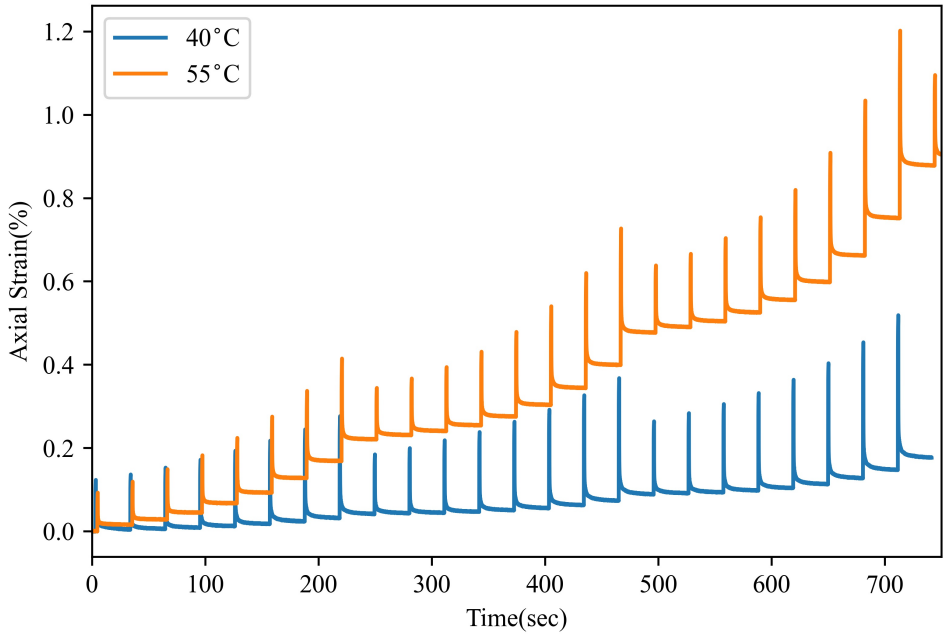

Figure 4.4: Axial strain response of asphalt mixtures when subjected to different temperatures

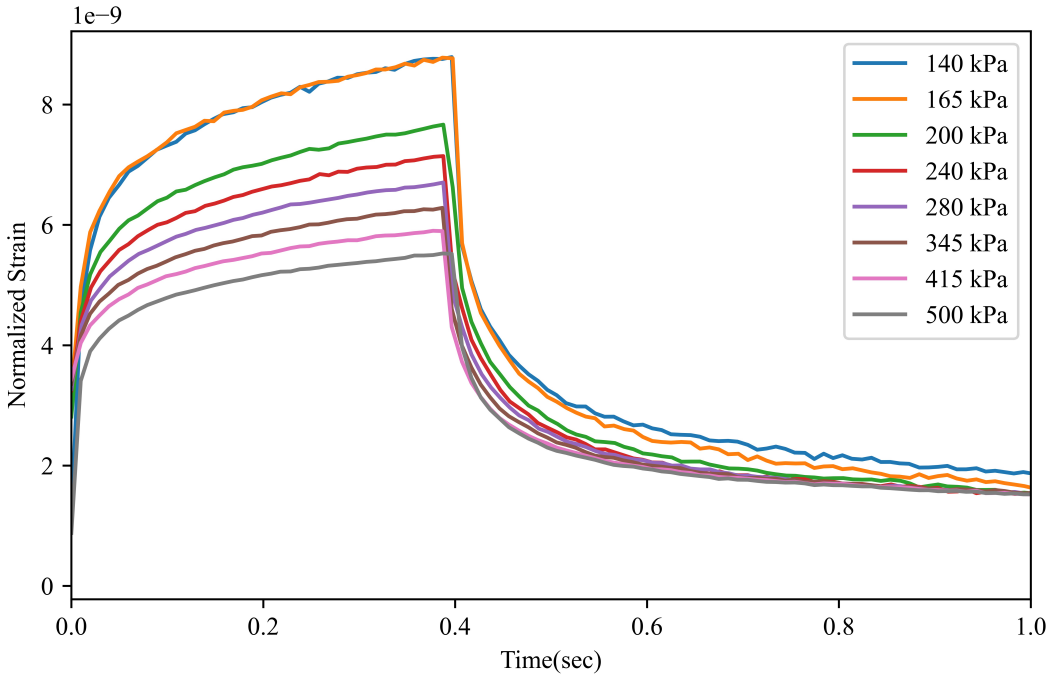

Figure 4.5: Normalized strain for the asphalt mixtures at 40° C

4.4 Nonlinear Viscoelastic Model

4.4.1 Preliminaries

Let κ_t denote the configuration of a body B at the current instant of time t. Let **x** and **v** denote the position and velocity of any particle of the body at this instant *t*, respectively. The velocity gradient is denoted by **L**:

$$\mathbf{L} = \frac{\partial \mathbf{v}}{\partial \mathbf{x}} \tag{4.1}$$

During any mechanical process that the body undergoes, the balance of mass, linear momentum, angular momentum, and laws of thermodynamics must be satisfied. The equations corresponding to the laws of the balance are:

$$\dot{\rho} + \rho \text{div}\mathbf{v} = 0, \tag{4.2}$$

$$\rho \mathbf{v} = \text{div}\mathbf{T}, \tag{4.3}$$

$$\mathbf{T} = \mathbf{T}^{\text{T}}, \tag{4.4}$$

where ρ is the density, **T** is the cauchy stress, and $\dot{A}$ represents the material time derivative:

$$\dot{A} = \frac{\partial A}{\partial t} + \frac{\partial A}{\partial \mathbf{x}}\mathbf{v}. \tag{4.5}$$

The balance of energy is given by

$$\mathbf{T} \cdot \mathbf{D} - \rho\dot{\epsilon} - \text{div}\mathbf{q} + \rho r = 0. \tag{4.6}$$

The Clausius-Duhem inequality is given by,

$$\rho\dot{\eta} + \text{div}\frac{q}{\theta} - \rho\frac{r}{\theta} \geq 0. \tag{4.7}$$

where **D** is the symmetric part of the velocity gradient, ϵ is the internal energy, **q** is the heat flux being supplied to the body, r is the heat supply to the body, θ is the temperature, and η is the

specific entropy. Combining Equations 4.6 and 4.7, the inequality can be expressed as

$$\mathbf{T} \cdot \mathbf{D} - \rho\dot{\epsilon} + \rho\theta\dot{\eta} - \frac{\mathbf{q} \cdot \text{grad}\theta}{\theta} = \xi \geq 0. \tag{4.8}$$

Here, ξ is the rate of dissipation at a material point. In this study, we express the inequality in terms of Gibbs free energy following the framework established by [96]. We define a quantity $\mathbf{T}_M$:

$$\mathbf{T}_M = \mathbf{T} - 2\widetilde{\eta}_d\mathbf{D}_d - 2\widetilde{\eta}_s tr(\mathbf{D})\mathbf{I}, \tag{4.9}$$

where $\widetilde{\eta}_d$ and $\widetilde{\eta}_s$ are the material parameters. The Gibbs free energy (G) is assumed to be a function of $\mathbf{T}_M$ and θ:

$$G = \hat{G}(\mathbf{T}_M, \theta), \tag{4.10}$$

The internal energy is related to Gibbs free energy as follows:

$$\epsilon = G - \frac{\partial G}{\partial \mathbf{T}_M} \cdot \mathbf{T}_M. \tag{4.11}$$

Assuming the deformation occurs at a constant temperature, these inequality reduces to

$$\mathbf{T} \cdot \mathbf{D} - \rho\dot{\epsilon} = \xi. \tag{4.12}$$

Substituting Equation 4.11 into Equation 4.12, the inequality then becomes

$$\mathbf{T} \cdot \mathbf{D} - \rho\left\{\frac{\partial^2 G}{\partial^2 \mathbf{T}_M}[\dot{\mathbf{T}}_M]\right\} \cdot \mathbf{T}_M = \xi \geq 0. \tag{4.13}$$

4.5 Development of Constitutive Relations

To complete the assignment of the constitutive equations, it is necessary to assume the Gibbs free energy and rate of dissipation to obtain the constitutive relation. The rate dissipation function

ξ is assumed to be of the form:

$$\xi = 2\eta_d \|\mathbf{D}_{p_d}\|^2 + 2\eta_s tr(\mathbf{D}_p)^2 + 2\widetilde{\eta}_d \|\mathbf{D}_d\|^2 + 2\widetilde{\eta}_s tr(\mathbf{D})^2, \tag{4.14}$$

where $\eta_d, \eta_s, \widetilde{\eta}_d$, and $\widetilde{\eta}_s$ are material viscosities, $\|\mathbf{A}\|$ denotes the Frobenius norm of $\mathbf{A}$, and $\mathbf{A}_d$ is the deviatoric part of the of $\mathbf{A}$.

Let C and $\mathbf{D}_p$ be defined such that,

$$C = 2\eta_d \|\mathbf{D}_{p_d}\|^2 + 2\eta_s tr(\mathbf{D}_p)^2, \tag{4.15}$$

$$\mathbf{D}_p = \mathbf{D} + \frac{\partial^2 G}{\partial^2 \mathbf{T}_M}[\dot{\mathbf{T}}_M] + \mathbf{H}, \tag{4.16}$$

with $\mathbf{H}$ being a tensor that satisfies $\mathbf{H} \cdot \mathbf{T}_M = 0$. $\mathbf{D}_p$ can be regarded as the rate of deformation of the configuration taken by the body when no external force is acting on the body. The inequality (Equation 4.13) can then be written as:

$$\mathbf{T} \cdot \mathbf{D} - \rho \left\{ \frac{\partial^2 G}{\partial^2 \mathbf{T}_M}[\dot{\mathbf{T}}_M] \right\} \cdot \mathbf{T}_M = C + 2\widetilde{\eta}_d \|\mathbf{D}_d\|^2 + 2\widetilde{\eta}_s tr(\mathbf{D})^2 \geq 0. \tag{4.17}$$

The above equation (4.17) can be written as,

$$\mathbf{T} \cdot \mathbf{D} - 2\widetilde{\eta}_d \|\mathbf{D}_d\|^2 - 2\widetilde{\eta}_s tr(\mathbf{D})^2 - \rho \left\{ \frac{\partial^2 G}{\partial^2 \mathbf{T}_M}[\dot{\mathbf{T}}_M] \right\} \cdot \mathbf{T}_M = C \geq 0, \tag{4.18}$$

$$\implies (\mathbf{T} - 2\widetilde{\eta}_d \mathbf{D}_d - 2\widetilde{\eta}_s tr(\mathbf{D})\mathbf{I}) \cdot \mathbf{D} - \rho \left\{ \frac{\partial^2 G}{\partial^2 \mathbf{T}_M}[\dot{\mathbf{T}}_M] \right\} \cdot \mathbf{T}_M = C \geq 0. \tag{4.19}$$

Substituting Equation 4.9 into Equation 4.19, we get:

$$\mathbf{T}_M \cdot \mathbf{D} - \rho \left\{ \frac{\partial^2 G}{\partial^2 \mathbf{T}_M}[\dot{\mathbf{T}}_M] \right\} \cdot \mathbf{T}_M = C, \tag{4.20}$$

Substituting Equation 4.16 into Equation 4.20 yields:

$$\mathbf{T}_M \cdot \mathbf{D}_p = C. \tag{4.21}$$

Next we follow the notion of maximizing C the method of Lagrange multipliers, the following auxillary function is defined:

$$\Phi = C + \lambda(C - \mathbf{T}_M \cdot \mathbf{D}_p). \tag{4.22}$$

Then we take derivative of C with respect to $\mathbf{D}_p$, and equate it to zero yields:

$$\frac{\partial \Phi}{\partial \mathbf{D}_p} = (1+\lambda)\frac{\partial C}{\partial \mathbf{D}_p} - \lambda \mathbf{T}_M = 0, \tag{4.23}$$

$$\Rightarrow (1+\lambda)\frac{\partial C}{\partial \mathbf{D}_p} - \lambda \mathbf{T}_M = 0, \tag{4.24}$$

$$\Rightarrow \frac{(1+\lambda)}{\lambda}\frac{\partial C}{\partial \mathbf{D}_p} = \mathbf{T}_M. \tag{4.25}$$

Lastly, we take the dot product of Equation 4.25 with $\mathbf{D}_p$

$$\frac{(1+\lambda)}{\lambda}\frac{\partial C}{\partial \mathbf{D}_p} \cdot \mathbf{D}_p = \mathbf{T}_M \cdot \mathbf{D}_p. \tag{4.26}$$

By substituting Equation 4.21 into Equation 4.26 we obtain:

$$\frac{(1+\lambda)}{\lambda}\frac{\partial C}{\partial \mathbf{D}_p} \cdot \mathbf{D}_p = C, \tag{4.27}$$

$$\Longrightarrow \frac{(1+\lambda)}{\lambda} = \frac{C}{\frac{\partial C}{\partial \mathbf{D}_p} \cdot \mathbf{D}_p}. \tag{4.28}$$

Next we calculate $\frac{\partial C}{\partial \mathbf{D}_p}$ using Equation 4.15

$$\frac{\partial C}{\partial \mathbf{D}_p} = 4\eta_d \mathbf{D}_{p_d} + 4\eta_s(tr(\mathbf{D}_p))\mathbf{I}. \tag{4.29}$$

By substituting the expressions for C (Equation 4.15) and $\frac{\partial C}{\partial \mathbf{D}_p}$ (Equation 4.29) in equation 4.28 we obtain

$$\frac{(1+\lambda)}{\lambda} = \frac{1}{2}. \tag{4.30}$$

The resulting constitutive equation is, therefore,

$$2\eta_d \mathbf{D}_{pd} + 2\eta_s tr(\mathbf{D}_p)\mathbf{I} = \mathbf{T}_M. \tag{4.31}$$

In this study, the Gibbs potential is assumed to be of the form:

$$G = -\frac{1}{18\mu_s}(tr\mathbf{T}_M)^2 - \frac{1}{4\mu_d}\|\mathbf{T}_{Md}\|^2, \tag{4.32}$$

where μ_s and μ_d are material stiffness parameters, and T_{Md} is the deviatoric part of the stress tensor T_M. Following Equation 4.16, $\mathbf{D}_p$ becomes,

$$\mathbf{D}_p = \mathbf{D} - \frac{1}{3\mu_s}\frac{tr(\dot{\mathbf{T}}_M)}{3}\mathbf{1} - \frac{1}{2\mu_d}\dot{\mathbf{T}}_{Md} + \mathbf{H}, \tag{4.33}$$

To ensure a frame indifference of $\mathbf{D}_p$, $\mathbf{H}$ is assumed to be:

$$\mathbf{H} = \frac{1}{2\mu_d}(\mathbf{WT} - \mathbf{TW}), \tag{4.34}$$

where $\mathbf{W}$ is the skew-symmetric part of the velocity gradient. Substituting Equation 4.34 into equation 4.33, yields:

$$\mathbf{D}_p = \mathbf{D} - \frac{1}{3\mu_s}\frac{tr(\overset{\omega}{\mathbf{T}}_M)}{3}\mathbf{1} - \frac{1}{2\mu_d}\overset{\omega}{\mathbf{T}}_{Md}, \tag{4.35}$$

where $\overset{\omega}{(\cdot)}$ is the Green-McInnis-Naghdi rate given by:

$$\overset{\omega}{\mathbf{A}} = \dot{\mathbf{A}} + \mathbf{AW} - \mathbf{WA}. \tag{4.36}$$

Hence, the constitutive equation will be of the form:

$$\mathbf{T} = 2\widetilde{\eta}_d \mathbf{D}_d + 2\widetilde{\eta}_s tr(\mathbf{D})\mathbf{I} + \mathbf{T}_M, \tag{4.37}$$

$$\mathbf{T}_M = 2\eta_d \mathbf{D}_{p_d} + 2\eta_s tr(\mathbf{D}_p)\mathbf{I}, \tag{4.38}$$

$$\mathbf{D}_p = \mathbf{D} - \frac{1}{3\mu_s}\frac{tr(\overset{\omega}{\mathbf{T}}_M)}{3}\mathbf{1} - \frac{1}{2\mu_d}\overset{\omega}{\mathbf{T}}_{Md}. \tag{4.39}$$

4.6 Kinematics

To simulate the binder behaviors obtained from various test protocols, we adopted a semi inverse method (i.e., the deformation or the velocity is assumed to be of a certain form). In this case, the deformation is assumed to be homogeneous, thus the equation of motion in the cylindrical polar coordinates are expressed as:

$$r = kR; \quad \theta = \Theta; \quad z = \lambda Z, \tag{4.40}$$

where R, Θ, and Z are coordinates in the undeformed configuration; r, θ, and z are coordinates in the deformed state; and k and λ are the stretches. The deformation gradient for the motion expressed as:

$$\mathbf{F} = \text{diag}\big(k, k, \lambda\big), \tag{4.41}$$

The corresponding velocity gradient (**L**) is expressed as:

$$\mathbf{L} = \text{diag}\left(\frac{\dot{k}}{k}, \frac{\dot{k}}{k}, \frac{\dot{\lambda}}{\lambda}\right). \tag{4.42}$$

The corresponding symmetric part of the velocity gradient (**D**) and the skew-symmetric part of the velocity gradient are given by (**W**):

$$\mathbf{D} = \frac{1}{2}(\mathbf{L} + \mathbf{L}^T) = \text{diag}\left(\frac{\dot{k}}{k}, \frac{\dot{k}}{k}, \frac{\dot{\lambda}}{\lambda}\right), \tag{4.43}$$

$$\mathbf{W} = \frac{1}{2}(\mathbf{L} - \mathbf{L}^T) = \Big(\mathbf{0}, \mathbf{0}, \mathbf{0}\Big). \tag{4.44}$$

$\mathbf{T}_M$ is assumed to be of the following form:

$$\mathbf{T}_M = \begin{bmatrix} T_{Mrr} & 0 & 0 \\ 0 & T_{M\theta\theta} & 0 \\ 0 & 0 & T_{Mzz} \end{bmatrix}. \tag{4.45}$$

$\mathbf{T}$ is assumed to be of the following form:

$$\mathbf{T} = \begin{bmatrix} T_{rr} & 0 & 0 \\ 0 & T_{\theta\theta} & 0 \\ 0 & 0 & T_{zz} \end{bmatrix}. \tag{4.46}$$

By substituting Equation 4.45 Equation 4.34, $\overset{\omega}{\mathbf{A}}$ can be written as follows:

$$\overset{\omega}{\mathbf{A}} = \dot{\mathbf{A}} + \mathbf{AW} - \mathbf{WA} = \dot{\mathbf{A}}, \tag{4.47}$$

$$\implies \overset{\omega}{\mathbf{T}}_M = \dot{\mathbf{T}}_M + \mathbf{T}_M\mathbf{W} - \mathbf{W}\mathbf{T}_M = \dot{\mathbf{T}}_M. \tag{4.48}$$

Using Equation 4.9, $\dot{\mathbf{T}}_M$ can written as:

$$\dot{\mathbf{T}}_M = \dot{\mathbf{T}} - 2\widetilde{\eta}_d\dot{\mathbf{D}}_d - 2\widetilde{\eta}_s tr(\dot{\mathbf{D}})\mathbf{I}. \tag{4.49}$$

Now $tr(\overset{\omega}{\mathbf{T}}_M)$ can be written as:

$$tr(\overset{\omega}{\mathbf{T}}_M) = tr(\dot{\mathbf{T}}_M) = tr(\dot{\mathbf{T}}) - tr(2\widetilde{\eta}_d\dot{\mathbf{D}}_d) - tr(2\widetilde{\eta}_s tr(\dot{\mathbf{D}})\mathbf{I}), \tag{4.50}$$

$$\implies tr(\overset{\omega}{\mathbf{T}}_M) = tr(\dot{\mathbf{T}}_M) = tr(\dot{\mathbf{T}}) - 6\widetilde{\eta}_s tr(\dot{\mathbf{D}}). \tag{4.51}$$

$\overset{\omega}{\mathbf{T}}_{Md}$ can be written as:

$$\overset{\omega}{\mathbf{T}}_{Md} = \dot{\mathbf{T}}_{Md} = \dot{\mathbf{T}}_d - 2\widetilde{\eta}_d\dot{\mathbf{D}}_d - 2\widetilde{\eta}_s tr(\dot{\mathbf{D}})\mathbf{I}_d, \tag{4.52}$$

$$\dot{\mathbf{T}}_{Md} = \dot{\mathbf{T}}_d - 2\widetilde{\eta}_d\dot{\mathbf{D}}_d. \tag{4.53}$$

Substituting Equation 4.51 and 4.53 into equation 4.39, yields:

$$\mathbf{D}_p = \mathbf{D} - \frac{1}{3\mu_s}\frac{tr(\dot{\mathbf{T}}) - 6\widetilde{\eta}_s tr(\dot{\mathbf{D}})}{3}\mathbf{1} - \frac{1}{2\mu_d}(\dot{\mathbf{T}}_d - 2\widetilde{\eta}_d\dot{\mathbf{D}}_d). \tag{4.54}$$

The deviatoric part and trace can be calculated using the above equation, which can then be substituted into Equation 4.38 to calculate $\mathbf{T}_M$ as:

$$\mathbf{T}_M = 2\eta_d\left(\mathbf{D}_d - \frac{1}{2\mu_d}(\dot{\mathbf{T}}_d - 2\widetilde{\eta}_d\dot{\mathbf{D}}_d)\right) + 2\eta_s\left(tr(\mathbf{D}) - \frac{1}{3\mu_s}(tr(\dot{\mathbf{T}}) - 6\widetilde{\eta}_s tr(\dot{\mathbf{D}}))\right)\mathbf{I}. \tag{4.55}$$

Substituting Equation 4.55 into Equation 4.37 yields:

$$\mathbf{T} = 2\widetilde{\eta}_d\mathbf{D}_d + 2\widetilde{\eta}_s tr(\mathbf{D})\mathbf{I} + 2\eta_d\left(\mathbf{D}_d - \frac{1}{2\mu_d}(\dot{\mathbf{T}}_d - 2\widetilde{\eta}_d\dot{\mathbf{D}}_d)\right) + 2\eta_s\left(tr(\mathbf{D}) - \frac{1}{3\mu_s}(tr(\dot{\mathbf{T}}) - 6\widetilde{\eta}_s tr(\dot{\mathbf{D}}))\right)\mathbf{I}. \tag{4.56}$$

Equation 4.56 can be rearranged as:

$$\mathbf{T} = a(\mathbf{D}_d) + b(tr(\mathbf{D})\mathbf{I}) - c\left(\dot{\mathbf{T}}_d - 2\widetilde{\eta}_d\dot{\mathbf{D}}_d\right) - d\left(tr(\dot{\mathbf{T}}) - 6\widetilde{\eta}_s tr(\dot{\mathbf{D}})\right)\mathbf{I}, \tag{4.57}$$

where a, b, c, and d are expressed as:

$$a = 2\widetilde{\eta}_d + 2\eta_d, \tag{4.58}$$

$$b = 2\widetilde{\eta}_s + 2\eta_s, \tag{4.59}$$

$$c = \frac{2\eta_d}{2\mu_d}, \tag{4.60}$$

$$d = \frac{2\eta_s}{2\mu_3}. \tag{4.61}$$

Assuming the tensors $\mathbf{D}_d$, $\mathbf{T}_d$ are of the following form:

$$\mathbf{D}_d = \begin{bmatrix} \frac{2}{3}D_{rr} - \frac{1}{3}(D_{\theta\theta} + D_{zz}) & 0 & 0 \\ 0 & \frac{2}{3}D_{\theta\theta} - \frac{1}{3}(D_{rr} + D_{zz}) & 0 \\ 0 & 0 & \frac{2}{3}D_{zz} - \frac{1}{3}(D_{rr} + D_{\theta\theta}) \end{bmatrix}$$
$$= \begin{bmatrix} D_{drr} & 0 & 0 \\ 0 & D_{d\theta\theta} & 0 \\ 0 & 0 & D_{dzz} \end{bmatrix}, \tag{4.62}$$

$$\mathbf{T}_d = \begin{bmatrix} \frac{2}{3}T_{rr} - \frac{1}{3}(T_{\theta\theta} + T_{zz}) & 0 & 0 \\ 0 & \frac{2}{3}T_{\theta\theta} - \frac{1}{3}(T_{rr} + T_{zz}) & 0 \\ 0 & 0 & \frac{2}{3}T_{zz} - \frac{1}{3}(T_{rr} + T_{\theta\theta}) \end{bmatrix}$$
$$= \begin{bmatrix} T_{drr} & 0 & 0 \\ 0 & T_{d\theta\theta} & 0 \\ 0 & 0 & T_{dzz} \end{bmatrix}. \tag{4.63}$$

Substituting the symmetric part of **D** form Equation 4.44 and the stress tensor to be of the form in Equation 4.62, the governing equations during multiaxial compression can be written in terms of

a set of ordinary differential equations:

$$\begin{bmatrix} T_{rr} & 0 & 0 \\ 0 & T_{\theta\theta} & 0 \\ 0 & 0 & T_{zz} \end{bmatrix} = a \begin{bmatrix} D_{drr} & 0 & 0 \\ 0 & D_{d\theta\theta} & 0 \\ 0 & 0 & D_{dzz} \end{bmatrix} + b \begin{bmatrix} D_{rr}+D_{\theta\theta}+D_{zz} & 0 & 0 \\ 0 & D_{rr}+D_{\theta\theta}+D_{zz} & 0 \\ 0 & 0 & D_{rr}+D_{\theta\theta}+D_{zz} \end{bmatrix} - c \begin{bmatrix} \dot{T}_{drr} & 0 & 0 \\ 0 & \dot{T}_{d\theta\theta} & 0 \\ 0 & 0 & \dot{T}_{dzz} \end{bmatrix} + 2\widetilde{\eta}_d c \begin{bmatrix} \dot{D}_{drr} & 0 & 0 \\ 0 & \dot{D}_{d\theta\theta} & 0 \\ 0 & 0 & \dot{D}_{dzz} \end{bmatrix} - d \begin{bmatrix} \dot{T}_{rr}+\dot{T}_{\theta\theta}+\dot{T}_{zz} & 0 & 0 \\ 0 & \dot{T}_{rr}+\dot{T}_{\theta\theta}+\dot{T}_{zz} & 0 \\ 0 & 0 & \dot{T}_{rr}+\dot{T}_{\theta\theta}+\dot{T}_{zz} \end{bmatrix} + 6\widetilde{\eta}_s d \begin{bmatrix} \dot{D}_{rr}+\dot{D}_{\theta\theta}+\dot{D}_{zz} & 0 & 0 \\ 0 & \dot{D}_{rr}+\dot{D}_{\theta\theta}+\dot{D}_{zz} & 0 \\ 0 & 0 & \dot{D}_{rr}+\dot{D}_{\theta\theta}+\dot{D}_{zz} \end{bmatrix}. \quad (4.64)$$

The above equations can be simplified

$$T_{rr} - a(D_{drr}) - b(tr(D)) - c(T_{drr}) - d(tr\dot{T}) = p\dot{D}_{rr} + q\dot{D}_{zz}, \quad (4.65)$$

$$T_{zz} - a(D_{dzz}) - b(tr(D)) - c(T_{dzz}) - d(tr\dot{T}) = s\dot{D}_{rr} + r\dot{D}_{zz}, \quad (4.66)$$

where $p, q, r,$ and s are expressed as:

$$p = 12\widetilde{\eta}_s d + \frac{2}{3}\widetilde{\eta}_d c, \quad (4.67)$$

$$q = 6\widetilde{\eta}_s d - \frac{2}{3}\widetilde{\eta}_d c, \tag{4.68}$$

$$r = 6\widetilde{\eta}_s d + \frac{4}{3}\widetilde{\eta}_d c, \tag{4.69}$$

$$s = 12\widetilde{\eta}_s d - \frac{4}{3}\widetilde{\eta}_d c. \tag{4.70}$$

Multiplying Equations 4.65 with s and 4.66 with p yields:

$$sT_{rr} - as(D_{drr}) - bs(tr(D)) - cs(T_{drr}) - ds(tr\dot{T}) = ps\dot{D}_{rr} + qs\dot{D}_{zz}, \tag{4.71}$$

$$pT_{zz} - ap(D_{dzz}) - bp(tr(D)) - cp(T_{dzz}) - dp(tr\dot{T}) = sp\dot{D}_{rr} + rp\dot{D}_{zz}. \tag{4.72}$$

Subtracting Equation 4.71 from Equation 4.72 gives us:

$$\begin{aligned} pT_{zz} - sT_{rr} - ap(D_{dzz}) + as(D_{drr}) - bp(tr(D)) + bs(tr(D)) - cp(T_{dzz}) + cs(T_{drr}) \\ - dp(tr\dot{T}) + ds(tr\dot{T}) = rp\dot{D}_{zz} - qs\dot{D}_{zz}. \end{aligned} \tag{4.73}$$

Multiplying Equation 4.65 by r and Equation 4.66 by q yields:

$$rT_{rr} - ar(D_{drr}) - br(tr(D)) - cr(T_{drr}) - dr(tr\dot{T}) = pr\dot{D}_{rr} + qr\dot{D}_{zz}, \tag{4.74}$$

$$qT_{zz} - aq(D_{dzz}) - bq(tr(D)) - cq(T_{dzz}) - dq(tr\dot{T}) = sq\dot{D}_{rr} + rq\dot{D}_{zz}. \tag{4.75}$$

Subtracting Equation 4.75 from Equation 4.74 gives us:

$$\begin{aligned} qT_{zz} - rT_{rr} - aq(D_{dzz}) + ar(D_{drr}) - bq(tr(D)) + br(tr(D)) - cq(T_{dzz}) + cr(T_{drr}) \\ - dq(tr\dot{T}) + dr(tr\dot{T}) = sp\dot{D}_{rr} - pr\dot{D}_{rr}. \end{aligned} \tag{4.76}$$

Consequently, the constitutive equation reduced to two coupled ordinary differential equations(i.e., Equation 4.73 and 4.76).

4.7 Parametric Analysis

We conducted a comprehensive parametric analysis to determine the mixture response's sensitivity to the various model parameters. The parameters used in this analysis are shown in Table 4.1. To establish a reference material response and aid in the sensitivity study, we selected a reference parameter set (Set 1 in Table 4.1). All the simulations were conducted at creep stress of 140 kPa for 0.4 seconds, with a ramp-up time of 0.05 seconds and creep time of 0.35 seconds like the experimental protocol and a confinement pressure of 0 kPa.

Table 4.1: Model parameters used in the parametric study

Set#	μ_d	η_{d1}	μ_s	η_s	$\widetilde{\eta}_d$	$\widetilde{\eta}_s$	a	b	c
1	1E7	1E8	1E8	1E11	1E6	1E7	3E6	100	1
2	3E7	1E8	1E8	1E11	1E6	1E7	3E6	100	1
3	5E7	1E8	1E8	1E11	1E6	1E7	3E6	100	1
4	1E7	6E7	1E8	1E11	1E6	1E7	3E6	100	1
5	1E7	3E8	1E8	1E11	1E6	1E7	3E6	100	1
6	1E7	5E8	1E8	1E11	1E6	1E7	3E6	100	1
7	1E7	1E8	1E8	1E11	1E6	1E7	3E6	100	1
8	1E7	6E8	1E8	1E11	5E6	1E7	3E6	100	1
9	1E7	1E8	1E8	1E11	9E6	1E7	3E6	100	1
10	1E7	1E8	3E8	1E11	1E6	1E7	3E6	100	1
11	1E7	1E8	5E8	1E11	1E6	1E7	3E6	100	1
12	1E7	1E8	1E8	1E11	1E6	1E6	3E6	100	1
13	1E7	1E8	1E8	1E11	1E6	5E6	3E6	100	1
14	1E7	1E8	1E8	1E11	1E6	1E7	3E6	100	1
15	1E7	1E8	1E8	1E11	1E6	1E7	3E6	10	1
16	1E7	1E8	1E8	1E11	1E6	1E7	3E6	2	1

An example of the influence of μ_d with all the other parameters kept the same is shown in Figure 4.6. As expected, the slope of the strain during the ramp-up loading condition depends on the μ_d parameter as slope decreases with increased μ_d. This in turn affects the maximum strain experienced by the mixture.

The parameter η_d is considered a function of the spherical component of the stress tensor, as shown in the following equation:

$$\eta_d = \eta_{d_1} * \left[\frac{exp\Big((1 - \frac{tr(\mathbf{T})}{\mathrm{a}})/\mathrm{b}\Big)}{\mathrm{c}} \right]. \tag{4.77}$$

Analysis of the effects of η_{d_1} revealed that it controls when the mixture changes from a very low viscosity fluid-like behavior to a solid-like highly viscous fluid behavior. Figure 4.7, shows that η_{d1} controls the slope of the strain response during the creep loading because the slope of the strain response decreases as the value of η_{d1} increases . In Figure 4.7, the material with $\eta_{d1} = 5 * 10^8$ MPa.s was found to experience the shift much earlier than the other materials. The parameters *a*, *b*, and *c*, along with η_{d1} control the variation of η_d, as a function of $tr(\mathbf{T})$. The variations of the material response due to parameters a and b are shown in Figures 4.8, and 4.9. Parameter *a* controls the initial material response just as the creep loading begins immediately after the ramp-up loading. Parameter *b* acts as a normalizing parameter to the confinement pressure in the exponential function. It also and controls the sensitivity of η_d to the confinement pressure, thereby indirectly controlling the long-term slope of the strain during the ramp-up loading (as b decreases the slope is also found to increase).

The parameter μ_s is found to affect the long-term strain response during the creep loading over a long time. As shown in Figure 4.10 parameter $\widetilde{\eta}_s$ is mainly found to control the slope of the strain during creep loading, contributing to the change of the material response to a fluid-like behavior during the creep loading. The parameters $\left(\frac{2\eta_d}{3\mu_d}\right)$ and $\left(\frac{\eta_s}{\mu_s}\right)$ are the two relaxation times. The parameters η_s, η_d, $\widetilde{\eta}_d$, and $\widetilde{\eta}_s$ determine the zero shear viscosity of the material. The parameters η_{d1}, a, b, c account for the nonlinearity due to the applied confinement pressure.

Based on the parametric analysis and the physical significance of the model's parameters, we present here a summary of these parameters:

- Parameters μ_d and $\widetilde{\eta}_d$ control the slope of the axial strain during the ramp-up time (0-0.05 seconds).

- Parameter η_d, and η_d, the viscosity parameters, controls The long term response of the material. This is also controlled by parameters η_{d1}, a, and b

- Parameters μ_s and $\widetilde{\eta}_s$ control the slope of the axial strain response when subjected to creep loading. The relationship between the model's parameters and the axial strain response is illustrated in Figure 4.13.

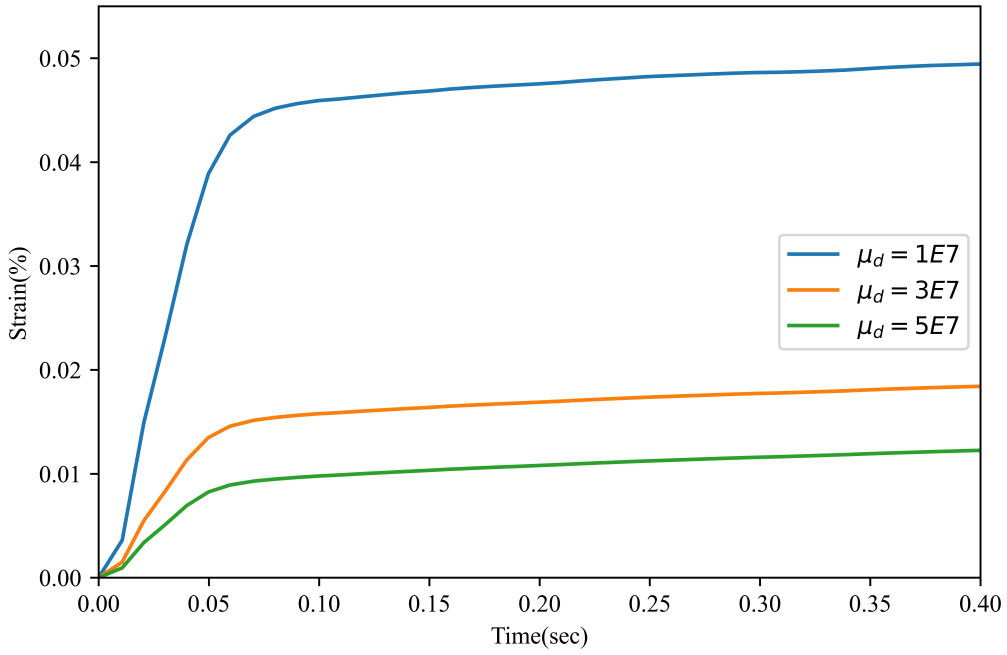

Figure 4.6: Analysis of the sensitivity of axial strain to μ_d

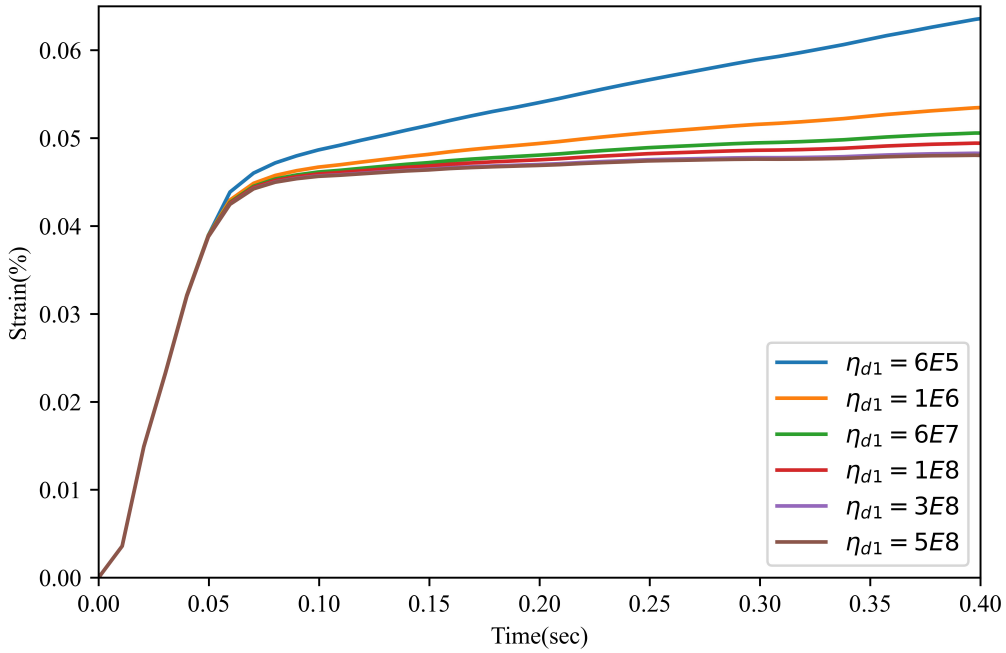

Figure 4.7: Analysis of the sensitivity of axial strain to η_{d1}

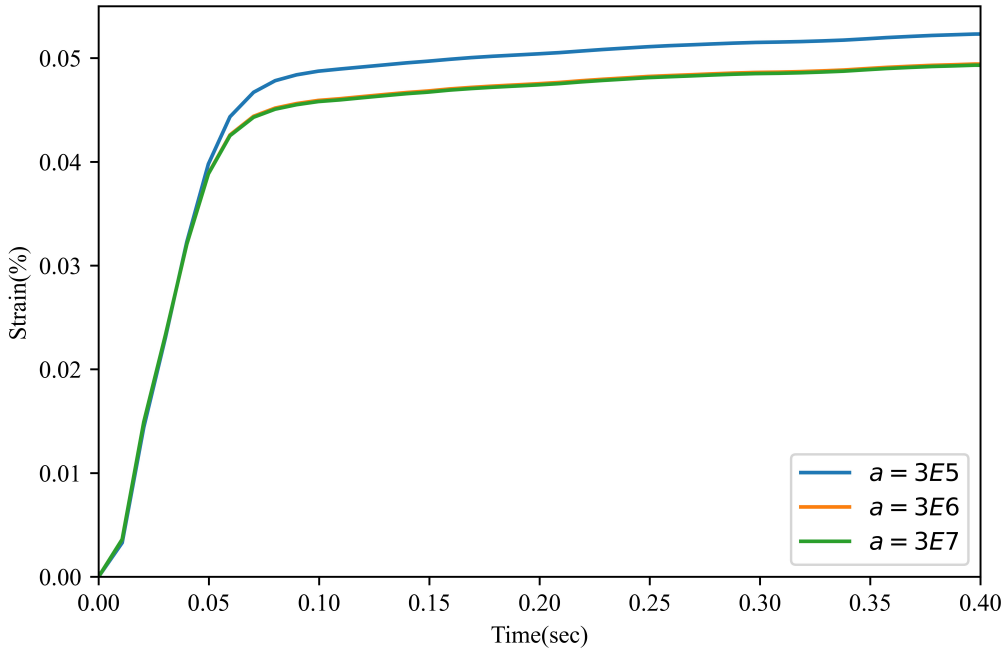

Figure 4.8: Analysis of the sensitivity of axial strain to a

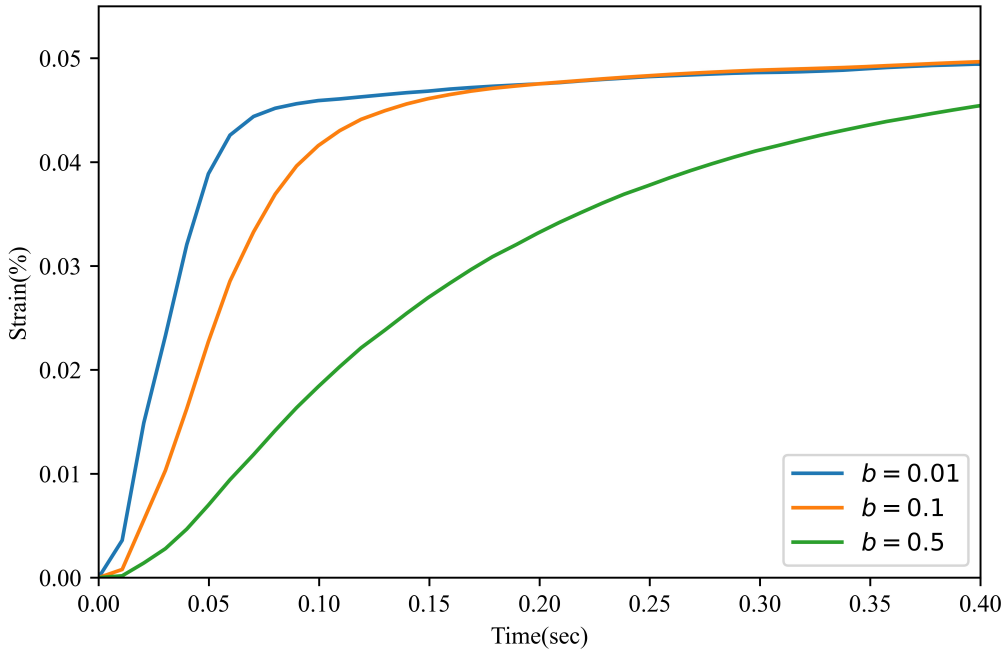

Figure 4.9: Analysis of the sensitivity of axial strain to b

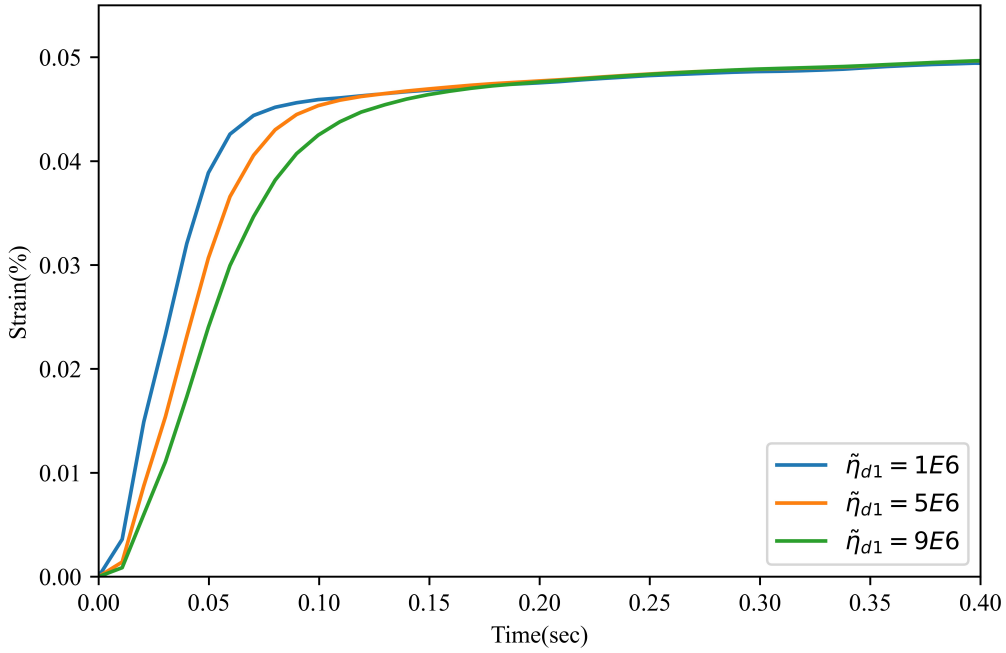

Figure 4.10: Analysis of the sensitivity of axial strain to $\widetilde{\eta}_d$

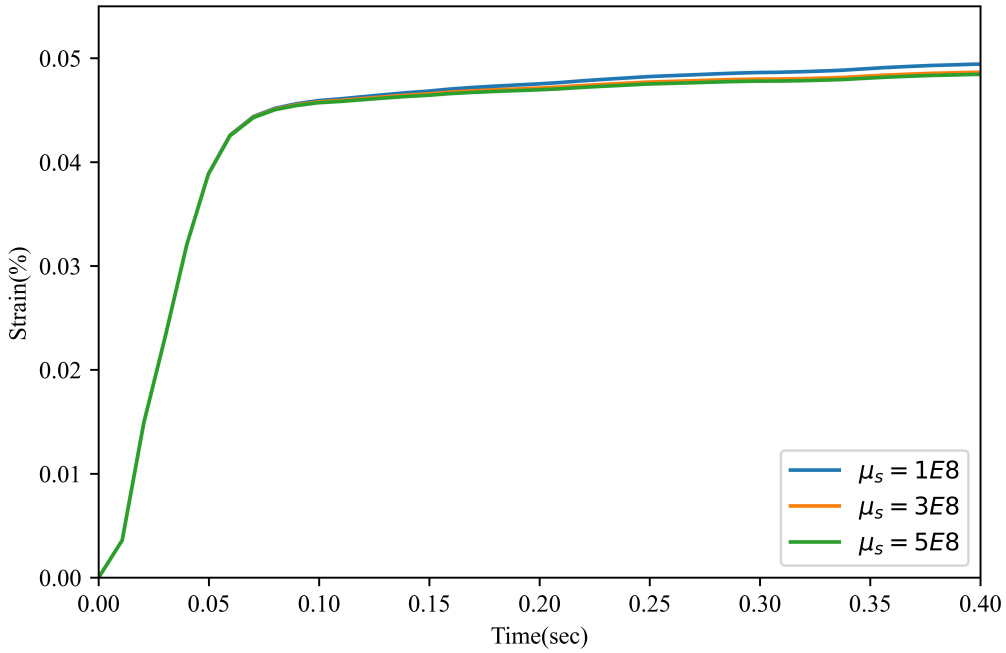

Figure 4.11: Analysis of the sensitivity of axial strain to μ_s

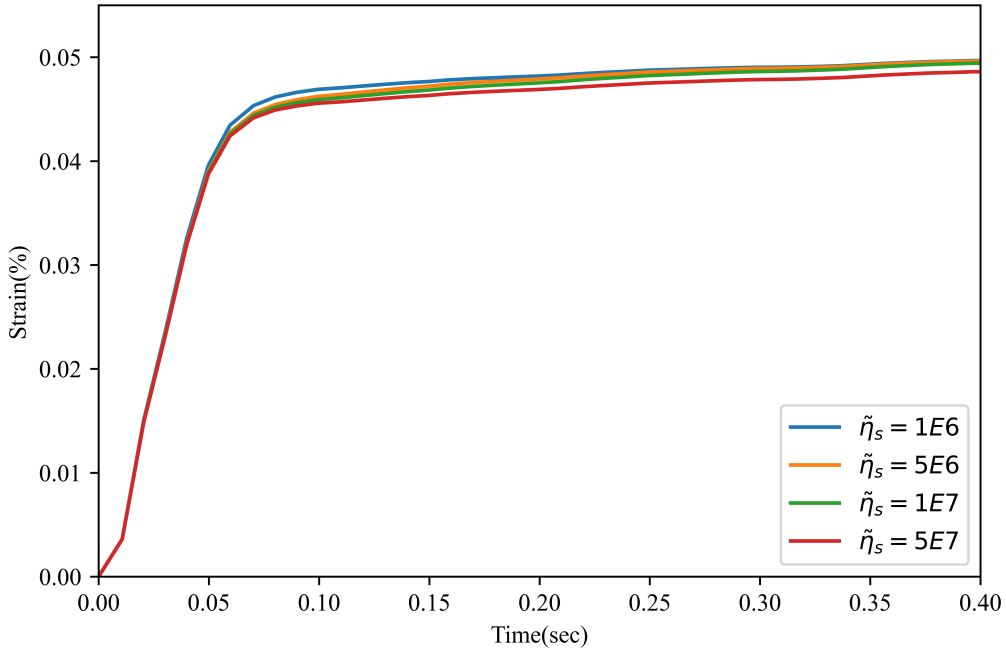

Figure 4.12: Analysis of the sensitivity of axial strain to $\widetilde{\eta}_s$

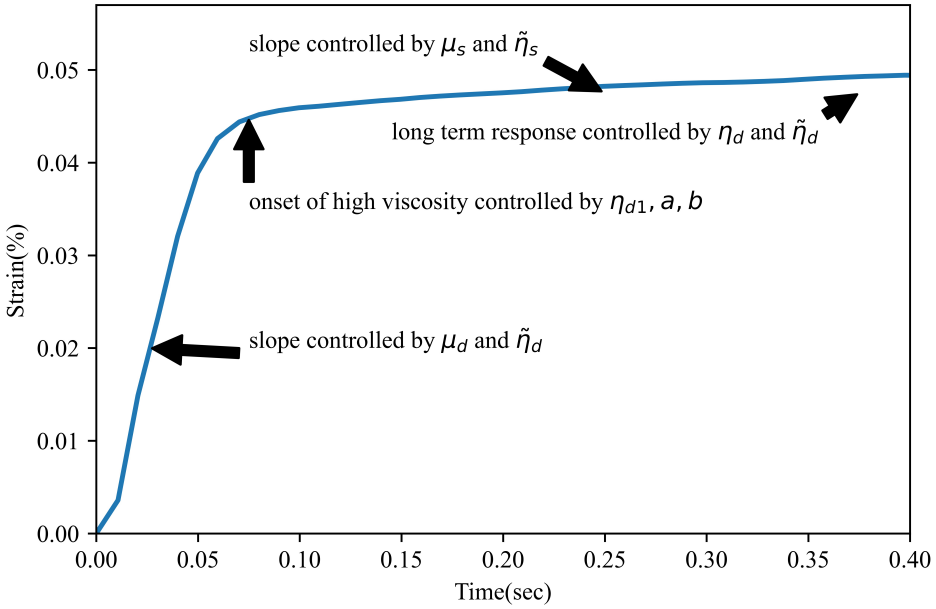

Figure 4.13: Illustration of the relationship of the model's parameters to the axial strain response.

4.8 Model Corroboration

The nonlinear viscoelastic model derived in section 4.7 assumes the mechanical processes to be isothermal. Experimental data is used to corroborate the model to obtain the appropriate calibrated material parameters for individual mixes at each temperature for the 0 kPa confinement case. The parameters were adjusted to better predict the material response (i.e., minimizing the error between the experimental data and the model prediction) using the findings from the parametric analysis. The obtained parameters were then used to predict the asphalt mixture's response at various confinement pressures. If the model prediction is not satisfactory (i.e., R^2 value > 0.9 for the axial strains at a 0 kPa confinement pressure and reasonable average error (%) value < 10% for the axial strains at other confinement pressures) for any of the confinement pressures, then the whole process starts again as shown in Figure 4.14. The obtained parameters for each temperature are shown in Table 4.2. The average error percentage for the model's predictions of 70, 140, and

380 kPa data is calculated as:

$$\text{Average Error}(\%) = Average\left(\frac{|x_{mt} - x_{et}|}{x_{et}} \times 100\right), \tag{4.78}$$

where x_{mt} is the modeling prediction at a given time t and x_{et} is the experimental value at a given time t. The average error percentages between the model prediction and experiment data throughout the experimental for 70, 140, and 380kPa data are shown in Table 4.3. The average error ($\%$) values are slightly high for the 55 C data due to low strain values obtained when the asphalt mixture samples were subjected to various confinement pressures and the accumulation of error with the progress of each creep and recovery cycle. The model captured the axial strain response well; however, it the model over-predicted the radial strain when the radial strain values were negative due to the constant application of confinement pressure even during recovery conditions.

Table 4.2: Model parameters at different temperatures

Temp	μ_d	η_d	μ_s	η_s	$\widetilde{\eta}_d$	$\widetilde{\eta}_s$	a	b	c
40^oC	9.25E7	9.37E12	9.45E10	9.17E11	5.05E6	3.25E7	1.76E6	100	1
55^oC	6.95E7	6.37E11	6.45E9	8.45E10	5.05E6	1.25E8	1.00E6	15	1

Table 4.3: Axial strain average errors between the model and experimental data at the end of each test

Confinement pressure	Temperature	Average error at the end of the test
70 kPa	40^o C	6.65$\%$
140 kPa	40^o C	2.55$\%$
380 kPa	40^o C	2.25$\%$
70 kPa	55^o C	6.65$\%$
140 kPa	55^o C	5.65$\%$
380 kPa	55^o C	6.57$\%$

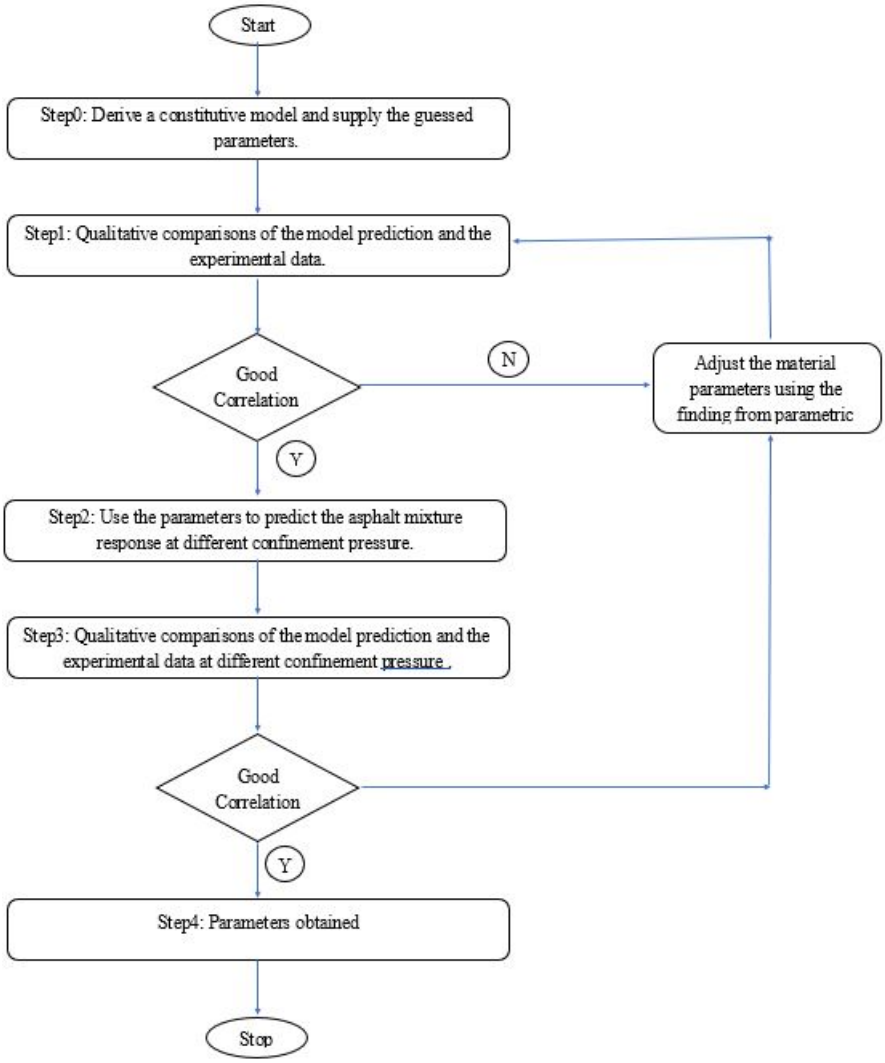

Figure 4.14: Flow chart of the model corroboration process

4.9 Summary

In this chapter, we developed a nonlinear viscoelastic model using the Gibbs-potential-based thermodynamic framework for describing the response of asphalt mixtures while accounting for the confinement pressure acting on the asphalt mixtures. The model also considers the fact that deforming materials like asphalt mixtures undergo microstructure changes in such a way, that the response to external stimuli depends on the current microstructure rather than the original microstructure. This was done by appealing to the idea that the material can have multiple natural

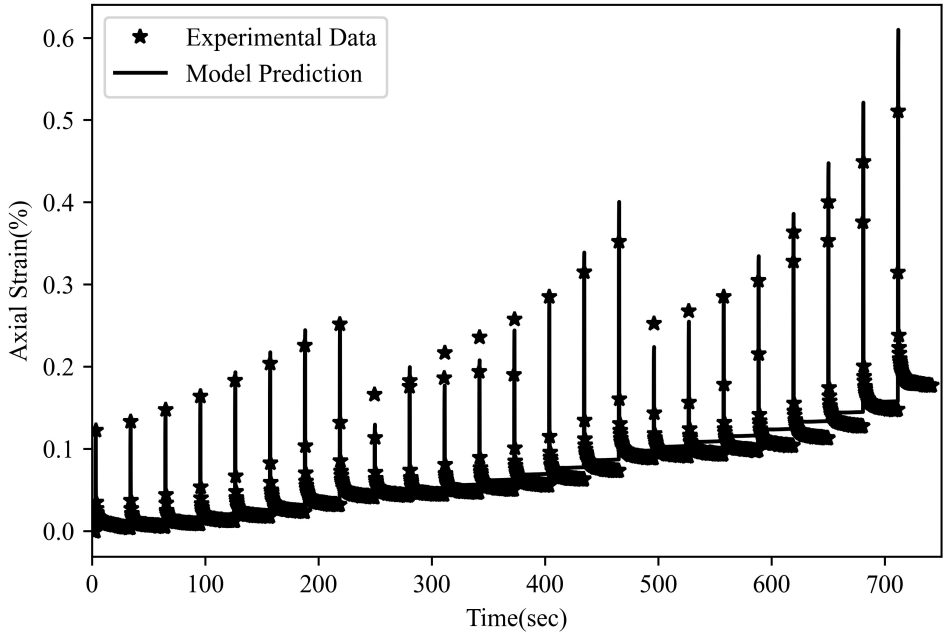

Figure 4.15: Analysis of axial strain values from the RCR experiments using nonlinear modeling at 40^oC and 0kPa confinement pressure.

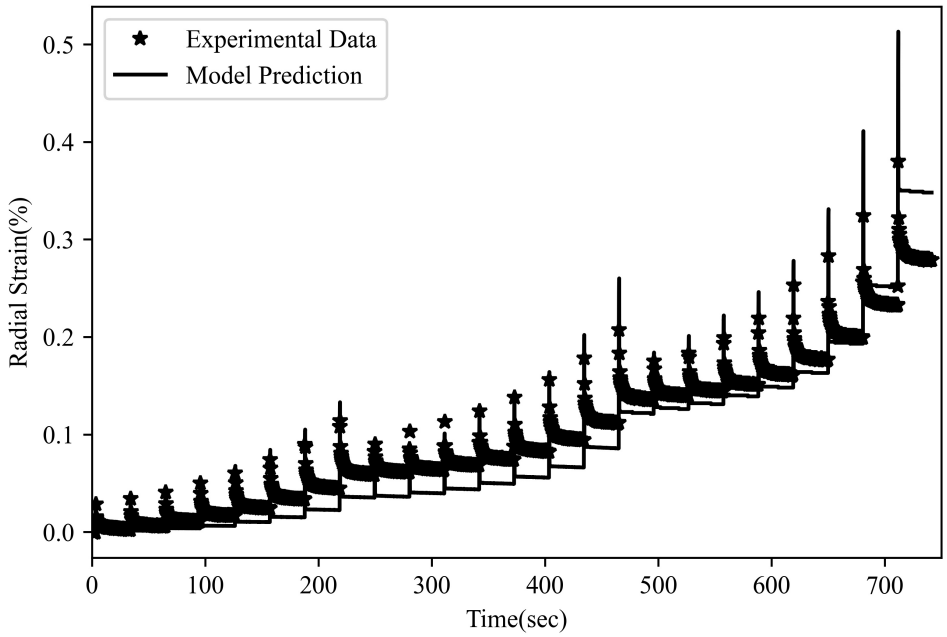

Figure 4.16: Analysis of radial strain values from the RCR experiments using nonlinear modeling at 40^oC and 0kPa confinement pressure

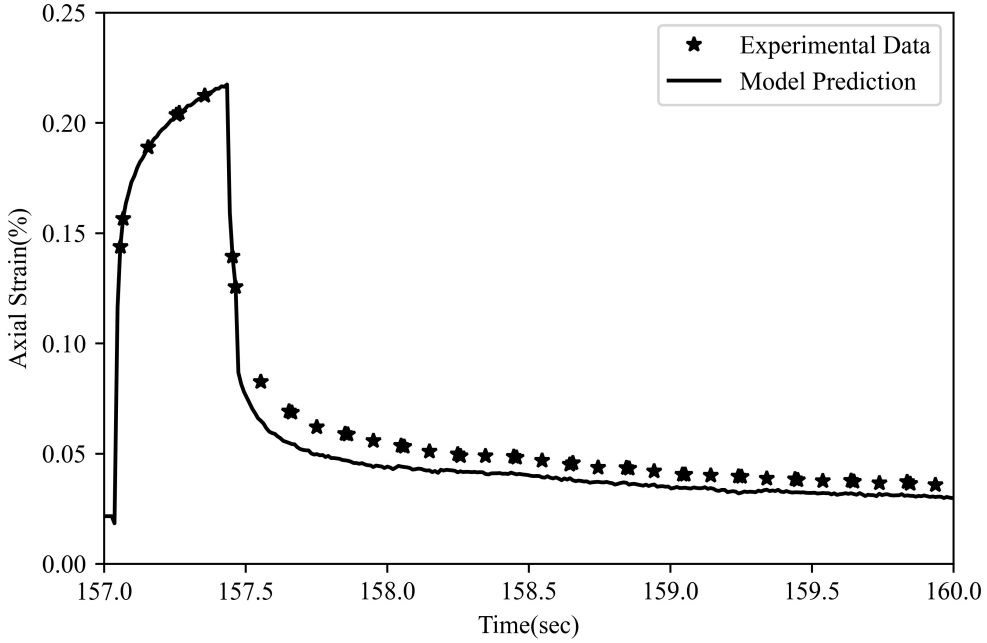

Figure 4.17: Close-up of axial strain analysis at 40^oC and 0 kPa confinement pressure.

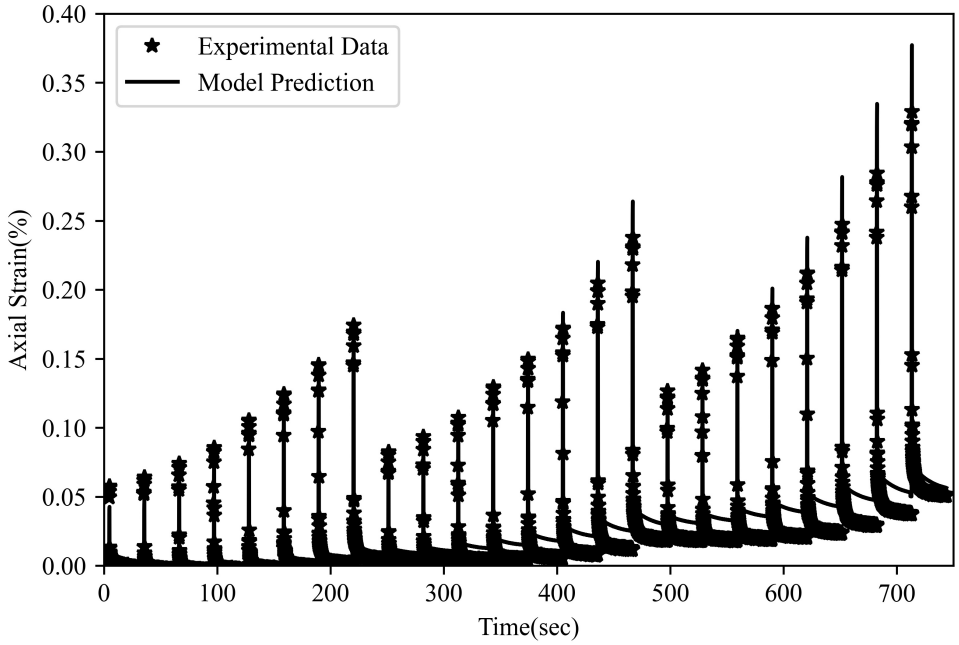

Figure 4.18: Analysis of axial strain values from the RCR experiments using nonlinear modeling at 40^o C and 70 kPa confinement pressure

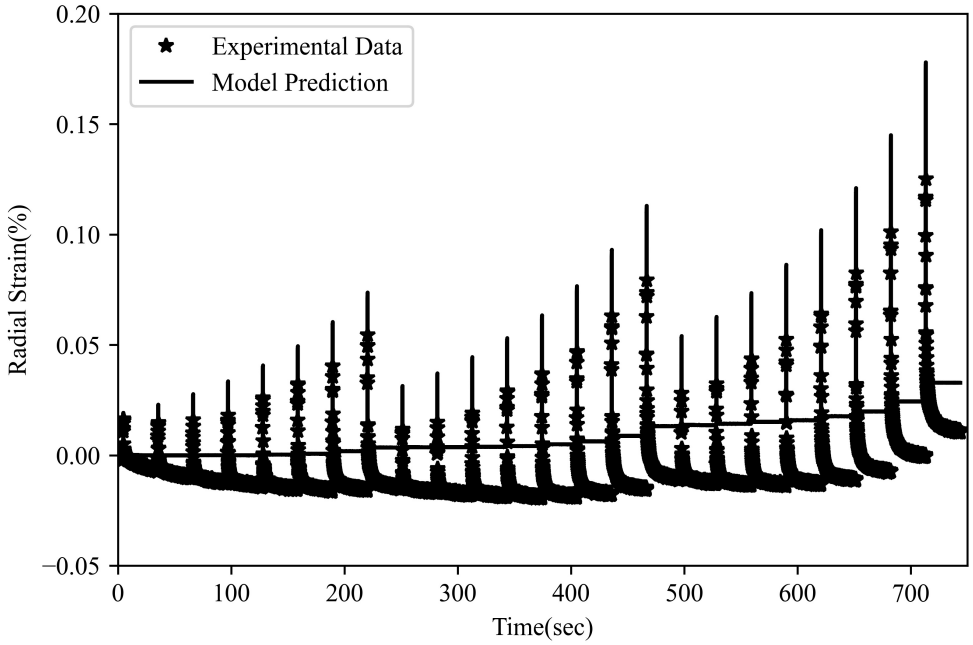

Figure 4.19: Analysis of radial strain values from the RCR experiments using nonlinear modeling at 40^o C and 70 kPa confinement pressure

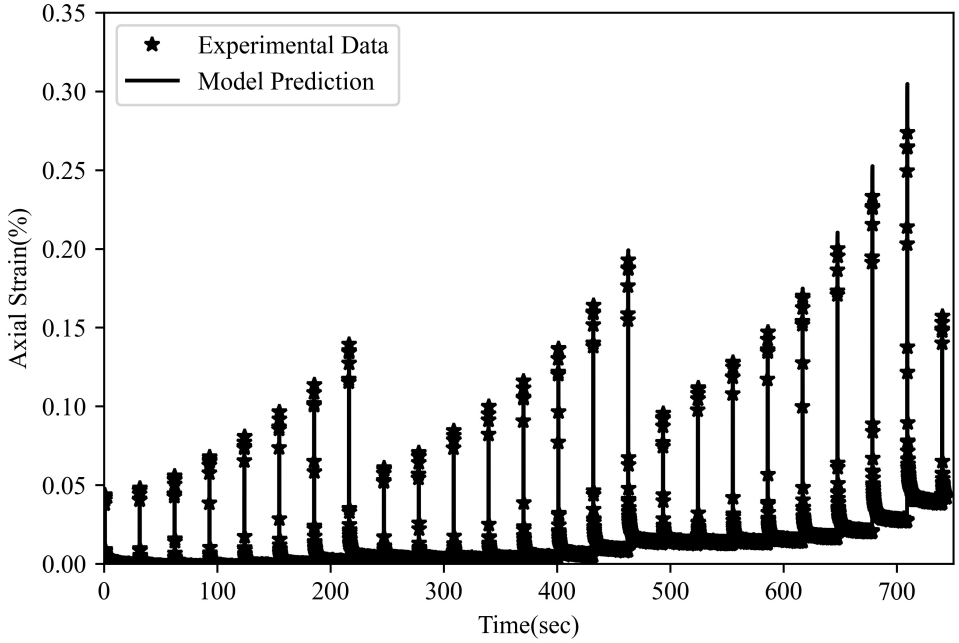

Figure 4.20: Analysis of axial strain values from the RCR experiments using nonlinear modeling at 40^o C and 140 kPa confinement pressure

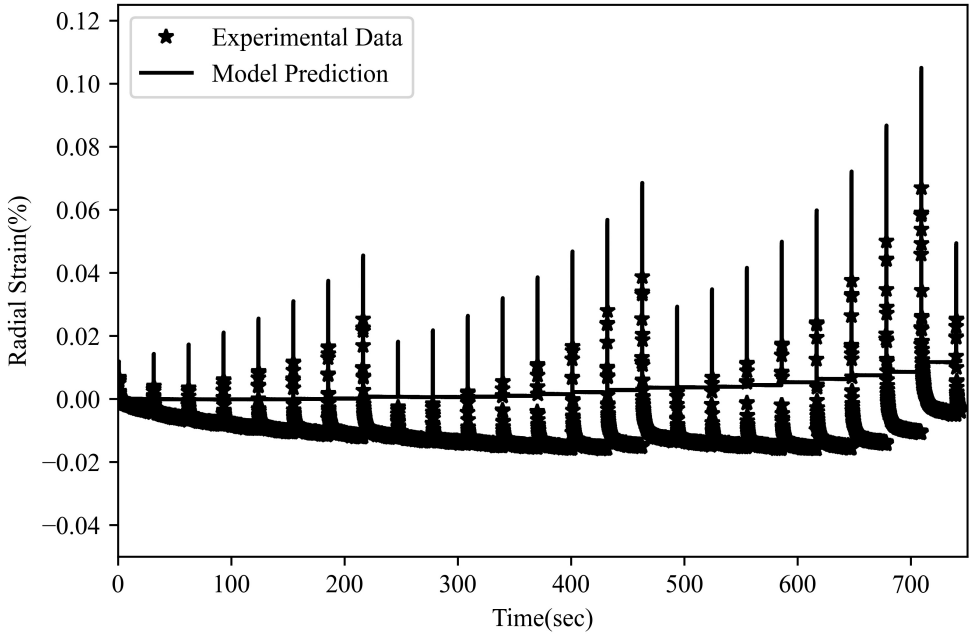

Figure 4.21: Analysis of radial strain values from the RCR experiments using nonlinear modeling at 40^o C and 140 kPa confinement pressure

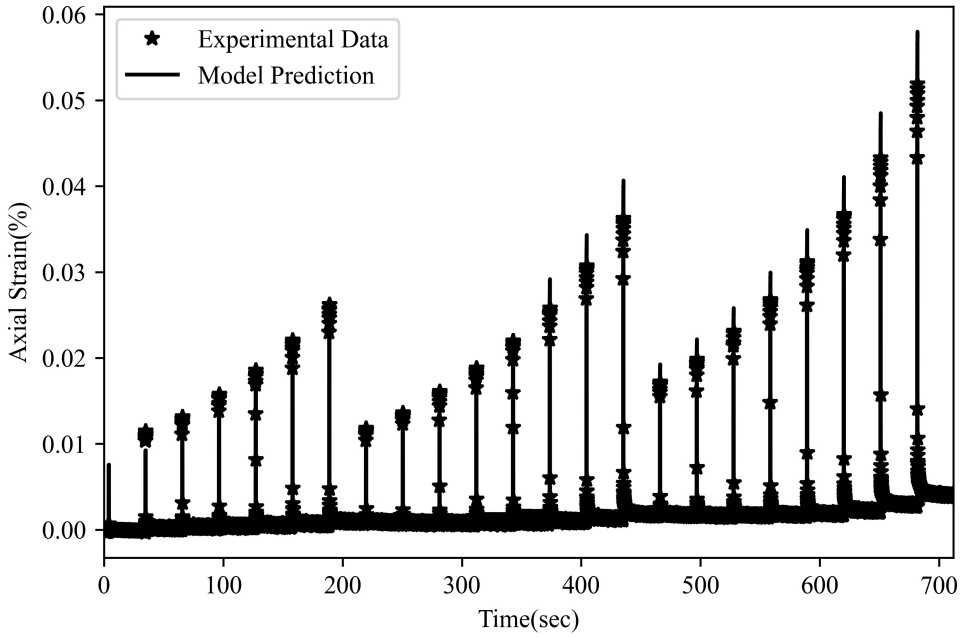

Figure 4.22: Analysis of axial strain values from the RCR experiments using nonlinear modeling at 40^o C and 380 kPa confinement pressure

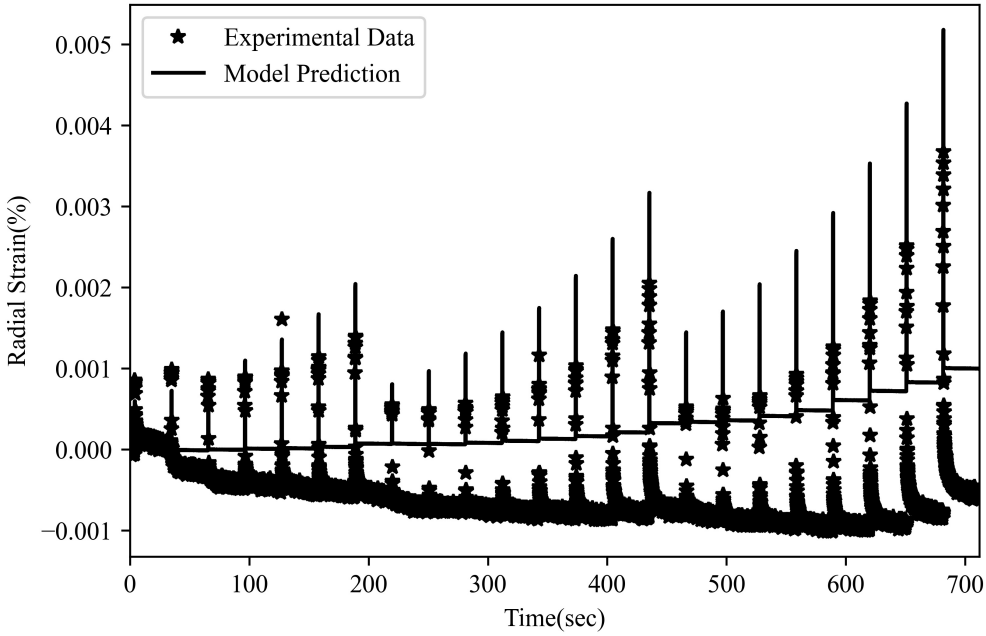

Figure 4.23: Analysis of radial strain values from the RCR experiments using nonlinear modeling at 40^o C and 380 kPa confinement pressure

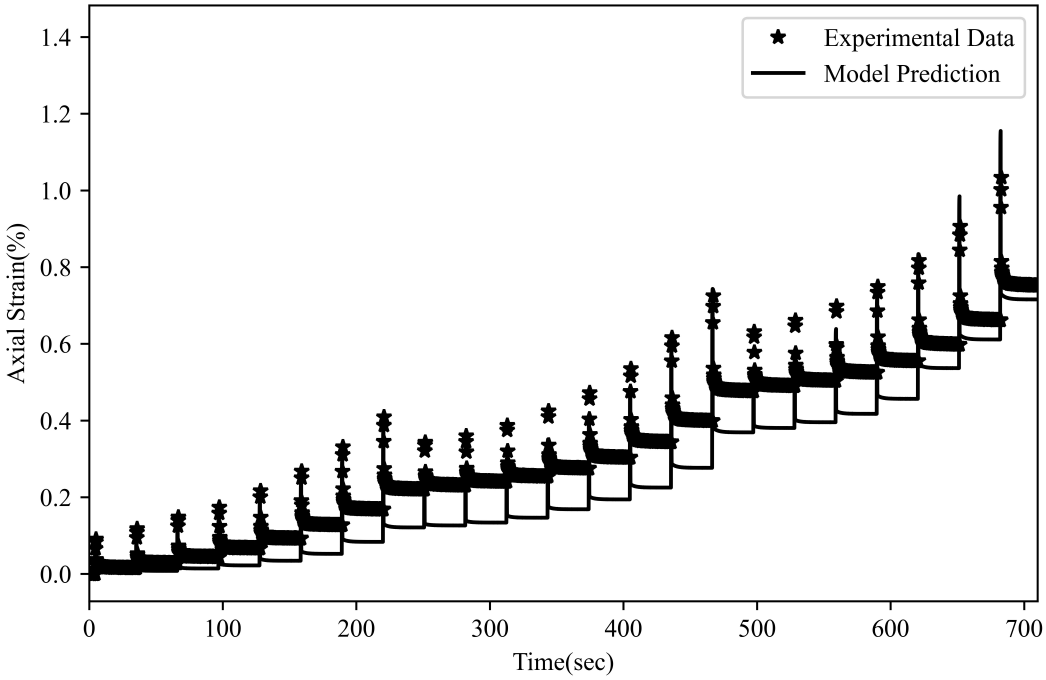

Figure 4.24: Analysis of axial strain values from the RCR experiments using nonlinear modeling at 55^o C and 0 kPa confinement pressure

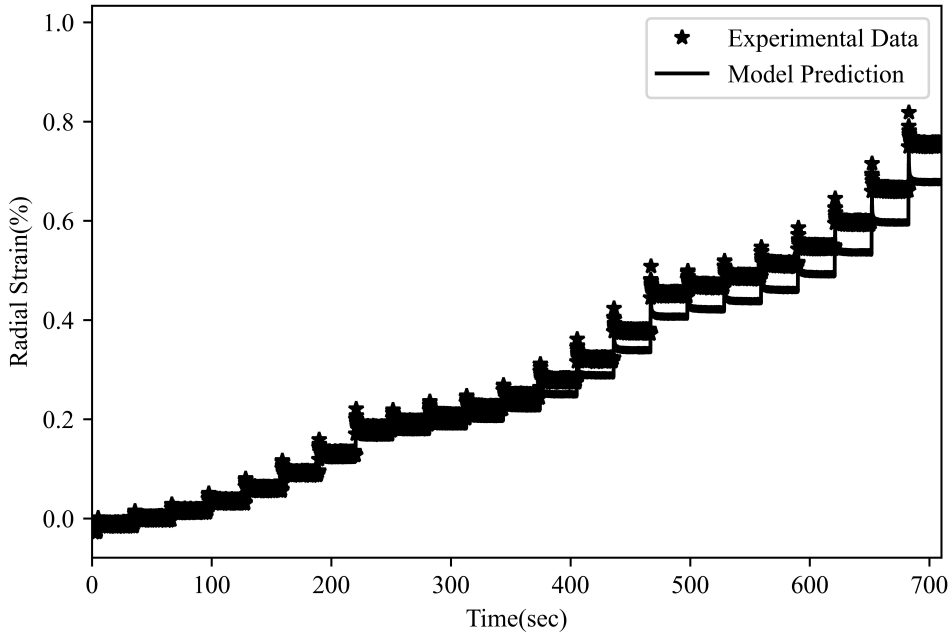

Figure 4.25: Analysis of radial strain values from the RCR experiments using nonlinear modeling at 55^o C and 0 kPa confinement pressure

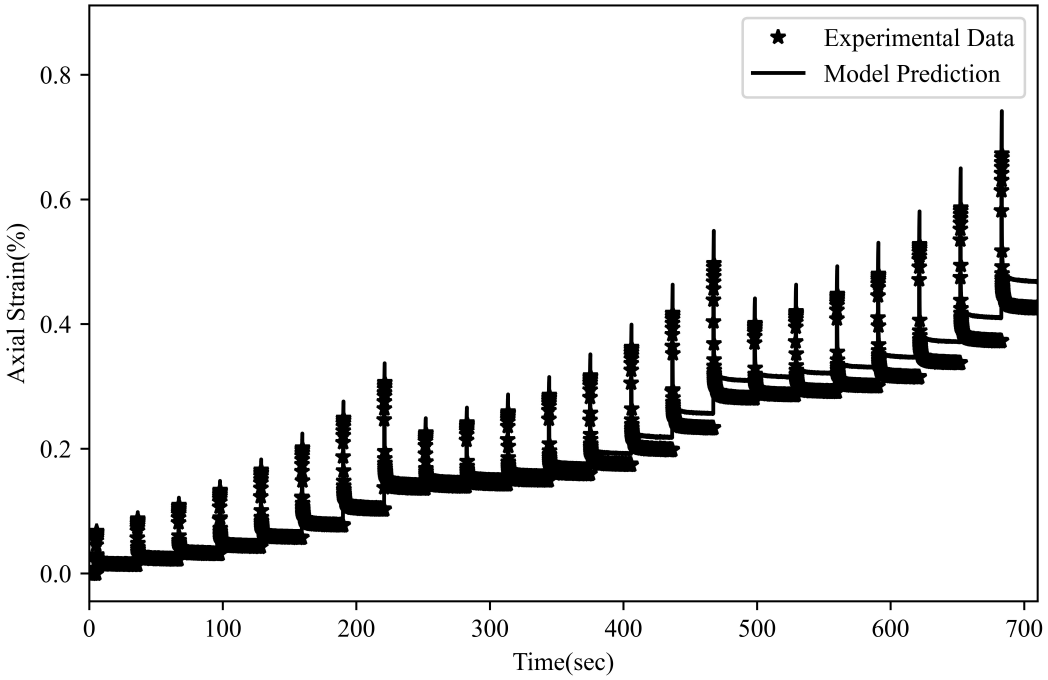

Figure 4.26: Analysis of axial strain values from the RCR experiments using nonlinear modeling at 55^o C and 70 kPa confinement pressure

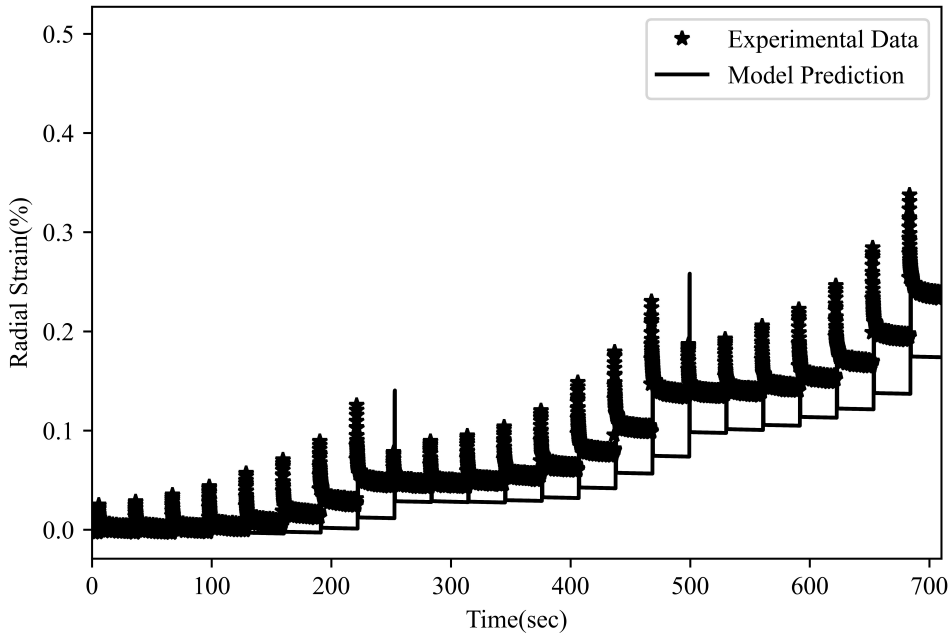

Figure 4.27: Analysis of radial strain values from the RCR experiments using nonlinear modeling at 55^o C and 70 kPa confinement pressure

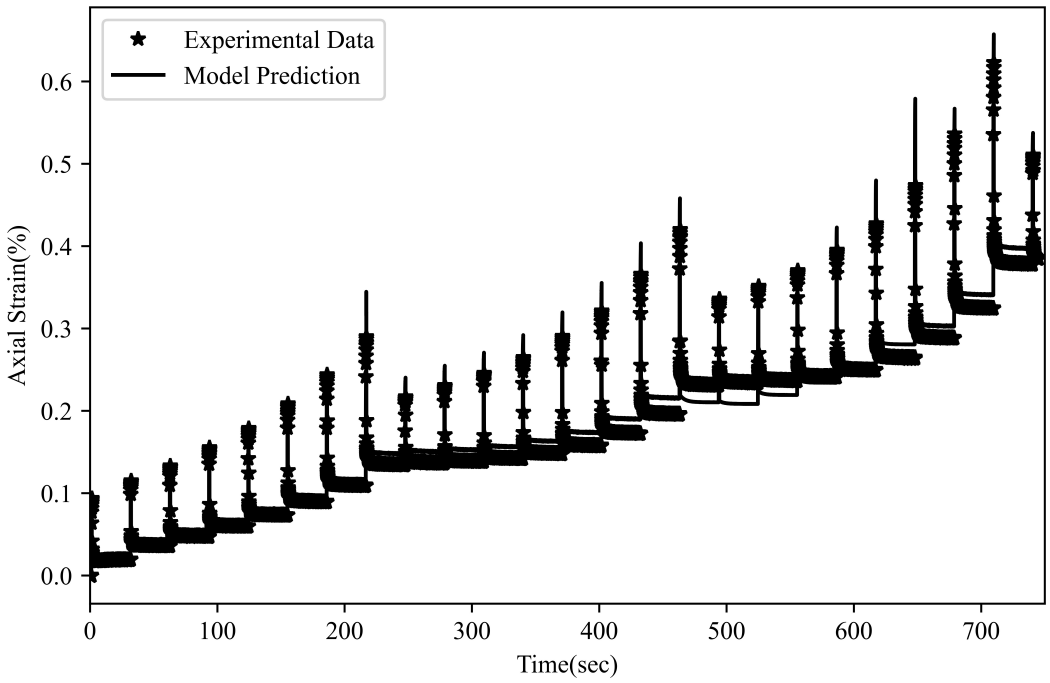

Figure 4.28: Analysis of axial strain values from the RCR experiments using nonlinear modeling at 55^o C and 140 kPa confinement pressure

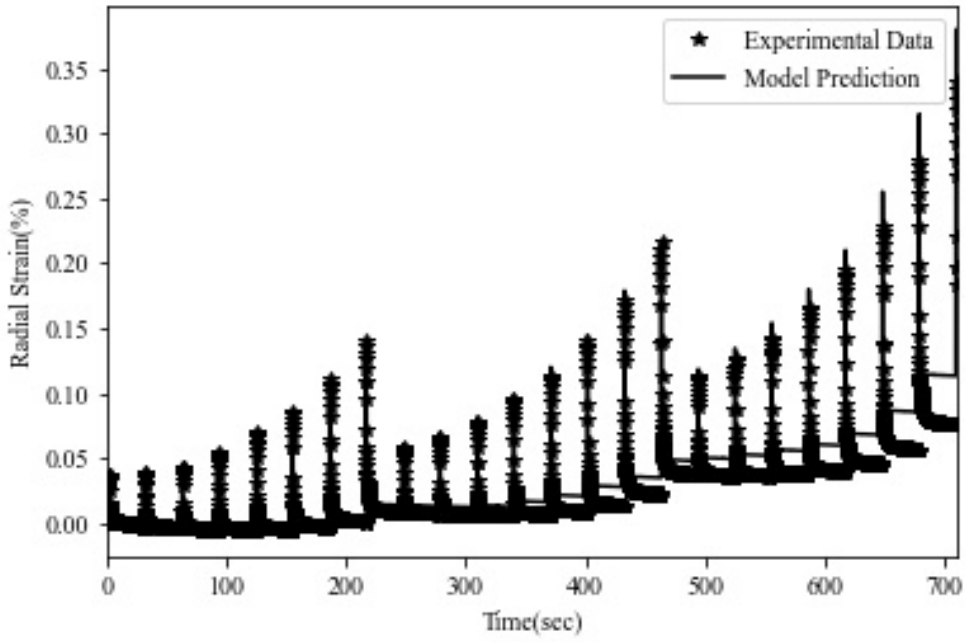

Figure 4.29: Analysis of radial strain values from the RCR experiments using nonlinear modeling at 55^o C and 140 kPa confinement pressure

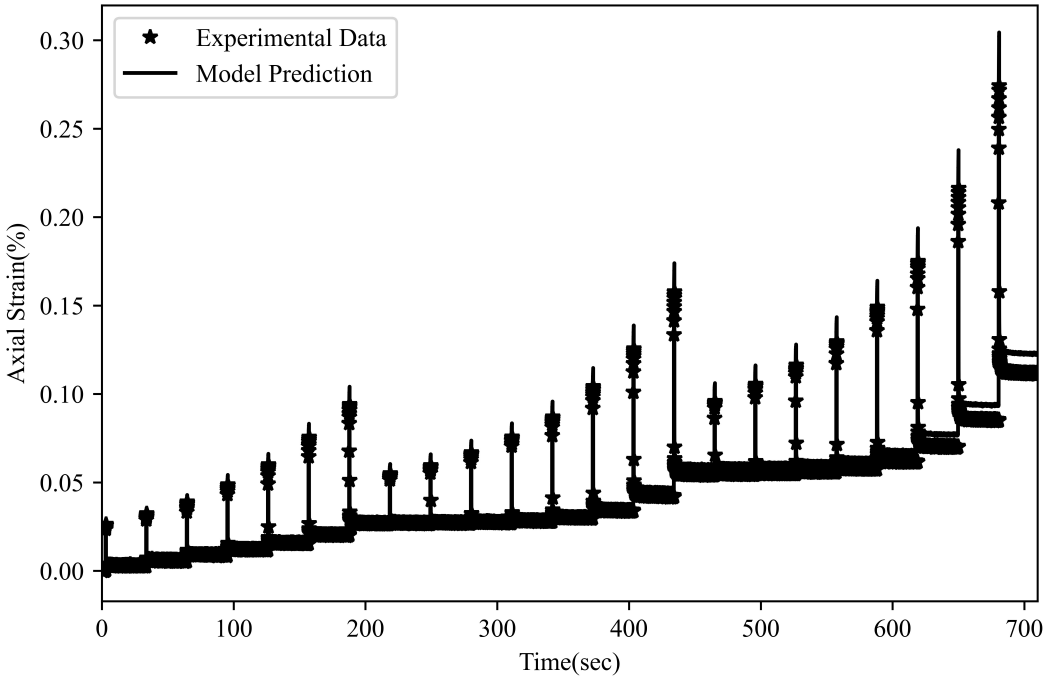

Figure 4.30: Analysis of axial strain values from the RCR experiments using nonlinear modeling at 55^o C and 380 kPa confinement pressure

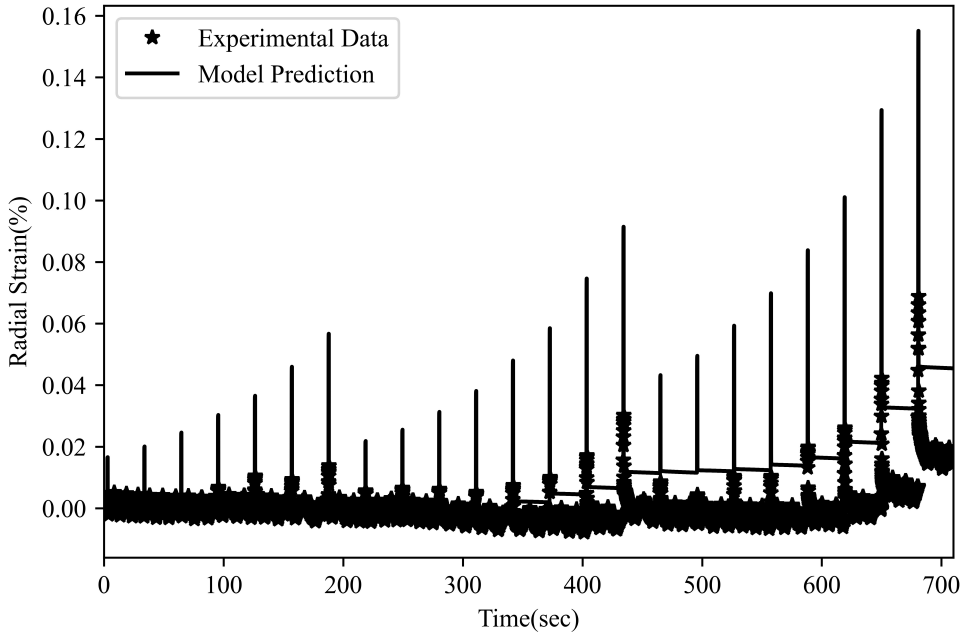

Figure 4.31: Analysis of radial strain values from the RCR experiments using nonlinear modeling at 55^o C and 380 kPa confinement pressure.

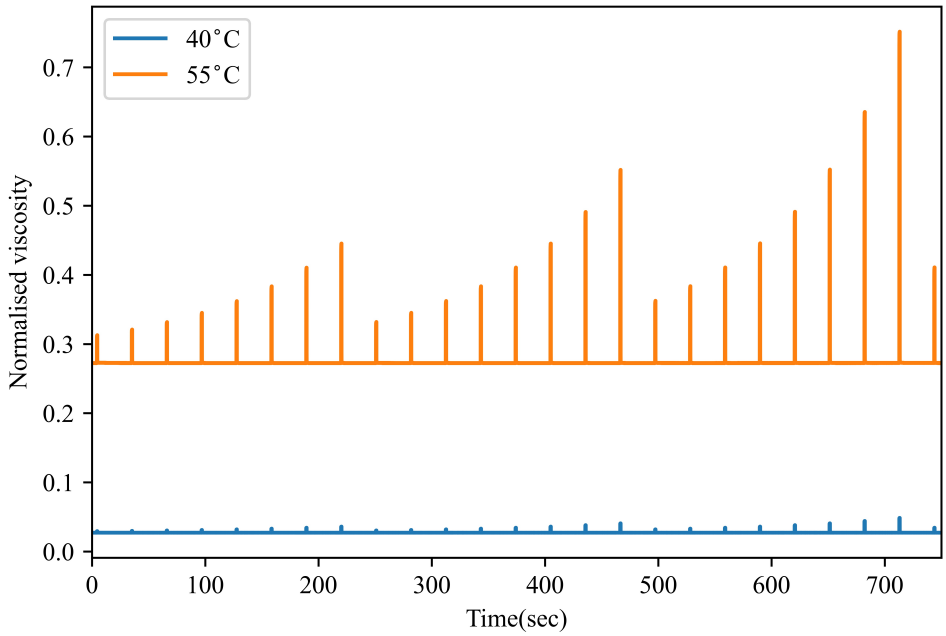

Figure 4.32: Axial strain response of asphalt mixtures when subjected to various confinement pressure

configurations, thereby keeping track of its current natural configuration.

When the model was corroborated against the obtained experimental data the model's predictions were found to describe the non proportional response of asphalt mixtures while accounting for the effect of confinement pressure well. Thus, the model can be used to describe the mechanical behavior of asphalt mixtures in isothermal processes at any temperature (as shown in Figure 4.16 at 40^oC and Figure 4.24 at 55^oC). The following conclusions can be drawn from the experimental studies, theoretical developments, and data analysis presented in this chapter:

- The viscoelastic properties of asphalt mixtures depend strongly on confinement pressure. This indicates the need for multiaxial laboratory testing conditions to realistically simulate the loading conditions experienced by asphalt pavements in the field.

- The viscosity of asphalt mixtures was found to depend on the confinement pressure (an exponential function of $tr(\mathbf{T})$).

- Temperature is also found to significantly influence binder stiffness as one would expect. All the viscosity and modulus parameters were observed to decrease with increased temperature as shown in Table 4.2

- The variation of normalized viscosity ($\frac{\eta_d}{\eta_{d_1}}$) due to confinement pressure, as shown in Figure 4.32, was found to be higher at higher temperatures. From this it can be deduced that the nonlinearity due to the confinement pressure is higher at higher temperatures.

5. SUMMARY AND CONCLUSIONS

5.1 Summary

As discussed in this dissertation, the response of asphaltic materials is dependent on time, temperature, stress or strain level, and confinement pressure. This makes the modeling of such materials a complex task. Hence, the primary objective of this study is to develop a thermodynamic constitutive model capable of modeling the complex behaviors exhibited by asphaltic materials, including its non-proportional response to external loading, its ability to stress relax, and its ability to recover when loading is removed, while accounting for the multi constituent nature of the material and its sensitivity to factors like confinement pressure, time, aging, and temperature.

The objective of this dissertation was achieved by using a thermodynamics-based nonlinear viscoelastic (NVE) model derived by Málek et al. [45] to capture the effects of various polymer additives, aging, and nonlinear creep and recovery response of asphalt mixtures. Additionally, this study established a framework to separate the contribution of individual constituents to the overall material response. The efficacy of this framework was tested to understand the effects of reclaimed asphalt pavement (RAP) content in the blended binder in chapter 3. Along with this, a detailed discussion of various experimental protocols that have been previously used to quantify permanent deformation in asphalt binders as well as their drawbacks in blended binders was provided. Consequently, a new protocol was also suggested in chapter 3 along with the required post-processing to better quantify permanent deformation. This framework has shown that a thermodynamic viscoelastic model derived based on the idea of natural configuration and maximization of the rate of dissipation can capture the complex response of asphalt mixtures and identify the contributions of its constituents.

Appealing to the idea of natural configuration and maximization of rate of dissipation, we derived a compressible NVE model within a Gibbs-potential-based thermodynamic framework, to model the effects of confinement pressure on the response of asphalt mixtures at various temper-

atures in chapter 4. The main reasons for the selection of the thermodynamics-based viscoelastic models are as follows:

- Asphaltic materials in the field exhibit nonlinearity even when subjected to small strains. The thermodynamics-based model was capable of capturing such nonlinearities.

- Asphaltic materials go through significant microstructure changes due to repeated loading in the field. These changes involve a reduction in air voids, rearrangement of aggregate, and changes in structure and aging of binders. The NVE model used in this study can account for these changes by appealing to the idea that a material can have multiple natural configurations simultaneously.• Asphaltic materials go through significant microstructure changes due to repeated loading in the field. These changes involve a reduction in air voids, rearrangement of aggregate, and changes in structure and aging of binders. The NVE model used in this study can account for these changes by appealing to the idea that a material can have multiple natural configurations simultaneously.

- The limited number of model parameters makes it possible to relate these parameters to mixture design. The framework established along with these parameters can be used to understand the effects of individual constituents, which can then be used to optimize mixtures and design of blended binders.

5.1.1 Modeling of Asphalt Mixtures with Warm Mix Additives

This study established a framework using the NVE model derived by Málek et al. [45], to separate the contributions of individual constituents to overall material response. The following conclusions can be made from this study:

- The model developed by Málek et al. [45] was used to capture the response of asphalt mixtures, including various warm mix additives. The efficacy of the model was evaluated by capturing the material behavior when subjected to different loading conditions using a single set of parameters.

- Warm fine aggregate mixtures (WFAM) samples exhibited nonlinearities in the form of non-proportional response and generation of normal stress when sheared.

- Aging has a significant effect on the stiffness of the WFAM samples in comparison to their viscosity. The dissipation parameter (μ3) is responsible for the viscous behavior which is almost unaffected due to aging of WFAM samples.

5.1.2 Linear and Nonlinear Modeling of Reclaimed Asphalt Binders

The framework established in chapter 2 was utilized to analyze the effects of binder recovered from reclaimed asphalt pavement on the response of a binder blend. Additionally, a new protocol was established to analyze the rutting resistance of blended binders. The main findings are:

- The loading conditions in the standard multiple stress creep and recovery (MSCR) test protocol are not ideal to analyze rutting in blended binders because applied stress levels are not sufficient to capture their NVE behavior, which is the case in the field.

- The recovery time in MSCR is constant irrespective of the load magnitude. This time may not be sufficient for the binder to recover completely under high loading conditions.

- The standard protocol of calculating non-recoverable creep compliance (Jnr) has shown disagreement in the values obtained from the MSCR and repeated creep and recovery with multiple stress levels (RCRMS) tests. In the case of the MSCR test, the Jnr value was constant up to 25% RAP, after which its value decreased with the addition of more RAP content. In the case of the RCRMS test, the Jnr value gradually decreased with the addition of RAP until 35% RAP.

- The stiffness and viscosities of the blended binders increased with the increase in RAP content. This is to be expected as aged binder in the field becomes stiffer and viscous.

- The viscosity parameter correlates well with the rutting of binders irrespective of loading unlike the commonly used J_{nr}, which was found to depend on the stress being applied on the binders.

5.1.3 Modeling Effects of Confinement Pressure and Temperature

A new compressible NVE model was derived, using the thermodynamic framework established by Rajagopal and Srinivasa [96], to capture the effects of confinement pressure on the response of asphalt mixtures. The conclusions of this are as follows:

- The constitutive model developed using a Gibbs-potential-based thermodynamic framework was able to capture the NVE response of asphalt mixtures. The model parameters were iteratively adjusted to capture the material response at all confinement pressures.
- It is clearly shown that the NVE properties of asphalt mixtures strongly depend on the confinement pressure. Therefore, the nonlinear properties obtained from the uniaxial creep and recovery tests cannot be used effectively to predict the response of asphalt pavements in the field.
- The nonlinearity induced by the confinement pressure increases with an increase in temperature.

5.2 Contributions of the Research

The primary contributions of this research are as follows:

- This research will pave the way for the development of a fundamental understanding of the influence of factors like confinement, aging, temperature, and polymer additives on asphaltic materials. Such understanding can be used to evaluate and predict the various distresses experienced by the pavement in the field.
- This research showcased the inadequacies of test protocols commonly used to quantify rutting resistance of asphalt binders and proposed a new protocol addressing these inadequacies. This new protocol, along with the suggested post-processing (i.e., calculating apparent viscosity), can be used to better quantify the rutting resistance of various binders.
- The framework developed to separate the contribution of individual constituents to overall material response can be used to optimize mixture designs to get desired mixture properties.

- The sensitivity of the model parameters to the applied confinement pressure depends on the operating temperature. The parameters are more sensitive to pressure with increased temperature.

- Several aspects of the complex behavior of the asphaltic material are analyzed throughout this study including:

  - Non-proportional response to external stimuli.
  - Generation of normal force under shear loading.
  - Effects of various polymer additives on the response of asphalt mixtures.
  - Effects of aging on the response of asphalt mixtures.
  - Effects of RAP content in blended binders.
  - Effects of confinement pressure on the response of asphalt mixtures.
  - Effects of temperature on the response of asphalt mixtures.

5.3 Future Work

This study can be extended in the following ways:

- The model developed and implemented in this study can be modified to account for the effects of changes in temperature on material response. The non-isothermal model can then be used to simultaneously study internal thermal stress due to temperature gradients in the pavement and external stress due to the passage of vehicles.

- A finite element model for the NVE model can be used to model several complex boundary value problems and simulate the various loading conditions pavements are subjected to in the field, like the passage of wheels repeated.

- The model can also be modified to account for the anisotropy and porosity of asphalt mixtures.

REFERENCES

[1] RA Schapery. "On the characterization of nonlinear viscoelastic materials". In: *Polymer Engineering & Science* 9.4 (1969), pp. 295–310.

[2] KR Rajagopal and AR Srinivasa. "A note on a correspondence principle in nonlinear viscoelastic materials". In: *International Journal of Fracture* 131.4 (2005), pp. L47–L52.

[3] CY Cheung and D Cebon. "Experimental study of pure bitumens in tension, compression, and shear". In: *Journal of Rheology* 41.1 (1997), pp. 45–74.

[4] SPA Narayan. "A model for the nonlinear mechanical behavior of asphalt Binders and its Application in Prediction of Rutting Susceptibility". PhD thesis. 2013.

[5] B Vajipeyajula, E Masad, KL Roja, et al. "A two-constituent nonlinear viscoelastic model for asphalt mixtures". In: *Road Materials and Pavement Design* (2019), pp. 1–15.

[6] E Rahmani, MK Darabi, RKA Al-Rub, et al. "Effect of confinement pressure on the nonlinear-viscoelastic response of asphalt concrete at high temperatures". In: *Construction and Building Materials* 47 (2013), pp. 779–788.

[7] M Bazzaz, MK Darabi, DN Little, et al. "A straightforward procedure to characterize nonlinear Viscoelastic Response of Asphalt Concrete at High Temperatures". In: *Transportation Research Record* 2672.28 (2018), pp. 481–492.

[8] E Rahmani, MK Darabi, DN Little, et al. "Constitutive modeling of coupled aging-viscoelastic response of asphalt concrete". In: *Construction and Building Materials* 131 (2017), pp. 1–15. ISSN: 0950-0618.

[9] JF Rushing, MK Darabi, E Rahmani, et al. "Comparing rutting of airfield pavements to simulations using Pavement Analysis Using Nonlinear Damage Approach (PANDA)". In: *International Journal of Pavement Engineering* 18.2 (2017), pp. 138–159.

[10] J Bari and MW Witczak. “New predictive models for viscosity and complex shear modulus of asphalt binders: for use with mechanistic-empirical pavement design guide”. In: *Transportation Research Record* 2001.1 (2007), pp. 9–19.

[11] JM Krishnan and KR Rajagopal. “Review of the uses and modeling of bitumen from ancient to modern times”. In: *Applied Mechanics Reviews* 56.2 (2003), pp. 149–214.

[12] E Masad, N Somadevan, HU Bahia, et al. “Modeling and experimental measurements of strain distribution in asphalt mixes”. In: *Journal of Transportation Engineering* 127.6 (2001), pp. 477–485.

[13] C Van der Poel. *Road asphalt*. Vol. 9. Chapter, 1954.

[14] AR Lee and AHD Markwick. “The mechanical properties of bituminous surfacing materials under constant stress”. In: *Journal of the Society of Chemical Industry* 56 (1937), pp. 146–156.

[15] KE Secor and CL Monismith. “Analysis and interrelation of stress-strain-time data for asphalt concrete”. In: *Transactions of the Society of Rheology* 8.1 (1964), pp. 19–32.

[16] JM Krishnan and KR Rajagopal. “Thermodynamic framework for the constitutive modeling of asphalt concrete: Theory and applications”. In: *Journal of materials in Civil Engineering* 16.2 (2004), pp. 155–166.

[17] KR Rajagopal and AR Srinivasa. “A thermodynamic frame work for rate type fluid models”. In: *Journal of Non-Newtonian Fluid Mechanics* 88.3 (2000), pp. 207–227.

[18] UK Shell Bitumen. “The Shell bitumen handbook”. In: *Chertsey: shell Bitumen UK* (1990).

[19] JM Krishnan and KR Rajagopal. “On the mechanical behavior of asphalt”. In: *Mechanics of Materials* 37.11 (2005), pp. 1085–1100.

[20] KL Roja, E Masad, B Vajipeyajula, et al. “Chemical and multi-scale material properties of recycled and blended asphalt binders”. In: *Construction and Building Materials* 261 (2020).

[21] LW Corbett. “Composition of asphalt based on generic fractionation, using solvent deasphaltening, elution-adsorption chromatography, and densimetric characterization”. In: *Analytical Chemistry* 41.4 (1969), pp. 576–579.

[22] D Lesueur. “The colloidal structure of bitumen: Consequences on the rheology and on the mechanisms of bitumen modification”. In: *Advances in Colloid and Interface Science* 145.1-2 (2009), pp. 42–82.

[23] W. Lethersich. “The mechanical behaviour of bitumen”. In: *Journal of the Society of Chemical Industry* 61.7 (1942), pp. 101–108.

[24] SPA Narayan, JM Krishnan, AP Deshpande, et al. “Nonlinear viscoelastic response of asphalt binders: An experimental study of the relaxation of torque and normal force in torsion”. In: *Mechanics Research Communications* 43 (2012), pp. 66–74.

[25] E Masad, CW Huang, G Airey, et al. “Nonlinear viscoelastic analysis of unaged and aged asphalt binders”. In: *Construction and Building Materials* 22.11 (2008), pp. 2170–2179.

[26] J D’Angelo, R Kluttz, RN Dongre, et al. “Revision of the superpave high temperature binder specification: the multiple stress creep recovery test (with discussion)”. In: *Journal of the Association of Asphalt Paving Technologists* 76 (2007).

[27] JM Dealy. “Rheological properties of oil sand bitumens”. In: *The Canadian Journal of Chemical Engineering* 57.6 (1979), pp. 677–683.

[28] MZ Rahaman, Z Hossain, and M Zaman. “Nonrecoverable compliance and recovery behavior of polymer-modified and reclaimed asphalt pavement–modified binders in Arkansas”. In: *Journal of Testing and Evaluation* 46.6 (2018), pp. 2483–2497.

[29] A Bernier, A Zofka, and I Yut. “Laboratory evaluation of rutting susceptibility of polymer-modified asphalt mixtures containing recycled pavements”. In: *Construction and Building Materials* 31 (2012), pp. 58–66.

[30] J Zhang, GS Simate, X Hu, et al. “Impact of recycled asphalt materials on asphalt binder properties and rutting and cracking performance of plant-produced mixtures”. In: *Construction and Building Materials* 155 (2017), pp. 654–663.

[31] D Singh, D Sawant, and F Xiao. “High and intermediate temperature performance evaluation of crumb rubber modified binders with RAP”. In: *Transportation Geotechnics* 10 (2017), pp. 13–21.

[32] HU Bahia, WP Hislop, H Zhai, et al. “Classification of asphalt binders into simple and complex binders”. In: *Journal of the Association of Asphalt Paving Technologists* 67 (1998).

[33] HU Bahia, DI Hanson, M Zeng, et al. *Characterization of modified asphalt binders in superpave mix design*. Project 9-10 FY’96. 2001.

[34] S Biro, T Gandhi, and S Amirkhanian. “Determination of zero shear viscosity of warm asphalt binders”. In: *Construction and Building Materials* 23.5 (2009), pp. 2080–2086.

[35] JA D’Angelo. “The relationship of the MSCR test to rutting”. In: *Road Materials and Pavement Design* 10.sup1 (2009), pp. 61–80.

[36] G White. “Grading highly modified binders by multiple stress creep recovery”. In: *Road Materials and Pavement Design* 18.6 (2017), pp. 1322–1337.

[37] S Dreessen, JP Planche, and V Gardel. “A new performance related test method for rutting prediction: MSCRT”. In: *Advanced testing and characterization of bituminous materials* 1 (2009), pp. 971–980.

[38] A Golalipour. “Modification of multiple stress creep and recovery test procedure and usage in specification”. PhD thesis. 2011.

[39] A Alisov, T Hagner, and A Walther. “Quantification of polymer content in binder by modified MSCR-test”. In: *6th Eurasphalt & Eurobitume Congress, Proceedings, Prag*. Vol. 4. 2016.

[40] NH Gibson, ME Kutay, D Keramat, et al. “Multiaxial strain response of asphalt concrete measured during flow number performance test”. In: *Journal of the Association of Asphalt Paving Technologists* 78 (2009), pp. 25–66.

[41] S Saadeh, E Masad, and DN Little. “Characterization of asphalt mix response under repeated loading using anisotropic nonlinear viscoelastic-viscoplastic model”. In: *Journal of Materials in Civil Engineering* 19.10 (2007), pp. 912–924.

[42] TK Pellinen, MW Witczak, M Marasteanu, et al. “Stress dependent master curve construction for dynamic (complex) modulus”. In: *Asphalt Paving Technology: Association of Asphalt Paving Technologists-Proceedings of the Technical Sessions*. Vol. 71. Association of Asphalt Paving Technologist. 2002, pp. 281–309.

[43] B Dołżycki and J Judycki. “Behaviour of asphalt concrete in cyclic and static compression creep test with and without lateral confinement”. In: *Road materials and pavement design* 9.2 (2008), pp. 207–225.

[44] Y Zhao, H Liu, and W Liu. “Characterization of linear viscoelastic properties of asphalt concrete subjected to confining pressure”. In: *Mechanics of Time-Dependent Materials* 17.3 (2013), pp. 449–463.

[45] J Málek, KR Rajagopal, and K Tuma. “A thermodynamically compatible model for describing the response of asphalt binders”. In: *International Journal of Pavement Engineering* 16.4 (2015), pp. 297–314.

[46] F Bai, X Yang, and G Zeng. “Creep and recovery behavior characterization of asphalt mixture in compression”. In: *Construction and Building Materials* 54 (2014), pp. 504–511.

[47] O-V Laukkanen, H Soenen, T Pellinen, et al. “Creep-recovery behavior of bituminous binders and its relation to asphalt mixture rutting”. In: *Materials and Structures* 48.12 (2015), pp. 4039–4053.

[48] MK Darabi, RKA Al-Rub, EA Masad, et al. “A thermo-viscoelastic–viscoplastic–viscodamage constitutive model for asphaltic materials”. In: *International Journal of Solids and Structures* 48.1 (2011), pp. 191–207.

[49] MK Darabi, RKA Al-Rub, EA Masad, et al. “A thermodynamic framework for constitutive modeling of time-and rate-dependent materials. Part II: Numerical aspects and application to asphalt concrete”. In: *International Journal of Plasticity* 35 (2012), pp. 67–99.

[50] J Málek, KR Rajagopal, and K Tuma. “A thermodynamically compatible model for describing asphalt binders: solutions of problems”. In: *International Journal of Pavement Engineering* 17.6 (2016), pp. 550–564.

[51] KR Rajagopal. “Multiple configurations in continuum mechanics”. In: *Reports of the Institute for Computational and Applied Mechanics* 6 (1995).

[52] JM Krishnan and SPA Narayan. *Steady shear experiments on asphalt*. Tech. rep. Internal Report, IIT Madras, Chennai, India, 2007.

[53] I Menapace, E Masad, and M Sadeq. “Microstructure of warm mix asphalt binder exposed to UV light and heat”. In: *8th International Conference on Maintenance and Rehabilitation of Pavements, MAIREPAV8*. 2016.

[54] M Sadeq, E Masad, H Al-Khalid, et al. “New protocol utilising the accelerated weathering tester to age fine asphalt mixtures with warm mix asphalt additives”. In: *7th International EATA (European Asphalt Technology Association) Conference*. 2017.

[55] M Sadeq, CW Huang, E Masad, et al. “A framework for the analysis of damage and recovery characteristics of asphalt mixtures”. In: *Road Materials and Pavement Design* (2020), pp. 1–14.

[56] K Kannan and KR Rajagopal. “A thermodynamical framework for chemically reacting systems”. In: *Zeitschrift für angewandte Mathematik und Physik* 62.2 (2011), pp. 331–363.

[57] S Moon, F Cui, and IJ Rao. “A thermodynamic framework for the modeling of crystallizable triple shape memory polymers”. In: *International Journal of Engineering Science* 134 (2019), pp. 1–30.

[58] KR Rajagopal and AR Srinivasa. “On the thermomechanics of materials that have multiple natural configurations Part I: Viscoelasticity and classical plasticity”. In: *Zeitschrift für angewandte Mathematik und Physik ZAMP* 55.5 (2004), pp. 861–893.

[59] Kumbakonam R Rajagopal and Arun R Srinivasa. “On the thermodynamics of fluids defined by implicit constitutive relations”. In: *Zeitschrift für angewandte Mathematik und Physik* 59.4 (2008), pp. 715–729.

[60] W Noll and CA Truesdell. *The non-linear field theories of mechanics*. Springer-Verlag Berlin, 1992.

[61] J Málek, KR Rajagopal, and K Tuma. “A thermodynamically compatible model for describing the response of asphalt binders”. In: *International Journal of Pavement Engineering* 16.4 (2015), pp. 297–314.

[62] AR Coenen, ME Kutay, NR Sefidmazgi, et al. “Aggregate structure characterisation of asphalt mixtures using two-dimensional image analysis”. In: *Road Materials and Pavement Design* 13.3 (2012), pp. 433–454.

[63] MD Nazzal, W Mogawer, A Austerman, et al. “Multi-scale evaluation of the effect of rejuvenators on the performance of high RAP content mixtures”. In: *Construction and Building Materials* 101 (2015), pp. 50–56.

[64] MD Nazzal, E Holcombe, SS Kim, et al. “Nanoscale and macroscale characterization of the influence of RAP and RAS on cracking resistance of asphalt mixes”. In: *Journal of Materials in Civil Engineering* 30.12 (2018), p. 04018334.

[65] F Rashid, Z Hossain, and A Bhasin. “Nanomechanistic properties of reclaimed asphalt pavement modified asphalt binders using an atomic force microscope”. In: *International Journal of Pavement Engineering* 20.3 (2019), pp. 357–365.

[66] SN Nahar, M Mohajeri, AJM Schmets, et al. “First observation of blending-zone morphology at interface of reclaimed asphalt binder and virgin bitumen”. In: *Transportation research record* 2370.1 (2013), pp. 1–9.

[67] HU Bahia and DA Anderson. “Strategic highway research program binder rheological parameters: background and comparison with conventional properties”. In: *Transportation research record* 1488 (1995).

[68] FL Roberts, PS Kandhal, E R Brown, et al. “Hot mix asphalt materials, mixture design and construction”. In: *NAPA Educational Foundation, Lanham, MD* (1991).

[69] TLJ Wasage, Jiri Stastna, and L Zanzotto. “Rheological analysis of multi-stress creep recovery (MSCR) test”. In: *International Journal of Pavement Engineering* 12.6 (2011), pp. 561–568.

[70] J D’ANGELO and R Dongr. “Superpave binder specifications and their performance relationship to modified binders”. In: *Proceedings of the Forty-Seventh Annual Conference of the Canadian Technical Asphalt Association (CTAA): Calgary, Alberta*. 2002.

[71] R Delgadillo. *Nonlinearity of asphalt binders and the relationship with asphalt mixture permanent deformation*. 2008.

[72] A Loizos, MN Partl, T Scarpas, et al. “A new performance related test method for rutting prediction: MSCRT”. In: *Advanced Testing and Characterization of Bituminous Materials, Two Volume Set*. CRC Press, 2009, pp. 1003–1012.

[73] R Kumar, N Saboo, P Kumar, et al. “Effect of warm mix additives on creep and recovery response of conventional and polymer modified asphalt binders”. In: *Construction and Building Materials* 138 (2017), pp. 352–362.

[74] AJ Barco Carrión, D Lo Presti, S Pouget, et al. “Linear viscoelastic properties of high reclaimed asphalt content mixes with biobinders”. In: *Road Materials and Pavement Design* 18.sup2 (2017), pp. 241–251.

[75] A Blasl, M Khalili, GC Falla, et al. “Rheological characterisation and modelling of bitumen containing reclaimed components”. In: *International Journal of Pavement Engineering* 20.6 (2019), pp. 638–648.

[76] S Mangiafico, H Di Benedetto, C Sauzéat, et al. “Influence of reclaimed asphalt pavement content on complex modulus of asphalt binder blends and corresponding mixes: experimental results and modelling”. In: *Road Materials and Pavement Design* 14.sup1 (2013), pp. 132–148.

[77] SPA Narayan, DN Little, and KR Rajagopal. “Analysis of rutting prediction criteria using a nonlinear viscoelastic model”. In: *Journal of Materials in Civil Engineering* 27.3 (2015), p. 04014137.

[78] MR Nivitha, SPA Narayan, and JM Krishnan. “Non-linear viscoelastic model based ranking of modified binders for their rutting performance”. In: *Materials and Structures* 51.4 (2018), p. 105.

[79] S Koneru, E Masad, and KR Rajagopal. “A thermomechanical framework for modeling the compaction of asphalt mixes”. In: *Mechanics of Materials* 40.10 (2008), pp. 846–864.

[80] KS Reddy, S Umakanthan, and JM Krishnan. “Constant strain rate experiments and constitutive modeling for a class of bitumen”. In: *Mechanics of Time-Dependent Materials* 16.3 (2012), pp. 251–274.

[81] R Vijay, AP Deshpande, and S Varughese. “Nonlinear rheological modeling of asphalt using White-Metzner model with structural parameter variation based asphaltene structural build-up and breakage”. In: *Applied Rheology* 18.2 (2008), 23214-1–23214–14.

[82] SPA Narayan, DN Little, and KR Rajagopal. “Nonlinear Viscoelastic Model for Describing the Response of Asphalt Binders within the Context of a Gibbs-Potential–Based Thermodynamic Framework”. In: *Journal of Engineering Mechanics* 141.2 (2015), p. 04014116.

[83] “Standard method of test for quantitative extraction of asphalt binder from hot mix asphalt (HMA)”. In: *AASHTO* (2014).

[84] "RHEA version 1 [Computer software]. Abatech Consulting Engineers, Blooming Glen, PA." In: ().

[85] TP70 AASHTO. "Standard practice for multiple stress creep recovery test of asphalt binder using a dynamic shear rheometer". In: *American Association of State Highway and Transportation Officials, Washington DC* (2010).

[86] "MATLAB [Computer software]. MathWorks, Natick, MA." In: ().

[87] D Kim et al. "Modulus and permanent deformation characterization of asphalt mixtures and pavements". In: *PhD thesis* (2015).

[88] Ls Gao, H Dan, and L Li. "Response analysis of asphalt pavement under dynamic loadings: loading equivalence". In: *Mathematical Problems in Engineering* 2019 (2019).

[89] JM Krishnan and KR Rajagopal. "Triaxial testing and stress relaxation of asphalt concrete". In: *Mechanics of Materials* 36.9 (2004), pp. 849–864.

[90] CW Huang, E Masad, AH Muliana, et al. "Nonlinearly viscoelastic analysis of asphalt mixes subjected to shear loading". In: *Mechanics of Time-Dependent Materials* 11.2 (2007), pp. 91–110.

[91] SPA Narayan, KAV Nag, JM Krishnan, et al. "Nonlinear viscoelastic response of asphalt binders in transient tests". In: *Road materials and pavement design* 13.1 (2012), pp. 191–202.

[92] A Mathruswamy, PK Athira, and SPA Narayan. "Compressible behaviour of bituminous mixtures in creep recovery test in confinement". In: *Functional Pavement Design: Proceedings of the 4th Chinese-European Workshop on Functional Pavement Design (4th CEW 2016, Delft, The Netherlands, 29 June-1 July 2016)*. CRC Press. 2016, p. 59.

[93] JM Krishnan, KR Rajagopal, E Masad, et al. "Thermomechanical framework for the constitutive modeling of asphalt concrete". In: *International journal of geomechanics* 6.1 (2006), pp. 36–45.

[94] B Vajipeyajula, KL Roja, E Masad, et al. “Analysis of reclaimed asphalt blended binders using linear and nonlinear viscoelasticity frameworks”. In: *Materials and Structures* 53.5 (2020), pp. 1–14.

[95] B Vajipeyajula, KL Roja, E Masad, et al. “Assessing permanent deformation of reclaimed asphalt blended binders using non-linear viscoelasticity theory”. In: *Advances in Materials and Pavement Performance Prediction II: Contributions to the 2nd International Conference on Advances in Materials and Pavement Performance Prediction (AM3P 2020), 27-29 May, 2020, San Antonio, TX, USA*. CRC Press. 2020, p. 372.

[96] KR Rajagopal and AR Srinivasa. “A Gibbs-potential-based formulation for obtaining the response functions for a class of viscoelastic materials”. In: *Proceedings of the Royal Society A: Mathematical, Physical and Engineering Sciences* 467.2125 (2011), pp. 39–58.